Cellulose – Polycarbonate Nanocomposites:

A novel automotive window alternative

by

Andrew Christopher Finkle

A thesis

presented to the University of Waterloo

in fulfilment of the

thesis requirement for the degree of

Master of Applied Science

in

Chemical Engineering (Nanotechnology)

Waterloo, Ontario, Canada, 2011

Author's Declaration

I hereby declare that I am the sole author of this thesis. This is a true copy of the thesis, including any required final revisions, as accepted by my examiners.

I understand that my thesis may be made electronically available to the public.

Abstract

Nanocrystalline cellulose (NCC) has great potential as a reinforcing agent in thermoplastics (such as polyesters, polyamides and polycarbonates) due to its high mechanical strength and aspect ratio – being compared with reinforcements like steel and carbon nanotubes. In order to maintain its strength when compounded with thermoplastics, the high-temperature processing must not damage the structural integrity of the nanocrystalline cellulose. The processing temperature for polyesters, polyamides and polycarbonates is relatively high and near to the onset of thermal degradation of cellulose bio products, therefore care must be taken to ensure the preservation of the structural integrity of nanocrystalline cellulose.

The thermal stability and the kinetics of thermal degradation of five different cellulose samples were studied using an Ozawa-Flynn-Wall method and thermogravimetric analysis data. To complete the characterization of the NCC for polymer processing applications, the crystallinity index was determined using X-ray diffraction; surface morphology was studied with scanning electron microscope, chemical composition was studied using FT-IR, and moisture content was measured using a moisture analyser. Each of these properties observed is essential to the end mechanical properties of the polymer nanocomposite as these properties will affect the dispersion and interfacial adhesion of the fibres to the polymer matrix.

After a complete investigation of the cellulose reinforcements, a procedure was developed for dispersion of the NCC fibres into a polycarbonate matrix followed by the moulding of specimen bars. The mechanical properties of the five cellulose-polycarbonate nanocomposites – for example, tensile modulus, flexural modulus and impact strength – were tested and compared to the homo-polycarbonate. The motivation for this project was to design a new material for use as strong, lightweight window substitute; an alternative to conventional residential/commercial windows and a lightweight alternative to conventional automotive glass, offering increased fuel efficiency.

Acknowledgements

I would like to express my sincerest gratitude to Dr. Leonardo C. Simon, my supervisor, for all his assistance, guidance and supervision through my graduate research.

I would like to thank Dr. Ting Tsui and Dr. Aiping Yu, my thesis committee members, for accepting to be readers of my thesis, and for all their help and guidance.

I would also like to thank all my friends and colleagues especially Dr. Ravindra Reddy, Dr. Sang-Young Anthony Shin, Yongseong Kim, Dr. Muhammad Arif, Diogenes Vedoy, Ben Lehtovaara, Graeme Marshman and Ralph Dickout for all their valuable assistance through the experimentation and writing of my thesis.

Dedications

I would like to dedicate this thesis to my parents, Christopher and Susan Finkle for all their love and support throughout this stage of my life, I would never have accomplished this without you.

Table of Contents

List of Figures

List of Tables

Chapter 1 – Introduction

1.1 – Motivation and Objective

Plastics have increased in popularity for consumer end-use products, such as automobile components, because of attributes like ease of processing, low density relative to glass and metals, and little degradation (no corrosion) over time. The desire for materials with such attributes, and other attributes like thermal, electrical, and mechanical properties, has created a demand for polymer composite research and design. Designing new polymer-based composite materials, like nanocomposites, as well as new polymer processing methods, are necessary steps to reduce costs and other resources required to manufacture consumer goods, as well as to introduce new and innovative applications to the market. Polymer nanocomposites are emerging as new contenders because in some cases their properties are proven to be far superior to pure, homogeneous polymers, polymer blends and even traditional polymer composites with micro-scale fillers. This thesis will focus on the material design, processing, and characterization of a novel polycarbonate (PC) based nanocomposite with nanocrystalline cellulose (NCC) as a reinforcing agent. This is a novel material, since at this moment there is no literature available for high-temperature processing and little available for other NCC-polymer composites. The processing methods and its properties are not well understood yet. It is expected that the NCC would improve mechanical properties and scratch resistance while maintaining a good amount of the polycarbonate's transparency.

The automotive industry is very strong in Canada. In the past 10 years the province of Ontario has ranked among the top jurisdictions in North America on the number vehicles assembled every year. Ontario, Michigan and Ohio are the largest automotive manufacturers in the world. A continuing trend in the automobile manufacturing industry is the reduction of weight of different components of vehicles, resulting in improved fuel economy. An approach materials engineers have taken in weight reduction is the replacement of heavier metal and glass vehicle components with plastics or polymer-based materials, such as composites. This can lead to a component weight reduction of 40% or more in some components, with about 15% expected in glazing applications, seen in Figure 1.1 [Smock 2010]. Historically, these automotive polymer composite materials contained synthetic additives like talc, glass fibres, Kevlar, and carbon fibres with loadings of 30-70% by volume [Bolton 1995]. This filler loading is done mainly to reduce the volume of costly polymer required, while maintaining the physical properties such as stiffness, impact resistance, bending strength, and tensile strength of the material by incorporating less-expensive filler materials in the place of polymer. Using polymers, manufacturers can also decrease tooling investment up to 70% over a metal alternative.

Polycarbonate is a frontrunner among transparent polymers, on the verge of penetrating a large portion of the auto-glass and glazing market. Manufacturers such as Bugatti and Ford, among their competition, are designing vehicle models equipped with polycarbonate sunroofs, side windows, and car tops [Smith 2010, Vink 2010]. One downside polycarbonate has over traditional silica glass windows is that it can be easily scratched, which is a significant problem on personal vehicles, whose windows' lifetime expectancy would be greater than 10 years.
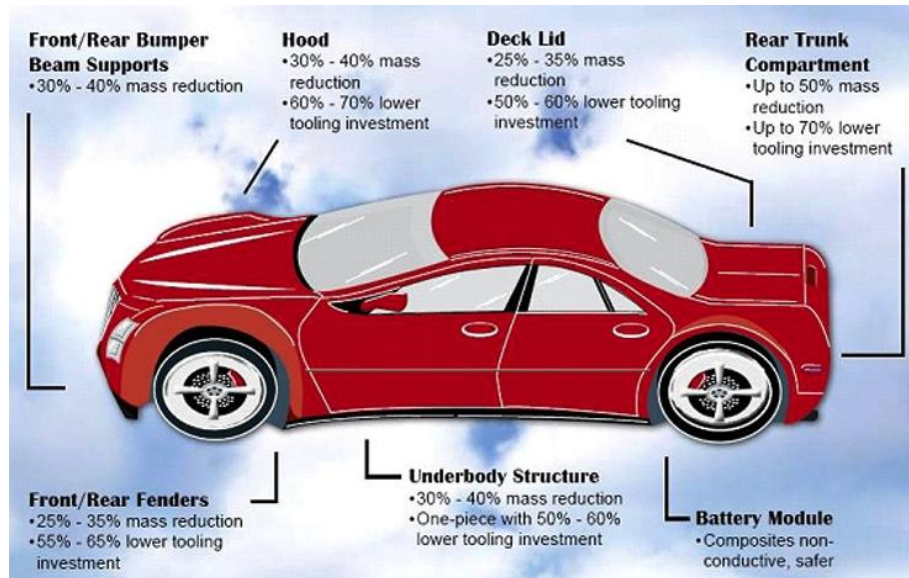
Figure 1.1 – Weight reduction available in a typical midsize vehicle by component

Another industry with a very Canadian identity is the forestry industry. As a commodity industry, it has suffered tremendously with low lumber prices. It has been hit very hard because of the recent recession and the collapse of housing market in North America. The forestry industry in Canada is looking for new, innovative uses of their vast forestry resource due to the recent decrease in demand for lumber, pulp and paper. Some of the causes behind the decrease in demand for lumber, pulp and paper are falling newsprint capacity, US housing market downturn, building and packaging moving to plastics, and information moving from paper to digital storage. Several initiatives in Canada and around the world are exploring the manufacturing of nanocrystalline cellulose from forestry or agricultural feedstock. This is a nanomaterial that is getting a lot of attention in both the polymer nanocomposite field and the automotive sector [Hubbe 2005, Leão 2011]. The nanocrystalline cellulose is abbreviated as NCC. NCC is a potentially higher-value material for the forestry industry to now profit from if novel applications can be developed [Klem 2006].

NCC is created by refining and purifying natural fibres to a purely cellulose material. Cellulose is a crystalline material present in the primary cell wall of a plant. The main responsibilities of cellulose are to protect the cell and provide strength to the plant stem. The crystalline cellulose fibres are held together in the plant by amorphous or semi-crystalline materials, lignin and hemicellulose. As the lignin and hemicellulose are removed by chemical,

3

enzymatic or physical means, cellulose remains in the form of nanofibrils, approximately 20 nm in diameter and 200 nm in length [Chakraborty 2005, Bondeson 2006, Janardhnan 2006]. Being at the nano-scale, these NCC particles would appear transparent if dispersed well in solution or polymer, a definite advantage when considering transparent applications. Also with successful dispersion, improved reinforcing properties should also be realized, repurposing the load-bearing portion of a plant or tree into a polymer reinforcement [Bledzki 1999].

The purpose of this thesis was to document the validation process of a new material that demonstrates the effective dispersal of nanocrystalline cellulose within a polycarbonate matrix for use as a strong, lightweight window substitute. The composites developed herein, provide a high strength material as an alternative to conventional residential/commercial windows and a lightweight alternative to conventional automotive glass, thereby resulting in increased fuel efficiency. The finished product is a demonstration of the ability to successfully disperse 4 different sources of nanocrystalline cellulose into a polycarbonate matrix, while demonstrating a level of optical transparency sufficient for automotive glazing. The four different sources are: NCC-FP, from FP Innovations in Quebec, Canada; NCC-Alb, from Alberta Innovates in Alberta, Canada; and MF 40-10 and UFC-100 from JRS Inc. in Germany.

When nanocrystalline cellulose is to be used as reinforcing material in a polymer nanocomposite, special attention should be paid to the thermal degradation of this organic material, as it is much lower than typical inorganic counterparts. This problem was apparent throughout previous research, a preliminary project set out to overcome the proper dispersion of nanocrystalline cellulose from FP Innovations within a polycarbonate matrix for application as an automotive window alternative. The team achieved success in the dispersion of the NCC, creating a harder and stronger material, but ran into issues with thermal degradation of the cellulose. As the processing temperature of polycarbonate was 300°C, degradation of the NCC was observed as browning in colour in the final nanocomposite. [Finkle 2010]

The molten processing of thermoplastics is a required processing step to make the desired final shape. When NCC is added to the formulation of a thermoplastic, the processing temperature and time may cause the NCC to degrade. Transparency is a critical parameter when designing a window replacement, thus it is imperative to understand what is causing the

degradation and see if there are any changes that can be done to reduce it. This can be achieved by determining the kinetic parameters of the thermal degradation of NCC. In the case of the NCC-polycarbonate (NCC-PC) nanocomposite, quantifying the kinetics of cellulose degradation hints at some process improvements, by determining the onset of degradation and the activation energies of burning in air and nitrogen.

The NCC-PC nanocomposites were prepared and characterized for each of the NCC sources. The strategy used for preparation of the nanocomposites included dispersion of NCC and PC in a solvent, drying, mixing with PC in an extruder, and compression moulding. The properties were measured and compared with the pure polycarbonate. The mechanical tests completed were flexural, tensile, and impact resistance testing. The thermal properties were investigated with thermogravimetric analysis (TGA) and differential scanning calorimeter (DSC). The optical properties were investigated in the visible spectrum (transparency). The surface chemical properties were investigated by Fourier transform infrared (FTIR). The morphology was determined through scanning electron microscopy (SEM). The characterization of this new material provided valuable information to better understanding its use as a window replacement, address any issues discovered during experimentation, possibly give unforeseen application, and give future project direction.

1.2 – Thesis Layout

The overall layout of this thesis is presented in Figure 1.2. This graphic layout brings together the relevant sections of this document, thus allowing the reader to quickly grasp the nature of this research work, its scope, materials and methodology. The graphic also gives quick reference to the section numbers of the content.

Chapter 2 – Literature Review: This chapter covers relevant background information from literature that should be sufficient to understand the study of the design of Nanocrystalline Cellulose-Polycarbonate nanocomposites. Specifically, the idea of a nanocomposite is introduced and each component phase is carefully defined to help the reader understand how they can come together to create a new material with desired properties. Also in this section, the characterization techniques to be used to study the properties of polycarbonate,

nanocrystalline cellulose, and the NCC-PC nanocomposites are introduced, including any important theoretical background. The different processing techniques for polycarbonate and the NCC-PC nanocomposite are discussed.

Chapter 3 – Materials: This chapter covers all of the polycarbonate and cellulose sources used in the preparation and design of the nanocomposites including supplier and any known properties.

Chapter 4 – Methodology: This chapter covers in detail, the procedural specifics of the polymer processing and each characterization technique used to classify the properties of polycarbonate, nanocrystalline cellulose, and the NCC-PC composite materials.

Chapter 5 – Results and Discussion: The results of the preparation and the characterization processes are presented. A discussion of the data and results are presented, including justifications, theoretical calculations and other references to the literature. This chapter should help the reader accomplish a good understanding of the benefits of the NCC-PC nanocomposite material.

Chapter 6 – Conclusions: This final chapter will summarize the main conclusions addressed by this study, how they can contribute to scientific literature, and address any work or direction that the study should take in the future.
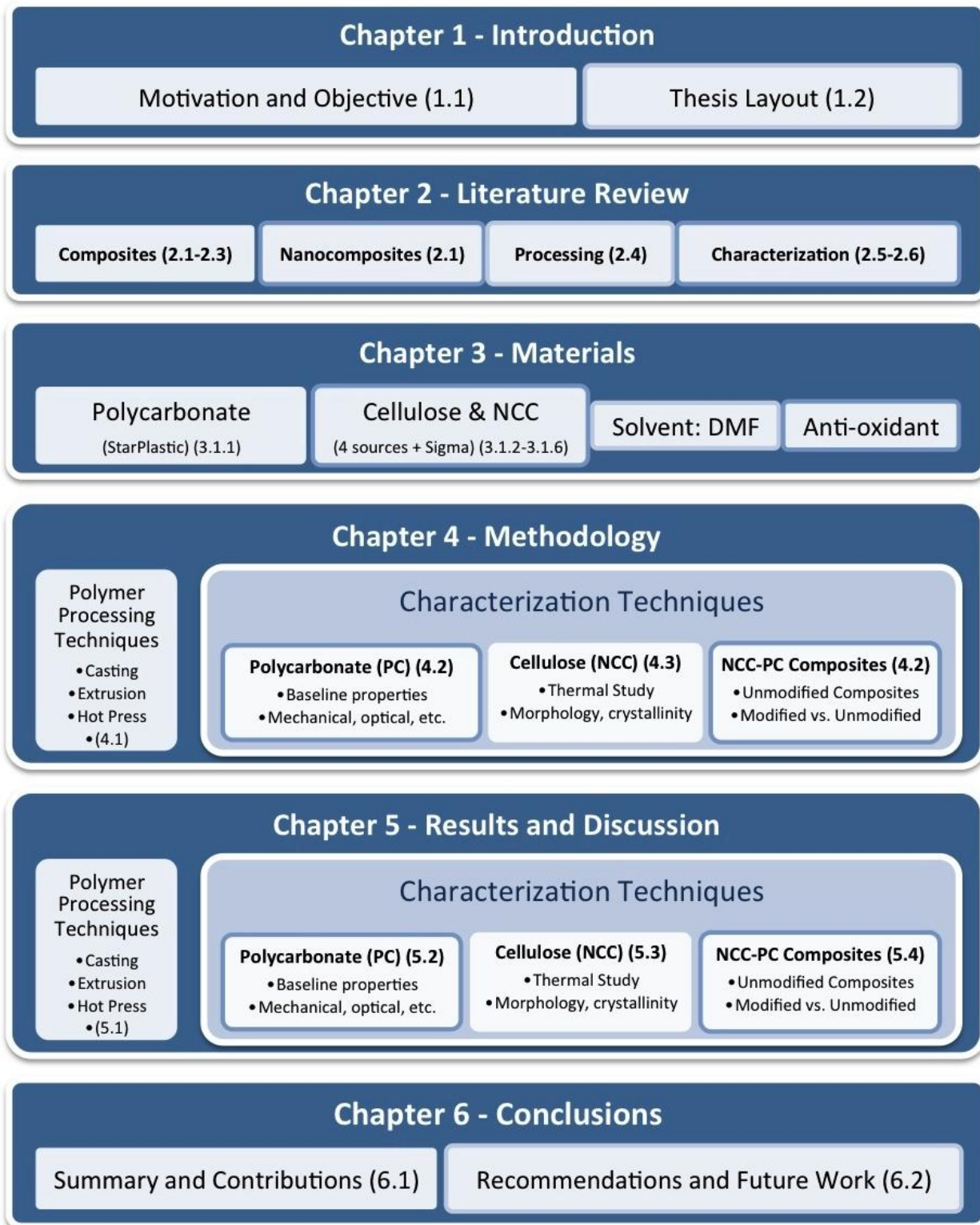
Figure 1.2 – Flow diagram showing layout of this thesis including section references

Chapter 2 – Literature Review

2.1 – Polymer Composites Overview

A composite is a multiphase material with significant proportions of each phase. The different phases can consist of metals, ceramics and/or polymers. A typical reinforced or filled polymer composite would consist of two component phases: a continuous polymer phase called the matrix; and a dispersed particulate or networked phase called the filler or reinforcement, this concept is depicted in Figure 2.1. The motivation for designing a polymer composite is to obtain properties that are not possible from each of the phases alone, such as chemical properties, physical properties or cost. A common commercial example of a polymer composite is a glass-reinforced plastic, which uses short glass fibres in some plastic matrix. Glass-fibre reinforced composites (FGRC) combine the best properties of each of its components: strength from the glass fibres and toughness and processability from the polymer. By combining the different phases, properties behave different; the result is a material superior to either of the phases on their own. Additional additives that are typically present in a composite material are anti-oxidants, plasticizers, stabilizers, flame-retardants, colorants or pigments - these also help provide specific characteristics to the composite but will not be directly addressed in this thesis.
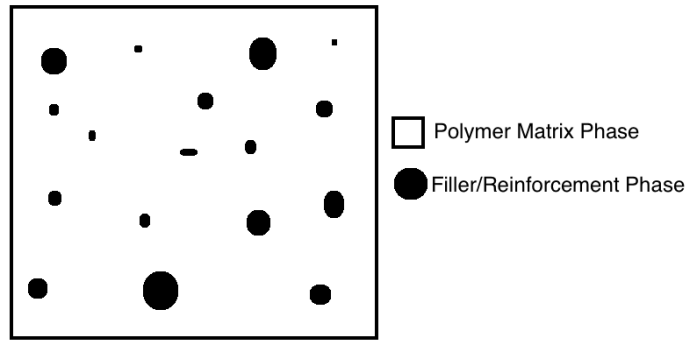
Figure 2.1 – Simple diagram of a two-phase polymer composite material

Thermoplastics are polymers that soften when the temperature is increased, thus allowing easy processing. The polymer softens because the polymer melts (like in polyethylene) or because the temperature is raised above the glass transition (like in polystyrene). In thermoplastic composites the processing happens by increasing the temperature and melting the matrix, without melting or softening of the dispersed phase. Thermoplastics have relatively low melting temperature as compared to metals or glasses, thus the manufacturing costs can be lower. The role of the polymer matrix in a composite is to comprise a majority of the material's volume, yet transfer a good portion of the stresses to other stronger reinforcement phases of the material. The polymer matrix holds the reinforcements in place and also acts as a barrier to protect the reinforcing phases from environmental effects and damage.   A composite's matrix can be comprised of other materials such as ceramics or metals, but the primary focus in this thesis is on thermoplastic-based composites, in particular polycarbonate.

The dispersed filler enhances the inherent properties of the matrix. In a polymer composite, this is often seen as an increase in elastic modulus, uniaxial stress, tensile strength, flexural strength, creep resist, and density, to name a few attributes. The filler strengthens the polymer by restricting chain mobility, but is typically used as a volume replacement, providing stability and reducing costs. Reinforcements, as a specific type of filler, are used to improve strength and stiffness of the polymer by absorbing a good portion of the applied stresses because of a high aspect ratio. Good interfacial bonding between the polymer and reinforcement within the composite and complete dispersion of the fibre reinforcements is essential in achieving the optimal enhanced properties, maximizing transfer of stress.

If the matrix is intimately bonded to the reinforcing fibres the strain of both the matrix and the fibres should be the same, this is called isostrain. This condition is held true even if the elastic moduli of each composite component are quite different, in fact, this condition holds true for most material properties giving a nice equation to predict composite properties based on those the individual components. This equation assumes linearly oriented fibres within the matrix. This relationship for composite material properties, X_c, is expressed in Equation 2.1.

$$X_c = v_m X_m + v_f X_f \hspace{4cm} \textit{(Equation 2.1)}$$

Where X can represent elastic modulus, E_e; diffusivity, D, thermal conductivity, k; or electrical conductivity, σ; and v represents the volume fraction of the matrix (m) and reinforcing fibres (f). A multiplying factor for the $v_f X_f$ term of 3/8 can be used for a uniform statistical planar distribution of the reinforcing fibres or 1/6 for a uniform statistical three-dimensional distribution. The derivation of Equation 2.1 can be found in the text, "Principles of Polymer Composites" by Alexander Berlin [Berlin 1985].

There are a number of complications when dealing with polymer composites that should be outlined and considered herein. Attention should be given to these five possible factors that will result in a less than ideal polymer composite:

1. A major effect of incorporation of filler within the polymer matrix is a change in the recrystallization mechanism, resulting in a much different crystallization of the composite compared to an unfilled polymer.
2. Porosity can also be formed easily through the production process, as poor wettability of the fibre by the polymer matrix, or degassing of the fibre, will create voids around the surface of the fibre; voids are initiation points for cracks and thus the strength is compromised.
3. Coefficients of thermal expansion between polymer and filler often differ by 10 times, which leads to residual stresses within the composite.
4. Shear and heat during processing must be controlled in order to minimize fibre degradation.

5. Agglomeration of the filler particles can also lead to reduced strength as the surface area between the polymer and filler is reduced, this is especially a problem when dealing with nano-scale fibres. [Berlin 1985, Gardner 2008]

2.1.1 - Nanocomposites

Nanotechnology is the emerging field of not only observing features in the nano-scale, but also controlling these features in functional engineering design. The nano-scale refers to the size-range between 1 and 100 nanometres, but this range is flexible depending on field of study and application. As a polymer materials engineer, designing nano-scale functional devices is of lesser importance than understanding the relationship between chemical structure and bulk properties of a material: the cornerstone of materials science and engineering. For example, maintaining small grain sizes on the nano-scale can significantly improve mechanical properties of the bulk material, like the yield strength [Mittal 2010].

Dispersing nanoparticles, like NCC, into a polymer matrix to add and improve electrical, thermal, and mechanical properties creates a polymer nanocomposite [Azizi 2005]. Nanoparticles have been used in the past to create more desirable attributes in materials such as unusual combinations of stiffness and toughness, among other properties. For example, carbon nanotubes can be used in a polymer nanocomposite to improve strength, conductivity, and thermal conductivity to name a few attributes [Mittal 2010]. Because this is such a new industry, this nanocomposite research has been more empirical (learning through experimentation), especially with a new material like NCC and Equation 2.1 presented earlier for material property predictions is no longer valid. A prime example of this empirical nanotechnology is automotive tires; carbon black nanoparticles have been used to reinforce the elastomeric rubber in tires long before it was understood 'why' the carbon black improved strength, toughness, and permeability to air. Now, as more resources are being focused on advanced materials, polymer nanocomposites can be better understood, and new materials can be better engineered. This thesis will contribute to the bank of knowledge being generated for NCC composites.

Materials at the nano-scale have unique surface characteristics; going from a bulk material to the nano-scale causes the surface area to volume ratio to increase exponentially. This allows for stronger interactions with the polymer matrix as the exposed surface is much greater and the

distance between the particles is decreased. As the filler particles reach the nano-scale, the proportion of atoms on the surface of the particles becomes very significant; as does the amount of interfacial material and thus surface properties will dominate. This effect is depicted in Figure 2.2; a decrease in the reinforcing particles diameter by one order of magnitude – from 10μm to 1μm – will increase the number of particles 1000 times and increase the available surface area by an order of magnitude. Decreasing from micro- to nano-scale – 1μm to 10nm particles – increases the number of particles by 1 million times and the surface area shoots up by two orders of magnitude. [Tam 2008]
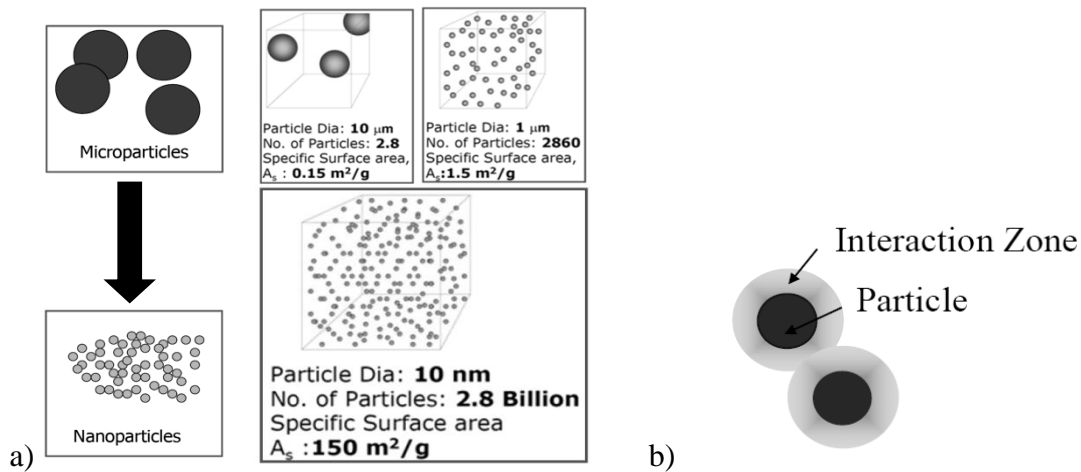
Figure 2.2 – Effect of the nano-scale on (a) number of particles and surface area and (b) the interaction zone between the filler particle and matrix

When dealing with nano-scale reinforcements, incorporation of only a few percentages by mass into the matrix is required to achieve mechanical properties that were achieved previously with greater than 30% microparticle incorporation. This effect of decreasing particle size versus the resulting elastic modulus is shown in Figure 2.3, it is seen that a much smaller concentration of nanotubes is required to achieve the same modulus as reinforcing the polypropylene with talc, about 2% and 35% respectively for an increase in modulus from 1.37 GPa to 3.5GPa. This increase in properties is once again because a good portion of the matrix located at the nanofibre interface, and conversion of bulk polymer into interfacial polymer is the key to improved property profiles.

Modulus vs Filler Type and Concentration
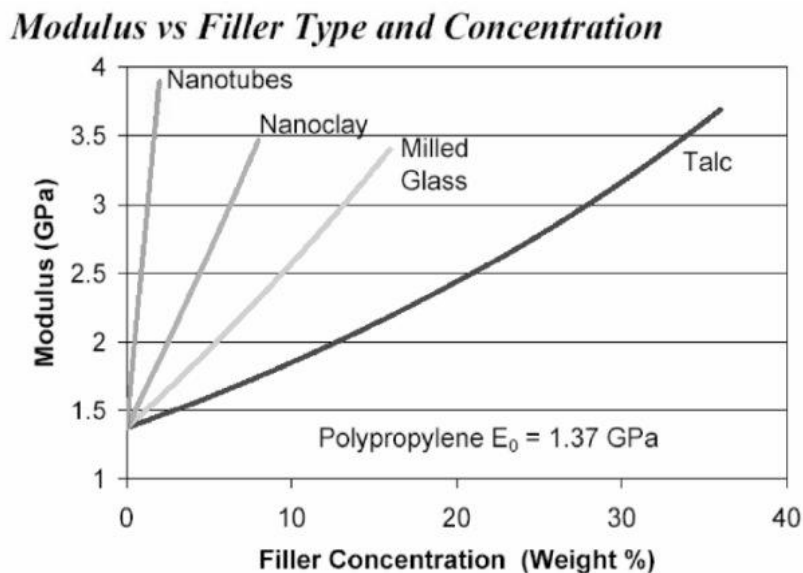
Figure 2.3 – Effect of particle size on filler concentration in polypropylene

When working with nanoparticles, it is important to consider the problems that can be faced. Nanoparticles tend to flocculate or agglomerate when dry, making it difficult to properly disperse them in the matrix with traditional mixing methods like melt-blending. This agglomeration is especially important to control in the nanocomposite being pursued in this thesis, as light transmission is particle-size dependant and to maintain the desired transparency, our particle size should remain below about 100 nm on as many dimensions as possible.

2.1.2 – Natural Fibres as Thermoplastic Reinforcements

A trend in automotive manufacturing is the use of natural fibres as the filler or reinforcing material in polymer composites. Among the driving forces are: high specific properties, utilization of renewable feedstock, lower energy for processing and aspects related to the crashworthiness of the materials. In the context of this thesis, the term natural fibre is limited to plant fibre and does not include natural inorganic fibres (like asbestos for example). Long before the natural-fibre revolution, that we are now beginning to see in the automotive sector, Henry Ford constructed a car with components made of hemp-reinforced epoxy resins [Small 2002]. The idea of using natural fibres as polymer reinforcement has been around since the 1920's, when Ford recognized the utility of hemp fibres in his vehicles. Similar to Ford in the 1920s, we too face a time of uncertainty and financial recession, requiring polymer engineers to look to

natural fibres for cost reduction by replacing expensive polymer volume with natural fibre volume in auto manufacturing. These fibres can come from a variety of natural sources, for example: saw mill waste (trees); rice husk; banana leaves and stalk; coconut husk; groundnut shell; jute fibre; rice and wheat straw; sisal fibres; seaweed; and cotton stalk [Rai 2004, Rai 2010].

In the past, plant fibres have been one of the most popular choices for use as a filler material in polymers. Wood and wood flour had been the filler of choice until about the year 2000, when industry research shifted to focus on cellulosic and lignocellulosic plant fibres; the components of the plant that have the most appropriate properties for polymer composites. These properties include low-density, non-abrasive nature, high filler loading, biodegradability, renewability and mechanical strength. Less valuable components of the plant fibres, like hemicellulose, were removed using chemical and mechanical processes. More on this will be discussed in section 2.4.1 – Plant Structure, Composition, and Biopolymerization.

Cellulosic composites have the opportunity for use in numerous automotive applications, many of which are already incorporating bio-based fibres in their construction. The 2010 C-Class Mercedes Benz incorporates more than 50 components containing natural fibers in the vehicle. Global auto production in 2009 was around 61 million vehicles, each containing approximately 26 kg of textile products of which greater than 11% is non-woven biofibres [OICA 2009]. The amount of textiles is predicted to increase to 35 kg by 2020 in a drive towards vehicle weight reduction [Bansal 2010]. The demand is increasing and the use of biofibres makes the automotive equipment less oil dependant, easier to recycle, and cheaper to make. Currently, the auto industry uses flax and hemp fibres in polymer composites to make automotive components such as storage bins, trunk linings, dashboard, pillars, rear decks, and door panels. Dr. Leonardo Simon's laboratory has recently collaborated with materials suppliers and Ford Motors Company on the development of polypropylene-wheat straw for injection moulding. This material was successfully commercialized in 2009 and introduced in the Ford Flex 2010 model year that is built in Oakville, Ontario.

As it looks, the next generation of vehicles will begin to use more refined natural fibres, like nanocrystalline cellulose, as the reinforcing agents in composite materials [Leão 2011]. A recent

realization in the automotive industry is that a stronger nanocomposite material would require a reduced volume or mass compared to the original component material. This stronger nanocomposite material would allow for automotive component redesign and miniaturization [Small 2002]. For example, Mathew of Norwegian University of Technology and Science is working with the extrusion of NCC-Poly(lactic acid) for improved mechanical properties; he observed an increase in the composite's elastic modulus from 2.0 to 2.4 GPa, an increase of nearly 20% with only 5% incorporation of NCC [Mathew 2006]. Similarly, Petersson observed an increase in tensile strength by 12% with a solution casted Microcrystalline Cellulose-PLA composite [Petersson 2006]. In 2005, researcher Yano reported the first example of an optically transparent composite with bacterial cellulose loading as high as 70%, observing mechanical properties five times that of some engineered plastics [Yano 2005].

2.2 – The Polymer Matrix: Polycarbonate (PC)

2.2.1 – Polymers and Thermoplastics

Polymers are a category of materials formed by long chains obtained by polymerization. Typical classifications of polymers based on properties are: thermoplastics, thermosets and elastomers. Thermoplastics are typically ductile or deformable material that are available for many applications in fibres, thin-films, sheets, foams, moulding, and in bulk. Intermolecular forces hold the chains together, and depending on the chain length (the molecular weight) and crosslinking networks, the polymers can have different levels of rigidity or different working temperatures.

Thermoplastics are a subcategory of polymers that can lose rigidity or be melted with increased temperature and then become rigid or crystallize again after cooling. Thermoplastics are long-chain polymers, with a high molecular weight, that have weak intermolecular bonding. As temperature is elevated, intermolecular bonds like Van der Waals forces, hydrogen bonding, or dipole-dipole interactions are broken by thermal energy allowing the polymer to flow, when heat is removed these bonds strengthen. Some common commercial thermoplastics include polyethylene, polypropylene, polystyrene, polyvinylchloride, and polycarbonate. Thermoplastics

are processed using mainly injection moulding, extrusion moulding, blow moulding, and some compression moulding.

If the bonding between the individual polymer chains is permanent or irreversible, like covalent bonding, the polymer is considered a thermoset. It is nearly impossible to melt or reform a thermoset because a cross-linking chemical bond was formed between chains, through a chemical reaction that is not easily reversible. As a result of the more permanent polymer network in a thermoset, they are typically used for temperature and flame resistant applications and are not easily recycled. Thermosets are typically processed using compression moulding and transfer moulding.

2.2.2 – Polycarbonate Properties

Polycarbonate (PC) is an engineering thermoplastic with extraordinary properties making it an ideal contender for numerous consumer end use applications. These properties include high heat tolerance, impact resistance, glass-like transparency, outstanding optical properties, excellent electrical properties, dimensional stability, ability to mould, and great colourability. There are currently over 2800 grades of polypropylene and 182 different trade names; this includes some popular choices like Calibre from LG, Lexan from Sabic, and Makralon from Bayer [Matweb].

Typical applications of polycarbonate include machine parts, propellers, and transparent emergency barriers; PC also accounted for about 2.7 billion tons of the global annual polymer production in 2005, which represented about 25% of the engineering plastics produced [Jansen 2011]. The price per pound for polycarbonate is just under \$2 with a global demand of about \$3.3 billion. Table 2.1 shows the polycarbonate market changes over a 20-year period with predictions for 2011 [Freedonia 2003]. There is also research in the area of PC composites including nanocomposites, like Multi-walled carbon nanotubes in polycarbonate [Choi 2006, Chen 2007].

Table 2.1 – Polycarbonate market demand 1992 through 2011

	Polycarbonate (PC) demand				
Item	1992	1996	2001	2006	2011
PC demand (mil lbs)	460	835	1,120	1,440	1,780
$/lb	1.56	1.64	1.6	1.72	1.84
PC demand (mil $)	718	1,369	1,790	2,480	3,280
% polycarbonate	15.9	22.1	23.9	25.2	26
Engineering plastics demand (mil lbs)	2,893	3,772	4,685	5,710	6,850

Polycarbonate is a special type of polyester based on carbonic acid. Polycarbonate's chemical structure has functional groups connected through a series of carbonate groups (-O-(C=O)-O-). In polycarbonate formed from Bisphenol A (BPA) and phosgene monomers, the polymer backbone consists of two large aromatic groups that lead to the polymers high strength, through steric hindrance limiting bending of the molecule. The repeating unit for BPA-phosgene polycarbonate can be seen in Figure 2.4.
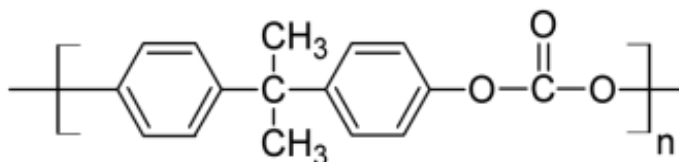
Figure 2.4 – Repeating unit of BPA-phosgene polycarbonate

The density of polycarbonate is 1.2 g/cm^3, it is about half of that of glass at 2.4 to 2.8 g/cm^3, making PC an economic choice for automotive and transportation applications, reducing the energy required to move the vehicle's load. The flexural modulus (tendency to bend) of PC is much lower than glass at 2.41 versus 18 GPa, but glass is brittle and will break with even little bending (low strain). The flexural strength (maximum stress to bend before deformation/break) is larger than glass at 89.6 MPa over 48 MPa. The impact strengths are very similar between the two materials, about 801 J/m, suggesting they have similar abilities to withstand impact, like a large object impacting a window while driving at high speed. Although it should be noted, un-notched PC can have an impact resistance 3 or 4 times higher which is more applicable to real-

world PC applications [Jansen 2011]. Table 2.2 shows some common mechanical properties for both the polycarbonate to be used in this thesis – StarPlastics PC743 Molding Grade PC - and standard silica glass [Appendix 1].

Table 2.2 – Mechanical properties of polycarbonate and silicate glass

Material	Density (g/cm^3)	Flexural Modulus (Gpa)	Flexural Strength (Mpa)	IZOD Impact Strength (J/m)
Polycarbonate	1.2	2.5	89.6	801
Silicate Glass	2.4-2.8	18	48	760

Some disadvantages of PC include poor resistance to marring, scratching, abrasion, and solvents [Ryntz 2002, Jansen 2011]. These shortcomings can be overcome with additives, stabilizers, and fillers. PC can be blended with other polymers such as ABS and thermoplastic polyesters to reduce some of these issues. The ductile to brittle transition temperature (DBTT), the temperature where above it failure is inherently ductile and below it is brittle, occurs around -10 to -20 °C for PC. This would limit some low temperature applications or geographic regions of a final window product. The DBTT can be improved with blending of other polymers or additives, but this could directly affect transparency and other desired properties. PC is typically injection moulded, but can also be compression moulded or profile extruded. [Freedonia 2003, Jansen 2011]

2.2.3 – Polycarbonate Applications

Polycarbonate, known for its temperature resistance, impact resistance, and optical properties, is a primary choice for applications such as window alternatives. Currently, the primary use PC is electronics and optical media, such as CDs, DVDs, or Blu-ray discs, with automotive applications being the second. The biggest applications for PC or reinforced PC in the automotive industry are headlamps, instrument panels, and wheel covers with glazing applications still open to be exploited. Other applications include housings for electrical equipment such as computers, printers, or cellular phones and other product and packaging. A complete breakdown of the polycarbonate demand by market can be seen in Table 2.3. Newer data was unavailable, but growth is expected over the past 5 years. [Freedonia 2003]

Table 2.3 – Breakdown of polycarbonate demand by market share from 1995 through 2006

Item	Polycarbonate demand by market (million pounds)			
	1995	1996	2001	2006
Polycarbonate demand	460	835	1,120	1,440
Electrical & electronic	140	339	437	567
Business machines	31	105	135	175
Information storage	20	120	170	230
Appliances	52	75	90	110
Other uses	37	39	42	52
Motor vehicles	61	158	260	350
Construction:	121	153	178	217
Glazing & skylights	107	135	155	187
Lighting	14	18	23	30
Consumer & institutional	101	123	167	210
Other markets	37	62	78	96

A significant difference between polycarbonate and its best contender, poly(methyl methacrylate) (PMMA), is the temperature at which the polymer begins to melt or flow. Polycarbonate is much more thermally stable than PMMA, PC has a melting point around 240℃ and PMMA has a melting point around 130℃. This opens polycarbonate up to many higher temperature applications that PMMA simply cannot fill, such as use in automobiles. A perfect example, the headlight covers in most vehicles are made out of a transparent polycarbonate; these lights can withstand the temperature fluctuations from cold winter to hot summer all while being only a few inches from a high output light bulb.

Figure 2.5 shows the open-source concept car, the c,mm,n (pronounced "common"), developed by the Netherlands Society for Nature & Environment and three Dutch universities [Tullo 2009] as well as a Ford Focus prototype spotted at the Chicago Auto Show. The windows of the vehicles are made from polycarbonate as part of an environmentally friendly design. The polycarbonate is a more environmentally friendly option because of reduced weight, improved aerodynamics, and recyclability.

Research in the area of polycarbonate composites is diverse; for example some focus now is on graphite, cellulose acetate buterate, and nano-clays [Kardos 1973, Jagadeesh 2008, Laskar 2004, Mitsunaga 2003, Nevalainen 2009, Yoon 2003].
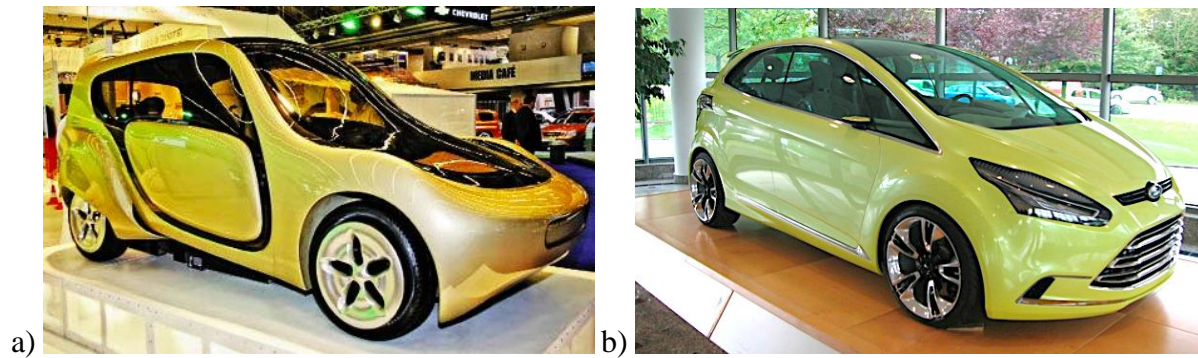
Figure 2.5 – a) Open source concept car the c,mm,n and b) Ford Focus prototype with PC windows and sunroof

2.3 – The BioFibre Reinforcement: Nanocrystalline Cellulose (NCC)

2.3.1 - Plant Structure, Composition, and Biopolymerization

With the use of Cellulose Whiskers, Cellulose Microfibrils, Cellulose Fibres, Nanocrystalline Cellulose, and other cellulose based fillers increasing rapidly in the polymer composites industry, there is a need to review the biosynthesis and microstructure in detail to aid in the understanding of its abilities as a reinforcing agent. There is also a need to clarify and define some nomenclature related to cellulose fibres, specifically the difference between cellulose fibres, microfibrils, microfibers, nanowhiskers, and nanocrystalline cellulose. To grasp the concept, it is best to give a top-down hierarchical approach to explaining the microstructure, starting with the structural molecular units up to the plant stem.

According to Muhlethaler, if the cell walls of different origin plant or tree are extracted with weak acid or alkali, random or parallel lines or textures will appear. This texture signifies the presence of non-cellulosic components like pectin, hemicellulose, and lignin between micron-scale cellulose fibrils. This is what is defined as a microfibril, the basic structural unit of a plant produced during photosynthesis, including not only cellulose, but also other natural impurities.

Different from an animal cell, a plant cell has a very strong protective wall, like a skeleton. This cell wall protects the nucleus from osmosis, external mechanical forces, and pathogens. Cell walls are categorized into primary and secondary cell walls. The primary cell wall is responsible for dividing and rapidly growing cells; its thickness remains constant but can increase in surface area several fold during growth. After growing, thickening of the secondary cell wall moves the

thinner primary wall close to the surface of the cell. Primary and secondary cell walls differ in chemical composition and structure, with the secondary cell walls being responsible for the mechanical strength; this is also where the industrial properties of these plant materials are determined. Twenty to thirty weight percentage of the dry mass in primary cell wall is cellulose and in the secondary cell wall this can increases to 90-95%. [Tarchevsky 1991]

Cell wall polysaccharides, polymeric carbohydrate polymers connected via glucosidic bonds, differ significantly in composition. Cellulose and callose contain glucose residues only whereas hemicellulose and pectic substances are heteropolysaccharides. These heteropolysaccharides contain hexoses, pentoses, and uronic acids. Due to the difference in composition, cellulose and callose are typically very linear whereas the hemicellulose and pectic substances are very branched polymers. Component monomers in cellulose are in the thousands but only 10s and 100s for the branched polysaccharides like hemicellulose and pectin. Cellulose's linear primary structure allows ordered supermolecular structure, found in the microfibrils via hydrogen bonding. Cellulose is important in a plant's cell wall, not only for its strong protection of the nucleus, but also because it forms the framework for other components of the plant to be deposited. [Tarchevsky 1991]

α-Cellulose is what remains after the removal of amorphous components (heteropolysaccharides), and consists of linear chains of β-(1,4) glucose. An oxygen bridge between carbons 1 and 5 connects these glucose rings, and when two glucose rings condense they form a cellobiose molecular structure. The hydroxyl groups of carbons 2, 3, and 4 are free to form hydrogen bonds with the hydroxyl moieties of the adjacent chains; this gives the superstructure considerable lateral order. Cellulose biopolymerization happens on the cell wall until there are approximately 3000-10000 structural units, variation depending on source, giving an overall molecular length of about 1.5 to 5μm. Figure 2.6 shows a section of a cellulose molecule with visible β-(1,4)-D-glucosidic bonds as well as the hydrogen bonding arrangement of α-cellulose [Chakraborty 2006]
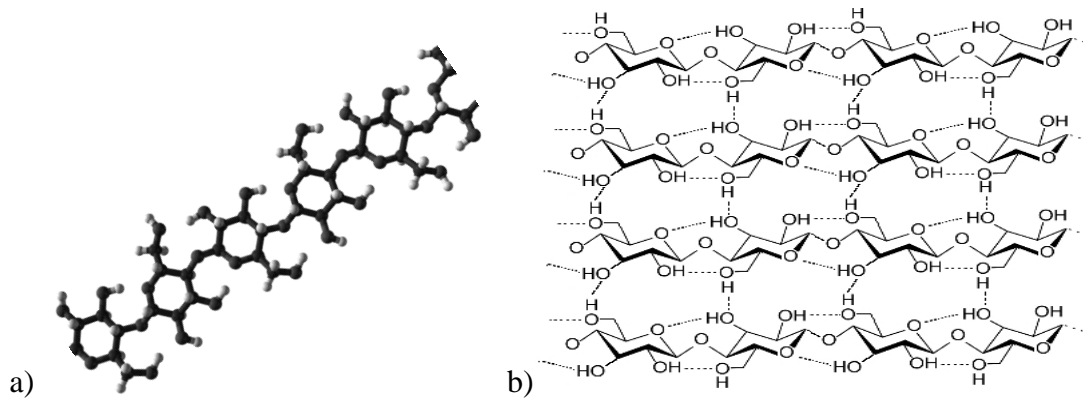
Figure 2.6 – a) segment of a single cellulose chain and b) the hydrogen bonding between multiple cellulose chains

The chain length of cellobiose is 1.03nm and they are separated from each other laterally by 0.83nm. The accepted crystalline elementary cell is monoclinic with a=0.83nm, b=1.03nm, c=0.79nm, and β=84°. The adjacent hydroxyl groups are only 0.25nm away from each other, confirming evidence of hydrogen bonding. The hierarchical structure down to the elementary cell can be seen in Figure 2.7. [Chakraborty 2006, Wang 2007]

In a higher plant (vascular plant), cellulose is polymerized at the plasma membrane at the surface of the plant cell by the rosette terminal complex (RTC) made of many cellulose synthase (CS) complexes. From the moment of synthesis, the cellulose does not only exist as a single glucosidic chain, but part of a composite of many chains, the elementary fibril. In the primary cell wall of plants, the elementary fibril is a microfibril of about 36 chains, but will vary depending on source and organism. The cellulose is catalysed at the plasma membrane by a cellulose synthase complex. Each complex is capable of producing one glucan chain via one synthetic subunit and one catalytic subunit. A cellulose synthase complex is expected to contain around 36 glucan chain producing units in a 25nm hexameric structure.

Each of the catalytic subunits accepts the substrate which is an activated form of glucose, it is assumed by plant biologists to be UDP-glucose. This UDP-glucose can come from the cytoplasm or may be donated from a membrane-associated form of sucrose synthase. The growing membranes are secreted through the membrane via a pore and a protein may assist the crystallization into α-cellulose configuration. It is very likely that the RTC contains many additional regulatory subunits, but they have been omitted here for simplicity. For more details

on the biosynthesis a great collection of articles to start with is "Cellulose: Molecular and Structural Biology; selected articles on synthesis, structure, and applications of cellulose," edited by M. Brown Jr. and I. Saxena [Brown 2007].

In bacterial cellulose, the complexes remain stationary and the cell is projected backwards in the medium in which the polymerization is occurring. In algae and higher plants, it is strongly believed that the complex moves through the fluid mosaic membrane and the direction of movement directs the pattern of the deposited cellulose. There is a series of microtubules that are adjacent or connected to the complexes that guides the complex. [Delmer 1995]

Several cellobiose groups from different cellulose chains together will form long thin crystallites called elementary fibrils or micelles. These sections are highly crystalline along the length with no segmentation by amorphous material discovered for ~37 molecules in one elementary fibril. The widths of these fibrils are on the order of 2 to 10 nm in width with a rectangular cross section similar to a ruler's edge. A cellulose molecule will have alternating regions of elementary fibrils, or crystalline domains, showing that the length of the crystal section is smaller than the length of the cellulose molecule. Each crystalline region contains about 120 glucose monomers, or 60 cellobiose structural units, resulting in about 60 nm in length of elementary fibre. Depending on the source, this crystallite can increase up to about 180 or 200 nm in length. A 'zero-defect' region, like the elementary fibril, is what 'cellulose whisker' refers to in literature, it has also been named cellulose nanowhisker in composite science. [Chakraborty 2006]
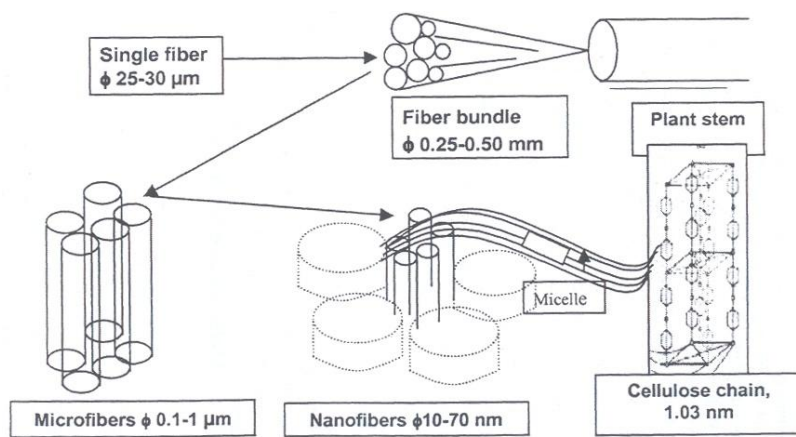
Figure 2.7 – Hierarchical structure of cellulose to fibre bundle

About 20 elementary fibrils or cellulose whiskers will configure itself into a microfibril, the texturized surface observed by Muhlethaler. The width of the microfibrils can be anywhere from 3 to 38 nm wide, but typically between 5 and 10 nm for wood sources. A scanning electron microscopy (SEM) micrograph shows that the microfibrils are actually composed of small rectangular units about 3 by 10 nm across. This is an elementary fibril, a structural subunit of the microfibril. Clowes and Juniper have also stated that thin cellulose threads, 8 by 30 nm in diameter and up to 5 μm in length, are comprised of several elementary fibrils and forms the skeleton of higher plants. A commonly considered configuration of the microfibril structure is that of a flat ribbon; with one dimension four times the other. It consists of several totally crystalline elementary fibrils, with loose glucose chains forming a paracrystalline region, and linkages may form between the outer surface of the microfibril and non-cellulosic polysaccharides, like lignin. Another less accepted hypothesis for the structure of the microfibril is that of a helical structure of elementary fibrils. [Chakraborty 2006]

An elementary fibril, or whisker, can have an aspect ratio of 20 to 70 depending on the source and length of the elementary fibril. Nanocrystalline cellulose typically is reported to have a length around 200 nm, much larger than the typically reported 60. Thus, it is expected that NCC refers to elementary fibrils on the higher end of the aspect ratio scale, i.e. closer to 70 and will vary with source. [Chakraborty 2006]

2.3.2 - Nanocrystalline Cellulose

This section on nanocrystalline cellulose will serve as an overview and brief history of the material, including its chemical structure as well as techniques for isolating the nanofibres, which will help in understanding the degradation mechanisms.

Nanocrystalline cellulose is a very new and innovative use for wood pulp, developed by Canadian researchers in association with the forestry industry of Canada. It is an unconventional nanomaterial with certain properties matching and exceeding that of current standard nanomaterials such as carbon nanotubes. Nanocrystalline cellulose has very unique optical, electrical, magnetic and strength properties. Some other inherent properties of the NCC fibres, which will prove beneficial, are that they are sustainable, biodegradable, non-toxic, and fully recyclable.

A typical nanocrystalline cellulose fibril is about 200 nm long and 10 nm wide and consists of a small bundle of the cellulose strands tightly bound together. Table 2.4 shows a comparison in sizes and the resulting surface area increase of 6000 times of NCC over traditional pulp fillers, which are also primarily cellulose based [FP 2008].

Table 2.4 – Comparison of the cellulosic dimensions of NCC and pulp

Dimension	Nanocrystalline Cellulose	Pulp
Fibre Length	200 nm	1.5m
Fibre Diameter	10 nm	30μm
Surface Area (Relative)	6000	1

Cellulose is naturally strong as its main function in nature is to provide strength and protection to the cell wall of a living plant. These inherent strengths, through hydrogen bonding, also make the isolation of individual nano-sized fibres quite difficult. It is reported that the tensile strength of typical Cellulose Nano Whiskers (CNWs) is about 10000 MPa with an elastic modulus of 150-250 GPa [Mathew 2006]. A whisker is classified as having an aspect ratio of approximately 20-60, whereas NCC often has an aspect ratio greater than 100.

Table 2.5 includes some potential, future applications for nanocrystalline cellulose [FP 2008].

Table 2.5 – Potential applications for Nanocrystalline Cellulose

NCC Applications
Reinforced polymers
High-strength spun fibers and textiles
Advanced composite materials
Films for better barrier and other properties
Additive for coatings, paints, lacquers & adhesives
Switchable optical devices
Pharmaceuticals and drug delivery
Bone replacement and teeth repair
Improved paper, packaging and building products
Additive for foods, cosmetics
Aerospace and transportation

Most of the research into NCC composites has been very recent, with most development happening after the year 2000. Dispersing microfibril cellulose into organic polymer composites for improved properties has been practiced for a few decades [Zadorecki 1989, Orts 2005]. As processing techniques for NCC were improved their applicability as a reinforcing agent with superior mechanical properties was quickly discovered [Nakagaito 2003, Nakagaito 2004, Nakagaito 2008]. Various matrices have been studied with a nanocrystalline cellulose source including poly(lactic acid) [Oksman 2006, Kvien 2007, Iwatake 2008, Ping 2009, Pandey 2009], polyurethane [Ozgurseydibeyoglu 2008], polyolefins [Soulestin 2007], and even an all-cellulose composite [Nishino 2004, Pullwan 2010].

2.3.3 - Isolation of Nanocrystalline Cellulose Fibres

As seen earlier in the chapter, the cellulosic macrostructure is held together by many hydrogen bonds requiring intensive processing methods to liberate the nanofibres. This has been a major challenge for researchers to find efficient ways to isolate the cellulosic fibrils from their source materials. Some specific examples of source materials are wood, agricultural residues, seaweed, and bacterial cellulose. There are a number of approaches being taken to free the nanocrystalline cellulose, which include chemical delignification, mechanical diminution, chemical diminution, and dissolution or different combinations of them. This section will provide a brief summary of these methods being investigated in research, and techniques likely used by the NCC manufacturers presented in this study.

The NCC isolation background is being included to give a full understanding of the material that is being tested for composite applications and what possible size distributions and impurities may be present. The size of the cellulosic bundles is a direct function of the processing that the original wood material undergoes. Understanding the processing may also indicate what impurities may be present and could affect the final properties of the composite.

Lignin is an amorphous region within the plant structure that holds the crystalline regions of cellulose together. Therefore, a first step in the liberation of NCC is the delignification process to separate the crystalline from amorphous regions of the plant. A common technique used in the pulp and paper industry is the Kraft Process, which removes the lignin from cellulose for papermaking applications. Wood chips are introduced to high pressures and a hot solution of

26

NaOH and Na₂S and the lignin component is progressively depolymerised, substituted and solubilised away. The pressure chamber, or digester, drops pressure rapidly and the fibrils further isolate themselves from each other. The resulting fibres are a tan-yellow in colour and must undergo a final bleaching to remove the final few percentage of non-crystalline material through oxidization of the lignin [Nakagaito 2004b, Bai 2009].

Mechanical diminution involves taking Kraft processed fibrils and refining further into nanofibrils. Passing fibril bundles in solution through rotating and stationary discs that have raised cones or bars separated by grove spaces to pulverize the bundles does this. This method, seen in Figure 2.8, requires very energy intensive processing and reports suggest that multiple passes (16 to 30 times) through the refiner are required to achieve dimensions on the nano-scale [Lima 2004]. Other mechanical diminution techniques used in research are passing microcrystalline cellulose bundles through a small nozzle at very high pressures or high intensity ultrasonic treatments [Lima 2004, Chakraborty 2005, Iwamoto 2007]. Cryocrushing is also a new method for liberating NCC fibres; liquid swollen cellulose crystals are immersed in liquid nitrogen and the crushed with a mortar and pestle. Intense cold makes the bundles brittle and mechanical force is used to break them apart [Morán 2008].
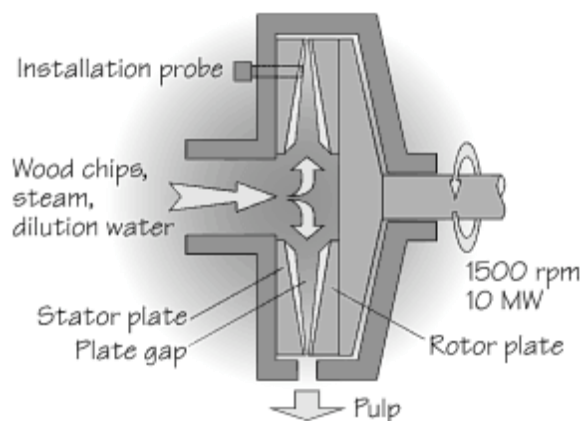
Figure 2.8 – Simple diagram of a refiner typically used in pulping

Chemical diminution includes acid hydrolysis and enzymatic treatment. One of these treatments is almost always used as a follow up procedure for the mechanical diminution processes described above. Acid hydrolysis works by breaking down the amorphous cellulose

with a strong acid and enzymatic treatment works by the selective attack by cellulase enzymes on the amorphous regions of the cellulose [Janardhnan 2006].

Canadian researchers at FP Innovations, Alberta Innovates, and BioVision have discovered economical processes for producing large quantities of nanocrystalline cellulose (NCC) and plan to reach a multi-ton per day facility within the year [Domtar 2010, Tetreau 2010, Biovision 2010]. The Canadian forestry industry believes that Nanocrystalline Cellulose will be a cost-effective nanoparticle available from an abundant renewable resource.

2.4 – Polymer and Nanocomposite Processing Background

2.4.1 – Solution Casting

Solution casting is a technique that can be used to make a polymer composite material. It is particularly effective at making well-dispersed nanocomposites. Solution casting works by dispersing or dissolving the different composite phases separately into a common miscible solvent, mixing the two dispersions or solutions, and then evapourating away the solvent. When the solvent is removed, the resulting composite is left in the form of a cake or thin film. When making the dispersions or solutions, it is helpful to use heat, stirring or ultrasonication to aid the mixing of the solute or dispersant with the solvent. A good dispersion will have avoided any aggregation or flocculation of the nanoparticles, maximizing the potential final properties. [Bhatnagar 2005]

If the resulting material is a powder or cake, the powder containing the nanoparticles and the thermoplastic can then be further melt-compounded with other polymers, additives or fibres via extrusion. Another option is to make a 'master batch' of composite material that contains a higher than desired concentration of the nanoparticle reinforcement, later in melt compounding, diluting the nanoparticle concentration to the desired level with additional polymer. Solution casting is feasible at the lab or bench-scale, but scaling up would require large amounts of solvent and may not be economically feasible. Figure 2.9 depicts the solution casting technique.

both A & B in solvent X   +heat/vac to remove X

Polymer A   Reinforcement B   Composite A/B
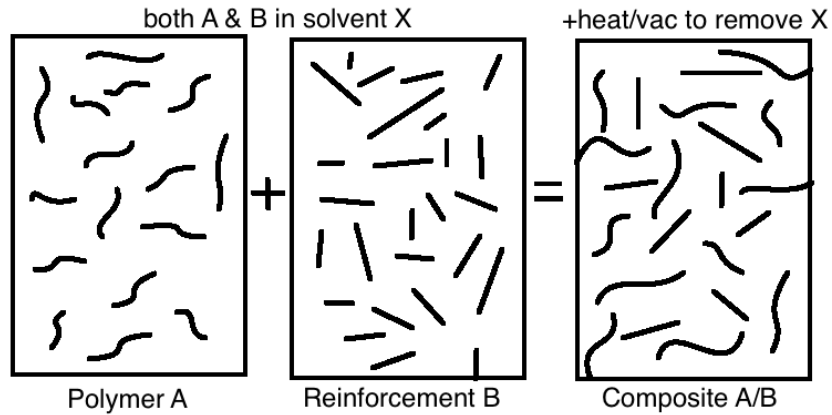
Figure 2.9 – Diagram depicting solution casting technique

2.4.2 – Melt-Compounding

Melt-compounding is a common industrial polymer processing technique. Melt-compounding mixes the reinforcement with the polymer matrix using an extruder. The twin-extruder has two heated screws that run in parallel, and apply shear force to mix the reinforcements into the molten polymer matrix. The co-rotating twin-screws are tapered and force the molten composite material through a small die after mixing. The molten string of polymer hardens and is cut into small polymer composite resin beads to be further processed. Figure 2.10 shows a bench-top twin-screw extruder with two-co-rotating screws that process the polymer through a small die.

a)   b)
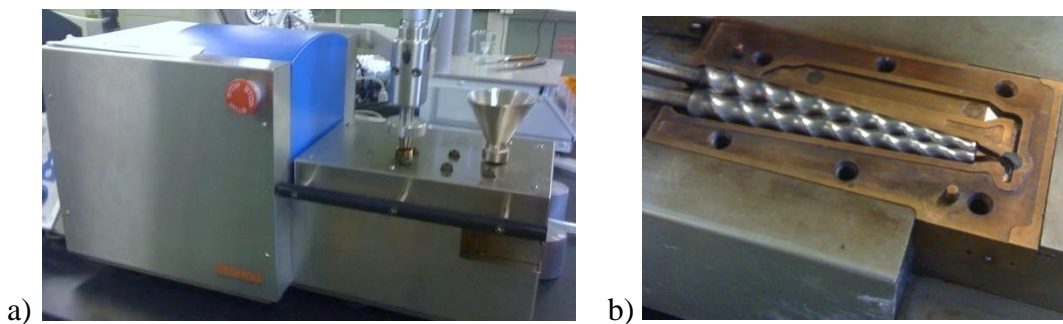
Figure 2.10 – a) Bench-top twin-screw extruder with b) co-rotating twin screws and die

This technique is not as effective at dispersing nanoparticles as it applies micro- and macro-scale shear. This leaves flocculations of the nanoparticles, which are usually added dry. This is why solution casting was chosen as an ideal first mixing technique. A solution casted batch of

nanocomposite can be processed with the extruder to melt the powder into a mouldable resin. [Nevalainen 2009]

2.4.3 – Compression Moulding

Compression moulding works by applying heat and pressure to a polymer or composite filled mould via the two large parallel plates of a hot press to form the polymer into a desired shape. The plates are heated above the melting point of the polymer and can be compressed to high pressures to aid formation. Compression moulding is a common industrial processing technique that can be easily scaled to process polymers or polymer composites in the lab and factory environment. This technique is how the material specimens are fabricated for further property testing from the extruded resin beads. Figure 2.11 depicts a standard bench-top parallel plate hot press, which can be used for compression moulding of polymer specimens.

Figure 2.11 – Parallel plate hot press

2.5 – Polymer and Nanocomposite Characterization Background

Engineering design in all disciplines requires understanding of material properties. This includes, but is not limited to: mechanical properties; thermal properties; processing properties; hygroscopic properties; and chemical structure properties. In this section, the characterization techniques used to study the properties of polycarbonate and the NCC-PC composite materials, synthesized using methods outlined in Section 2.4 will be introduced. This will include important theoretical background to gather a general understanding of the characterization techniques used herein.

Since the pure polycarbonate and the NCC-PC nanocomposites are of similar polymer morphology, they will be characterized in the same fashion. This characterization will cover: mechanical tests including tensile, flexural, and impact testing; thermal testing including DSC for glass transition and TGA for thermal stability; processing property tests including MFI for melt flow index; and chemical spectrum tests including FTIR spectroscopy for composition and UV-Vis spectroscopy for transparency.

2.5.1 – Mechanical Properties

Mechanical testing of the polycarbonate and NCC-PC composite materials will focus on the tensile, flexural, and impact testing that is typical when classifying a new material. The mechanical properties of the material are determined by numerous factors in the natural or synthetic design. This includes the materials structure at macro-, milli-, micro-, nano-, molecular, and atomic length scales, although shorter length scales will often have the greatest effects on the bulk material properties. Successful design of a material requires understanding of the structural considerations of that material, and how this translates to macro-scale or bulk properties. That being said, it is often not possible to predict the materials bulk properties from the sub-structure. Empirical data is collected using various techniques, including tensile, flexural and impact testing, and correlations are drawn between structure and properties. The techniques introduced here follow ASTM (American Society for Testing And Materials) technical standards D638 for the tensile testing of polymers, D1708 for the microtensile testing of polymers, and D256 for the impact resistance testing of polymers; these methods are transferrable to most solid materials.

The tensile properties of unreinforced and reinforced plastics are measured by the deformation of dog-bone shaped specimens under constant pulling speed. The dog-bone shaped specimens have a three-dimensional body, *a* x *b* x *c*, separating two larger grip-heads. The heads of the dog-bone specimens are gripped at each end, one fixed and one moves at a predefined speed, measured in mm/min. As one of the grip heads moves, the uniaxial force, *F*, required to maintain speed and elongate the sample, *Δc*, is recorded. Figure 2.12 shows the standard dog-bone mould for the ASTM D1708 microtensile specimen. [ASTM D1708]
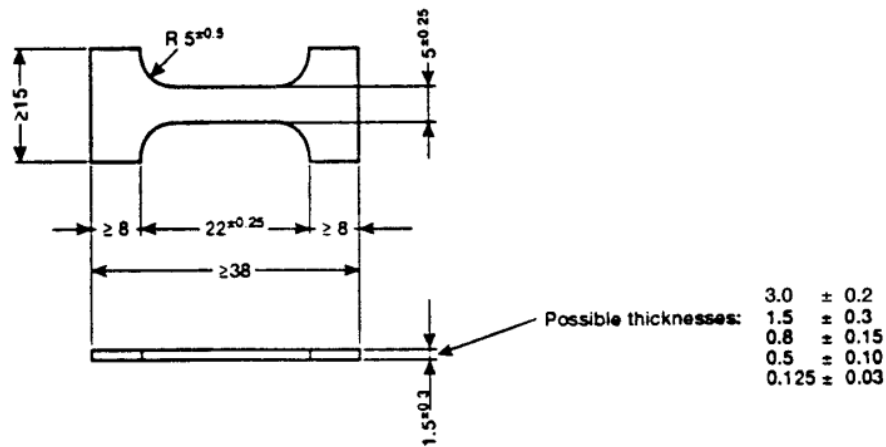
Figure 2.12 – Dog-bone shaped specimen for microtensile testing (dimensions in mm) [ASTM D1708]

The tensile stress, σ_t, is calculated by dividing the force recorded by the cross sectional area, *A*, of the centre of the specimen.

$$\sigma_t = F / A \qquad\qquad\qquad \text{(Equation 2.2)}$$

The strain, ε_t, of the material is the elongation, at some time, divided by the original length.

$$\varepsilon_t = \Delta c / c \qquad\qquad\qquad \text{(Equation 2.3)}$$

The stress, recorded in N/m^2 or Pa, is plotted against the strain, recorded in mm/mm, of the material to produce a typical stress-strain curve. The stress-strain curve can be used to determine important tensile properties like the elastic modulus, E_e. The elastic modulus is also known as the Young's modulus, Y_m, or tensile modulus, E_t, and is found by calculating the slope of the stress-strain curve in the linear elastic region. The elastic modulus has units of N/m^2 or Pa.

$$E_e = Y_m = E_t = \sigma / \varepsilon \qquad\qquad \text{(Equation 2.4)}$$

Other tensile properties that can be found from the stress-strain curve are:

- Yield strength, σ_y: the critical value of stress where the material begins to deform inelastically, below this value the material returns to its original shape after removing the load;
- Yield point, σ_e: the point at which a material will continue to elongate with no substantial increase in applied stress;
- Yield strain, ε_y: is related to the yield stress, and is a critical value of strain for a material, that when exceeded the material will deform inelastically (permanently);
- Ultimate tensile strength, σ_U: the maximum stress withheld before rupture; and
- Elongation at break, ε_B: the strain at the point of rupture.

Figure 2.13 shows the typical tensile stress-strain curves for a plastic material, a ductile material, a strong material that is not ductile, and a brittle material. The different tensile properties discussed above are labelled for the example of the ductile material. Clearly, not all tensile properties can be determined for each type of curve.
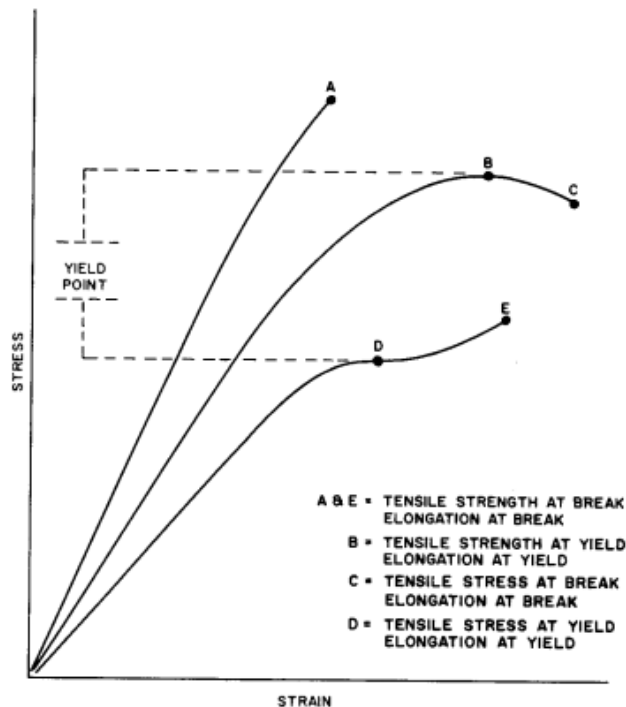
Figure 2.13 – Tensile stress-strain curves for plastic material, ductile material, strong and not ductile material and a brittle material [ASTM D638]

The flexural properties of unreinforced and reinforced plastics are measured by three point loading system. In this technique, a sample bar with rectangular cross section rests on two supports, and loading is applied to a third point, located at the midpoint on the top. The specimen is deflected until rupture occurs or until a maximum strain of 5.0% is reached, whichever occurs first. The rate at which the loading is applied is called the strain rate and is measured in units of mm/mm/min. This characterization technique is beneficial to the application as windows or barriers, as they will endure more flexural stresses in daily use than tensile. This mechanical test is also standardized through ASTM D790 for the flexural testing of polymers. [ASTM D790]

The flexural stress, σ_f, is calculated by solving the following equation, and typically reported in MPa.

$$\sigma_f = 3PL/2bd^2$$
(Equation 2.5)

Where P is the load at a given point on the load deflection curve in N; L is the support span between the two lower points in mm, b is the width of the specimen being tested in mm, and d is the depth of the specimen in mm.

The flexural strain, ε_f, is calculated by solving the following equation, typically reported in mm/mm.

$$\varepsilon_f = 6Dd/L^2$$
(Equation 2.6)

Where D is the maximum deflection of the centre of the specimen in mm; d is the depth in mm from above; and L is support span in mm from above.

The flexural stress, recorded in N/m^2 or Pa, is plotted against the flexural strain, recorded in mm/mm, similarly to tensile testing to produce a stress-strain curve. The stress-strain curve can be used to determine important tensile properties like the modulus of Elasticity of Bending (E_B). The E_B is also known as the flexural modulus, and is found by calculating the slope of the stress-strain curve in the linear elastic region. The modulus of elasticity of bending has units of N/m^2 or Pa.

Other flexural properties that can be found from the stress-strain curve are:

- Flexural strength (σ_{fM}): the maximum flexural stress sustained by the specimen during a bending test; and
- Flexural Stress at break (σ_{fB}): flexural stress at the breaking point of the specimen during a bending test.

Figure 2.14 shows the typical flexural stress-strain curves for a brittle material, a ductile material, and a strong material that is not ductile. The different tensile properties discussed above are labelled for the example of the ductile material. Figure 2.15 shows the setup of a typical 3-point bending test.
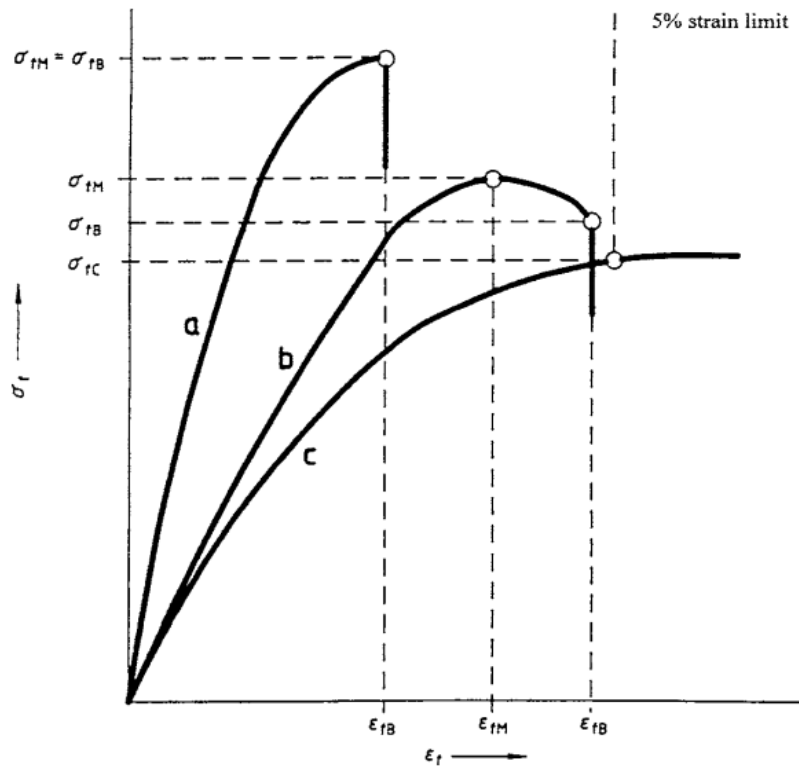
Figure 2.14 – Flexural stress-strain curve for a) a brittle material that breaks before yielding, b) a ductile material that yields and breaks before 5% strain, and c) a strong material that is not ductile that neither yields nor breaks before 5% strain [ASTM D790]
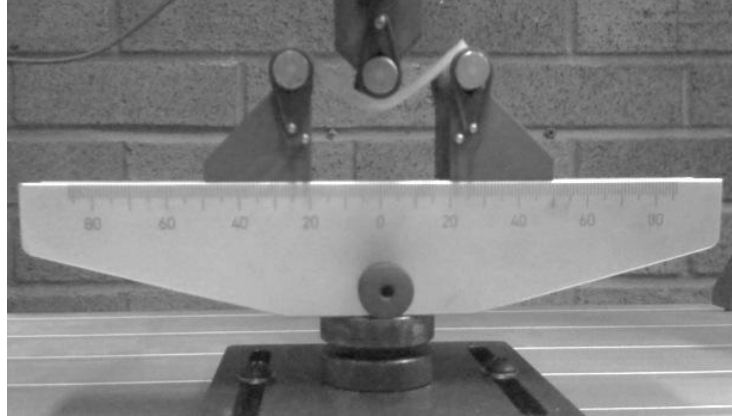
Figure 2.15 – Bench-top 3-point bending flexural test with sample being deflected

The technique used to measure impact strength is called a notched Izod pendulum test. In contrast to the tensile and flexural tests that are normally performed at slow strain rates, the pendulum impact test subjects the polymer specimen to a sudden blow, and consequently a rapid strain rate. With the IZOD impact test, the materials tested will appear more brittle than they did in the tensile and flexural tests. This technique determines the resistance of plastics to a standardized pendulum-type hammer, measuring the energy absorbing capacity of the material under sudden loading. The three-dimensional, *a* x *b* x *c*, IZOD specimens are required to have a milled notch to produce a stress concentration zone that increases the likelihood of brittle rather than ductile fracture. Dropping a pendulum and allowing it to strike the specimen in a standard way measured the amount of energy required to cleanly break a notched sample of the polymer. The energy is determined by noting the height difference between the starting point of the pendulum and the final height after striking the sample, *Δh*, and calculating the difference in potential energy, *ΔU*. [ASTM D256]

$$\mathit{\Delta U = mg\Delta h}$$ (Equation 2.7)

The impact resistance, *IR*, is then found by dividing the energy required to break the sample by the cross sectional area of the notched specimen, *a* x b_n, and is recorded in kJ/m^2, or more typically J/m, after being normalized by one dimension of the cross section according to the standard. The value b_n is the thickness after notching, the original thickness *b* minus the notch thickness.

$$IR = \Delta U \, / \, (a \times b_n) \qquad\qquad\qquad \textit{(Equation 2.8)}$$

This technique follows ASTM D256 method to ensure reproducibility and consistency. An example of a typical set-up for and IZOD impact test can be seen in the Figure 2.16 below.
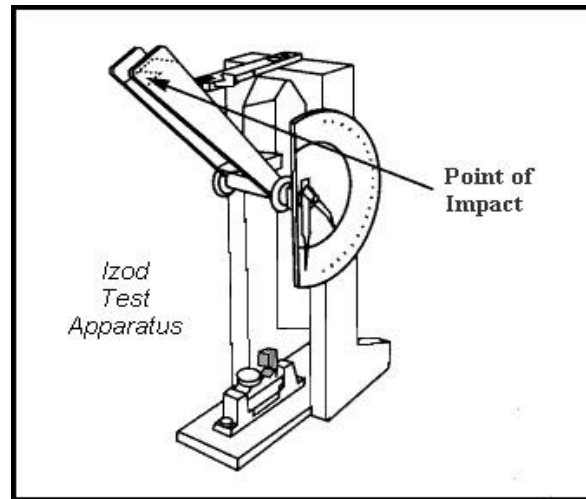
Figure 2.16 – Izod impact test apparatus, specimen location is near bottom centre (shaded)

2.5.2 – Thermal Properties

When characterizing new materials the melting point (T_m) and glass transition (T_g) temperatures should be noted, as they are important characteristics of a material often dictating many future applications and tests for the species. These thermal properties can also hint at other properties of the sample. Differential scanning calorimetry (DSC) is a thermodynamic technique used to determine these thermal properties like glass transition temperature and melting temperature. The DSC recognizes and records differences in heat (or energy) required heating a sample in a platinum or ceramic pan, compared to a reference empty pan. The analytical machine must ensure that the sample experiences the same temperature and rate of temperature change as the reference sample to make certain the data collected is accurate.

The melting of a crystalline solid to an amorphous solid phase is a transition that absorbs energy (endothermic) – this is because energy is required to break the intermolecular forces holding the material together in the crystalline state. Therefore, when the sample begins to melt, the DSC must provide more heat to the sample than the reference pan. Measurement of this energy allows the calculation of the enthalpy of phase transition. Consequently, the amount of

crystallinity in the material can be calculated. The crystallization of an amorphous solid occurs when the atoms or molecules arrange themselves into a long-range ordered crystal in order to reduce energy and be in the most stable configuration, this happens at a point called crystallization temperature. As a result, during the crystallization of the sample the DSC must reduce the amount of heat flow to the sample as it is undergoing an exothermic phase transition.

Thermogravimetric analysis (TGA) is an important analysis tool used in materials science research. TGA is a precise method used to find changes in the weight of a sample as the sample undergoes a pre-programmed heating profile in air or inert atmosphere. As the temperature increases in accordance to a pre-set rate (in degrees Celsius per minute) the apparatus measures weight change versus temperature. This data can be represented with a weight loss curve, temperature (or time) versus percentage of original weight, called a thermogram.

A property that limits the ability to process and the applications of a polymer is its thermal degradation point or onset of degradation. Thermal degradation is the molecular breakdown of a sample as a result of overheating. This temperature sets an upper limit as to the amount of heat the material can withstand, so with a higher thermal degradation temperature a material can be used in a wider variety of applications or processing procedures. It is also helpful to ensure that in NCC-PC nanocomposites the amount of the nanocrystalline cellulose incorporated does not significantly reduce this temperature. [Jang 2005, Tajvidi 2009]

2.5.3 – Processing Properties

The melt flow index of a polymer gives a relative value or metric as to how easy it will be to process the polymer. The principle behind melt flow indexing is quite simple; the polymer material is brought to a specific temperature and is only held there for a brief amount of time. A specific load is then applied to the material and it is forced through a small die. The sample is collected at timed intervals after passing through the die and is weighed. A measurement in grams per ten minutes is calculated and recorded as the MFI.

Some typical MFI values found for common polymers, as listed in ASTM D1238, 'The Standard Test method for Melt Flow Rates of Thermoplastics by Extrusion Plastomer,' are: LDPE, 1.74 g/10 min; HDPE, 5.35 g/10 min; Polypropylene, 10.94 g/10 min; and Polycarbonate,

13.59 g/10 min. Figure 2.17 below shows a schematic of the extrusion plastomer technique detailed above and tabulates some typical melt flow indices for common polymers.

LOAD

MATERIAL

TEMPERATURE

LDPE	1.74g/10 min
HDPE	5.35g/10 min
PP	10.94g/10 min
PC	13.59g/10 min

a)   b)
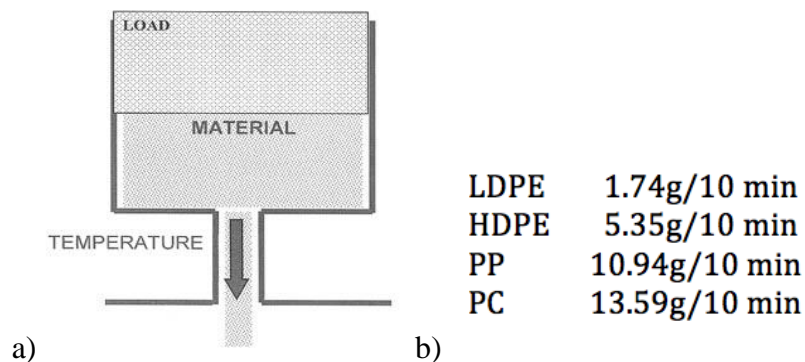
Figure 2.17 – a) Principle of melt flow index in extrusion plastomer and b) common polymer MFIs [ASTM D256]

2.5.4 – Chemical Properties

Fourier transform infrared (FTIR) spectroscopy is a characterization technique used to classify a substance based on the type of chemical bonds within the molecular structure. It is based on the principle that the atoms vibrate according to the chemical (type of bonding) environment. By probing the sample with electromagnetic waves over a spectrum of energies (i.e. frequencies), different bonds will interact differently absorbing energy at a wavelength that is characteristic to that molecular bond. This material analysis technique does not destroy the sample being probed and has simple sample preparation, simply pressing a thin film. The specific wavelengths that can be transmitted through the film are transformed into a plotted spectrum that contains bands at these specific wavenumbers (inverse of wavelength). FTIR spectroscopy probes over the range of wavelengths from 2.5 to 50 micrometres; considered as wavenumbers, the range is 4000 to 200 wavelengths per cm (cm^{-1}). The plot represents a curve that is specific to that sample often referred to as the characteristic fingerprint or infrared spectrum. [Davis 2001]

Another spectroscopic technique used to characterize polycarbonate is ultraviolet-visible spectroscopy (or UV-Vis for short). This technique probes within the electromagnetic range of ultraviolet and visible light. This technique will help characterize the transparency and any changes to the colour of the nanocomposite that may occur due to the addition of nanocrystalline

cellulose. The visible spectrum is between about 400 to 700nm wavelengths, and maximum visible transmission in this region is desirable for our transparent nanocomposite.

2.6 – Nanocrystalline Cellulose Characterization Background

2.6.1 – Particle Morphology and Size

Scanning electron microscopy is a characterization technique that aids in the analysis of the surface structure, surface morphology, and chemical composition. The scanning electron microscope (SEM) is very beneficial in materials science because it provides very high resolution and high depth of field images of the material of interest. Inorganic and organic samples can be analysed resolving micro and nano features of the surface. The SEM uses electrons to probe the surface rather than photons as in optical microscopy; the smaller wavelength of electrons allow for a much-improved depth of field and resolution over optical microscopy. Relatively simple sample preparation is another key attribute of the SEM. Moisture or volatiles should be removed by drying with heat or vacuum. The surface of the specimen is sputtered coated with gold or other conductive material to make the surface electrically conductive. The conductivity of the sample is important, as the image will appear distorted, very bright and/or blurry if the electron beam charges the sample.

The SEM operates on a much more complex set-up than a typical optical microscope. A metallic cathode filament, such as a tungsten hairpin gun, is heated by passing a voltage across it causing electrons to become free and accelerate towards an anode plate. Electrons accelerate past the anode plate and pass through a condenser lens concentrating the electrons into a beam approximately 1-5 nm in diameter. The electron beam then passes through an objective where the electrons experience longitudinal and radial magnetic fields that cause the electrons to follow a downward spiralling motion achieving the desired resolution. This beam passes over the surface in a raster fashion, meaning laterally back and forth moving down slightly each time. As the electron beam hits the surface the electrons will interact with the sample causing elastic scattering and absorption penetrating the sample in a teardrop shape. Secondary electrons are scattered near the surface of the sample, backscattered electrons penetrate a little deeper, and x-rays probe deep into the sample. The emitted electrons and x-rays are detected and transformed

into different images revealing information about the sample. The low energy secondary electrons give topographical information of the specimen. High energy backscattered electrons also give topographical information, but more importantly it allows the determination of the atomic number, Z, of atoms in the sample. X-rays emitted from the sample give information on the composition of the sample using Energy Dispersive X-ray (EDX). Together, this information collected by the scanning electron microscope can be used to significantly characterize the morphology, topology, and composition of the sample. [Watt 1985]

DLS, or 'Dynamic light scattering', is a well-established, non-invasive technique used characterize the size and size distribution of particles in mixtures and solutions, effective to beyond the nano-scale. The principle behind DLS is related to the Brownian motion of particles in solution: particles or molecules are illuminated with a light source – typically a laser – which cause time-dependent fluctuations in the scattering intensity that can be correlated to Brownian velocity, and therefore the particle size, using the Stokes-Einstein relationship.

2.6.2 – Crystallinity

X-Ray Diffraction (XRD) characterization uses inelastic scattering of X-rays as a result of their interactions with the arrangement of atoms within a sample, and can be used to determine the crystallinity of a sample as well as the size of these crystallite regions. XRD is a non-destructive technique that can be used to analyse different material samples from single crystals to powdered samples. The X-ray source, a cathode ray tube, produces a monochromatic and concentrated beam of X-rays that will interact with the sample over a range of different incident angles. By sweeping over a range of angles a complete analysis of the diffraction directions within the lattice can be probed.

If the X-rays that are incident with the sample satisfy Bragg's Law then constructive interference will occur and a diffracted X-ray will be emitted and detected producing a characteristic scattering pattern, or diffractogram, of the sample. Of the two types of XRD stated above, single crystal and powdered XRD, the characterization of cellulose will primarily use X-ray Powder Diffraction. [Bragg 1975]

X-ray Powder Diffraction analyses a finely powdered sample that could range from a highly amorphous sample to one or more crystal phases. The XRD diffractogram will not provide much information of the composition or molecular structure of the material but will provide both qualitative and quantitative information of the crystalline arrangement of cellulose including the cellulose crystallinity index and crystallite size. The cellulose Crystallinity Index (%CI) measures the amount of crystalline content within the sample by volume and is quantified as a percentage.

The technique used here for measurement of crystallinity consists of XRD peak deconvolution where an XRD diffractogram is modelled by several peaks corresponding to the different Miller Indices present in the sample [Zhao 2007]. For example, a cellulose diffractogram has five dominant crystalline peaks for the (001), (00-1), (021), (002), and (040) Miller Indices. There is also one low amplitude and very broad peak that corresponds to the amorphous regions of the cellulose sample that is centred on the Bragg angle of 21.5° and extends nearly to both ends of the spectrum (5° to 40°). Each of the five characteristic crystalline peaks of cellulose can be seen in Figure 2.18 where the sixth amorphous peak has already been subtracted. [Sottys 1984]

To determine the %CI, the area under the curve for the five crystalline phases is divided by the total area of all six curves, seen in Figure 2.18. The equation to find the Crystallinity Index is included below.
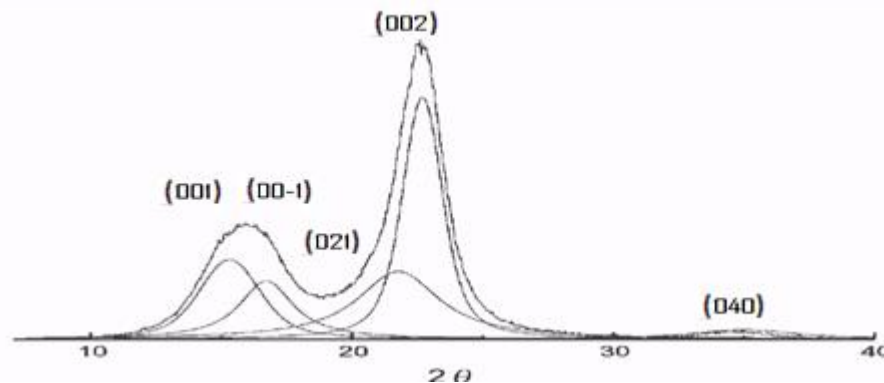
Figure 2.18 – Characteristic XRD diffractogram for cellulosic materials with amorphous regions baseline subtracted

$$\%CI = \frac{AUC_{001} + AUC_{00-1} + AUC_{021} + AUC_{002} + AUC_{040}}{AUC_{total}}$$

(Equation 2.9)

Where %CI is the percentage crystallinity for cellulose, AUC_{hkl} corresponds to the area under the curve for the peak of orientation hkl, and AUC_{total} is the total area under the curve for all six orientations.

The crystallite size, grain size, or mean size of the crystalline domains, can be calculated for cellulose samples as it is strongly believed that peak broadening in cellulose is a function of smaller crystalline domains. To determine the crystallite size, the Scherrer equation can be implemented to give the value of the lower bound of the grain size of our cellulose material. [Patterson 1939].

$$\tau = \frac{K\lambda}{\beta cos\Theta}$$

(Equation 2.10)

Where τ is the mean size of the ordered crystalline domain, K is a shape factor with a typical value between 0.9 and 1.0, λ is the wavelength of the X-ray source, β is the broadness of the peak measured as the full width at half maximum (FWHM), and θ is the Bragg angle [Garvey 2005].

2.6.3 – Hygroscopic Properties

Moisture content analysis is being conducted to quantify the water content that is inherent in the solid cellulose material in ambient conditions. Cellulose is known to be very hydrophilic; water is adsorbed from the surroundings (air) onto the surface of the material. It is beneficial to know the moisture content of our material in ambient conditions as it may cause compatibility issues when incorporated (as a reinforcement or filler) in polymeric materials during the manufacturing process. This analysis will also give an idea of drying required before processing with polycarbonate. A typical technique used to determine water content is to heat a conditioned sample to a constant temperature above the boiling point of water (like 110°C) and monitor the mass of the sample as a function of time. After the sample reaches a steady-state mass it can be assumed that a high majority of the moisture has been vapourized and no longer contributing to the sample mass. To calculate the moisture content, *%MC*, of the sample the following equation can be used:

$$\%MC = \frac{m_i - m_f}{m_i}(100\%)$$ (Equation 2.11)

Where m_i is the initial mass of the sample and m_f is the mass of the sample after reaching a steady-state mass during drying at elevated temperatures. This technique assumes that all of the weight loss is a result of the vapourization of water and does not account for any other volatile compounds that may be released at the temperature used.

2.6.4 – Thermal Stability

Thermogravimetric analysis (TGA) uses a programmed heating of a sample and its mass change is measured as a function of temperature or time. By measuring the weight change of a material during its heating, information can be gathered on the degradation kinetics of the material or activation energy required to transform from a solid to gas products. Typically a ramped heating program is used where the material is heated at an increasing temperature that is a linear function of time (the heating rate); this method is called non-isothermal TGA. The heating rate has units of degrees Celsius per minute. Another technique that can be used is isothermal TGA where the sample quickly reaches a programmed temperature and then remains there for a set time. The mass loss recorded is corresponding to a loss of a volatile component of the material where either the material changes phase into a gas (vaporization, volatilization) or there is a chemical reaction (like thermal oxidation) where the products are gases.

The results of a TGA experiment are given in a plot of mass versus temperature or time. The derivative of this plot gives the derivative thermogravimetry (DTG) curve. The DTG curve is more conveniently used to observe any overlapping reactions or to compare relative mass losses [Arseneau 1971, Chatterjee 1968a]. In this thesis the TGA will be performed on NCC fibers to better understand the degradation characteristics of the material and to gain a better idea of what happens during the processing with thermoplastic (polycarbonate) at high temperature (above 250 ^{o}C). To quantify this, kinetic parameters of thermal degradation will be calculated; this includes the activation energy and onset of degradation. This will be done in different atmospheres (air and nitrogen) and different heating rates. [Chatterjee 1966, Consea 1995, Milosavljevic 1995, Corradini 2009]

For a kinetic process, the rate of reaction, *r*, is the change of a reactant from one state to another, a product, and can be represented as the product of a temperature dependant function, *k(T)*, and a conversion dependant function, *f(X)*.

$$r = \frac{dX}{dt} = k(T)f(X)$$
(Equation 2.12)

Where *X* is the conversion of the reactant, *T* is the absolute temperature (K), and *t* is time (usually in s). The temperature dependant term, *k(T)*, is assumed to obey the Arrhenius relationship.

$$k(T) = A exp(-\frac{E}{RT})$$
(Equation 2.13)

Where *E* is the activation energy of the kinetic reaction, *A* is the pre-exponential factor, and *R* is the universal gas constant (8.3145 J/[mol K]). The conversion dependant function, *f(X)*, in Equation 2.12 is typically a very complex relationship, typically only valid for a particular temperature range. For now, a simple n-th order relation will be employed.

$$f(X) = (1 - X)^n$$
(Equation 2.14)

Where the *(1-X)* term can be represented by *W*, the remaining weight fraction of the sample, such that:

$$r = \frac{dW}{dt} = AW exp(-\frac{E}{RT})$$
(Equation 2.15)

and

$$\ln r = \ln A + n \ln W - \frac{E}{RT}$$
(Equation 2.16)

Most published models for deriving the kinetic parameters using non-isothermal TGA are derived from Equation 2.16. These models can focus on a single thermogram or multiple thermograms with different heating rates (kept constant in each thermogram). The constant heating rate, *β*, is the rate of temperature change over time, or *dT/dt*. [Flynn 1966, Ozawa 1970]

Flynn, Wall, and Ozawa have developed a method to determine the activation energy as a kinetic parameter of the thermal degradation of a material [Ozawa 1986]. Equation 2.17 below

shows the common activation energy calculation method known as Ozawa-Flynn-Wall (OFW) method.

$$\log \beta \approx 0.457 \left(\frac{-E_a}{RT} \right) + \left[log \left(\frac{AE_a}{R} \right) - \log F(\alpha) - 2.315 \right]$$ (Equation 2.17)

Where β is the heating rate used, E_a is the activation energy of the reaction, R is the gas constant (8.3144 J/kmol), T is the temperature in Kelvin, A is the pre-exponential factor and α is the percentage-degradation or conversion. The activation energy is the amount of energy required for a chemical reaction to proceed and can be determined from the slope of a plot of log β versus *-1/RT*. [Ozawa 1992]

The OFW method is a popular technique that can be applied to determine the activation energy, *E*, at different conversions. Take Equation 2.12 and integrating using separation of variables and substituting 2.13.

$$F(X) = \int_{\tau_0}^{\tau} \frac{A}{\beta} exp \left(\frac{-E}{RT} \right) dT$$ (Equation 2.18)

And using a linear empirical approximation limited to the range of {-20>-*E/(RT)*>-60} results in:

$$\log \beta = -0.4567 \frac{E}{RT} + \left(\log \frac{AE}{R} - \log F(X) - 2.315 \right)$$ (Equation 2.19)

Taking a plot of {log β} versus {*-1/RT*} at a constant conversion (multiple βs) will result in a line with a slope of $0.4567E_a$, thus the activation energy can be determined for any conversion.

Chapter 3 – Materials

3.1 – Polymer and Nanocrystalline Cellulose Materials

Listed below are the four sources of cellulose and the single source of polycarbonate that have been chosen for this research. The different cellulose samples originate from various locations including Alberta and Quebec in Canada, and Germany and have undergone varying amounts of refinery and cellulosic isolation. This difference in the cellulose processing will be apparent in the purity and morphology of our samples including properties such as particle size and thermal stability which will be discovered through material characterization. Three samples from Sigma-Aldrich have also been included in some characterization techniques for comparison purposes and are also included here. Below is a brief overview of each material sample chosen for the present study, including any material data that was supplied by the manufacturers.

For completeness, the solvents used for any cellulose or polymer processing were dimethylformamide (DMF), ethanol, and DI water. The polymer antioxidant used was Irganox 1098 from Ciba; a specification sheet has been included in Appendix 1.

3.1.1 – StarPlastic Polycarbonate

The polycarbonate sample that was received from PolyOne distributors, it was originally produced by StarPlastic Inc. of Millwood, WV. The trade name of the resin is StarPlastics PC743R-CLS112 Moulding Grade PC and the Lot number is 62896 dated June 16, 2009. It was

labelled safe for ultraviolet light, water exposure, immersion, and acceptability for outdoor use in accordance with UL 746C. The polymer also came with a specifications sheet detailing specific properties of this batch of PC. A more detailed specification sheet for the material has been found online. They have been included in Appendix 1.

3.1.2 – JRS Arbocel® UFC-100 Ultrafine Cellulose (UFC-100)

The Arbocel UFC-100 Ultrafine Cellulose from JRS Co. located in Germany is an ultrafine white powder. The cellulose powder is insoluble but partially dispersible in water near a neutral pH. The UFC-100 sample has a purity of 99.5 % cellulose. The average particle size is approximately 1μm according to JRS as measured using DLS techniques. The bulk density of the UFC-100 cellulose is 160 g/l with a whiteness measurement of >85% measured at 461 nm. The specification sheet for UFC-100 is included in Appendix 1.

3.1.3 – JRS Arbocel® NANO MF 40-10 Nano Disperse Celulose (MF40-10)

Arbocel cellulose fibres are environmentally friendly products derived from renewable raw materials. Among other applications they are used as thickeners, fibre reinforcements, absorbents, diluents, or as fillers/carriers in most manifold applications.

The Arbocel NANO MF 40-10 Nano Disperse Cellulose from JRS Co. – located in Germany – is a 10% dispersion of nanocellulose in water. The cellulose is insoluble but dispersible in water near a neutral pH. The average particle size is approximately 4.5 μm according to JRS as measured using dynamic light scattering (DLS) techniques. The MF 40-10 dispersion has a value of 92 on the CIE L* colour scale and a brightness of 85% when dry. The particle stability is a maximum of 2 months from time of preparation. The specification sheet for MF 40-10 is included in Appendix 1.

3.1.4 – Alberta Innovates – Technology Futures Nanocrystalline Cellulose (NCC-Alb)

The Nanocrystalline Cellulose from Alberta Innovates – Technology Futures is slightly yellowish in colour and is in the form of hard flakes >1mm in size. The cellulose flakes are insoluble but dispersible in water near a neutral pH leaving a nearly transparent dispersion at a

few percentages, suggesting it is a material reaching the nano-scale on some dimensions. The sample supplied by Alberta Innovates – Technology Futures was produced from cotton.

3.1.5 – FP Innovations Nanocrystalline Cellulose (NCC-FP)

The Nanocrystalline Cellulose from FP Innovations is slightly yellowish in colour and is in the form of thin translucent flakes that appear to be formed through a press-drying process. The cellulose powder is insoluble but dissolvable in water near a neutral pH leaving a transparent dispersion at a few percentages, suggesting a material on the nano-scale on one or more dimensions. The sample supplied by FP Innovations is based out of Quebec and the cellulose is a product of Canadian wood sources. The typical crystallite is 200nm long and 10nm in diameter. In 2010 FP Innovations announced plans to producing >1kg/day at a new facility to open in early 2012.

3.1.6 –Cellulose, fibrous, medium; SigmaCell 50; and SigmaCell 101

Cellulose fibres (medium), SigmaCell Type 50 and SigmaCell Type 101 were all obtained from Sigma-Aldrich Corporation of St. Louis, Missouri. Only SigmaCell 50 is provided with a nominal average particle size (50 μm); the manufacturer does not provide the particle sizes of the other two samples. SigmaCell Type 101 is marked as 'highly purified' by Sigma-Aldrich. All the samples are in the form of a white powder.

Chapter 4 – Methodology

4.1 – Polymer and Nanocomposite Processing Methodology

4.1.1 – Solution Casting

The cellulose sources were first dispersed by ultrasonication into dimethylformamide (DMF) solvent. A consistent mass of two grams of cellulose was incorporated in order to compare the different cellulose sources to be mixed with 100g of polycarbonate. The cellulose was dried at 125°C for 1 hour to remove any moisture prior to ultrasonication. After drying, the cellulose and 400mL of dimethylformamide (DMF) were added to a 1000 mL round bottom flask and ultrasonicated with heat. Ultrasonication was done past the point of visible dispersion; this took up to an hour depending on the cellulose source. A measured amount, 100 g, of polycarbonate was added to the cellulose-DMF dispersion. This mixture was then refluxed under heat and stirred until the polymer had dissolved and a homogeneous dispersion was obtained. [Viet 2006]

This composite dispersion was decanted into a large pan for slow evaporation of solvent in air for 48 hours. Slow evaporation of the solvents from the solutes resulted in a cellulose-PC nanocomposite powder or cake being cast. The cake was collected and dried under heat and vacuum to remove any remaining moisture or DMF. Mechanical blending aided in the drying of the composite.

4.1.2 – Melt Compounding

Processing of the composite powder into a polymer resin was completed with a bench-top extruder that applied heat and sheer stress to melt and mix the composite. The extruder used was made by Thermo Electron Corporation and the model was the Haake MiniLab. The extrusion processing temperature for the cellulose-PC composites was 250°C, this is lower than the recommended PC processing temperature of 300°C. The lower temperature was chosen to reduce the thermal degradation of the natural cellulose fibres and minimize change in colour in the nanocomposite material. The rotating speed of the twin-screws remained constant at 250 revolutions per minute (rpm). This RPM was chosen as it resulted in the least visible degradation of the polycarbonate. Feed of the composite was done manually through a small hopper on the top of the extruder using gravity and manual plunging. Processing times of the materials varied from 30 minutes to 1 hour, with a visible difference in ease of flow between the different cellulose composites. With the approximate time estimates, the feed rate of the composite varied between 100 and 200 g/hour.

4.1.3 – Compression Moulding

Compression moulding of the extruded composite materials was done to make the ASTM D256, D790, and D1708 sample bars for mechanical testing. Two 8" aluminium plates were covered in foil and a very thin layer of WD-40 applied with a wipe to aid cleaning and removal of the specimens after formation. An aluminium specimen mould - a plate with desired specimen shapes removed - was placed on one of the foil-covered plates. The plates and mould along with the hot press were heated to 220°C above the temperature at which PC begins to flow. A schematic diagram of the two moulds used to make ASTM specimen bars is included in Figure 4.1 (CAD done by Yongseong Kim).
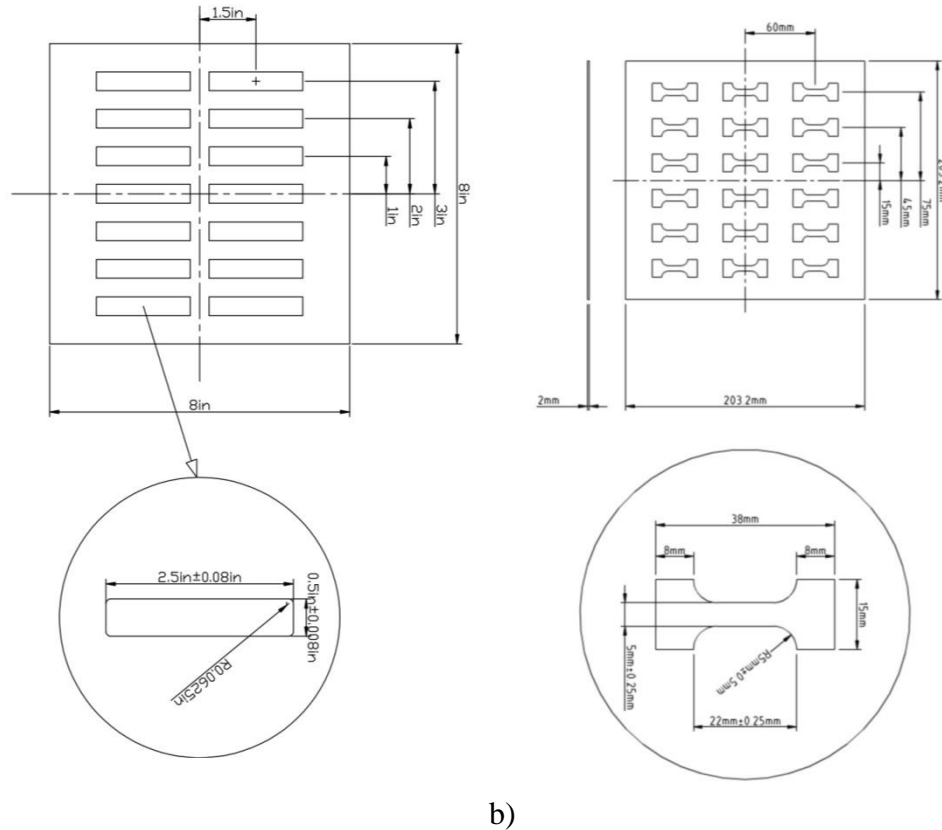
Figure 4.1 – Compression moulds used to make a) ASTM D256 and b) D1708 specimen bars for mechanical testing

The empty specimen moulds, set atop a foil-covered plate, were generously filled with the dried composite material and covered with the second foil-covered plate. This stack was then placed in the centre of the hot press. Initially, no pressure was applied; light contact was made between the stack and the parallel plates of the hot press to allow the polymer to flow. The polymer composite was allowed to heat for 10 minutes and then 10 kT of pressure was applied to the stack for 2 minutes. Next, the pressure was released for about 30 seconds, to allow some gas to escape, and then 25kT of pressure applied for a final 2.5 minutes, for a total of 15 minutes at 220°C. The stack was removed from the hot plate and quenched with hot tap water for 10 minutes. The specimens were carefully removed from the moulds and were ready for further testing. Thin films created as a by-product from making the specimen bars were collected for FTIR and UV-Vis spectroscopy.

4.2 - Polymer and Nanocomposite Characterization Methodology

4.2.1 – Mechanical Properties

Tensile and flexural tests were completed using the universal testing machine manufactured by TestResources Inc. MiniTec apparatus and IZOD impact tests were completed using the TestMachines Inc. (TMI) 43-02-01-0001 impact resistance apparatus. The specimen bars formed for the tensile testing were in a dog-bone shape as specified by ASTM D1708 for microtensile testing. The microtensile technique was chosen to avoid excess material processing and use. As seen in Figure 4.1, there is a thin rectangular section to be tested, suspended between two larger grip-heads. The rectangular cross-sectional area in the centre of the specimen has a gauge length of about 22 mm, a width of 5 mm, and a thickness of 2 mm. The specimen bars formed for the flexural testing were 63.5 mm in length, by 12.7 mm in width, by 2 mm in thickness as specified by ASTM D790. The specimen bars formed for the impact testing were also 63.5 mm in length, by 12.7 mm in width, by 2 mm in thickness as specified by ASTM D256. The IZOD impact specimens were notched using JinJian XQZ-1 Specimen Notch Cutter for a final notched width of 10.16mm.

Testing of at least five specimens for each polymer sample is required for significance in each tensile, flexural, and impact tests. All samples were conditioned in 23±2°C temperature and 50±10% relative humidity for 40 hours prior to testing.

4.2.2 – Thermal Properties

An approximate 6 mg mass of each composite sample was run on the TA Instruments Q2000 Differential Scanning Calorimeter. A heating cycle from 35 °C to 250 °C to 35 °C back up to 350 °C was used at a heating rate of 10°C/min. The samples were run in air at 50 ml/min flow rate. The results are output in a thermogram of heat released versus temperature.

An approximate 6 mg mass of each sample was run on the TA Instruments Q500 Thermogravimetric Analyser. A ramp from 35 °C to 600 °C was used at a heating rate of 10°C/min. The samples were run in air at 50 ml/min flow rate. The results are output in a thermogram of percentage of original mass versus temperature.

4.2.3 – Processing Properties

The melt flow index of each composite sample was determined using the Dynisco Polymer Test D4001DE MFI apparatus. The temperature was stabilized at 250°C and approximately 5 g of polymer or composite was added to the cylinder. The material was allowed to heat for exactly 7 minutes and a mass of 1.2 kg was added as per the ASTM D1238. Molten polymer composite is pressed through a heated die and these polymer extrudates were collected at a determined time interval. Samples were collected every 10-30 seconds - smaller intervals were used for faster flow rates - and weighed only if there were no bubbles present. The melt flow index is calculated and reported in grams per 10 minutes (g/10min).

4.2.4 – Chemical Properties

A film with approximate thickness of 100 to 250μm from the compression moulded composite materials was collected to probe with the Fourier Transform Infrared. The FTIR used for this study was a Bruker Tensor 27 / Hyperion 2000 FTIR System. The sample was scanned over a range of 4000 to 400 cm^{-1}. The thickness of each film was measured to determine any error assumed in comparing transmittance between one another.

Similarly, a thin film of each of the composite materials was probed by Ultraviolet-Visible spectrum analyser or UV-Vis. The UV-Vis used for this study was a Bruker Vector 22 UV-Vis-NIR System. The sample was scanned over a range of 200 to 700 nm to quantify the transparency of the composite materials.

4.3 – Nanocellulose Characterization Methodology

4.3.1 – Surface Morphology

The scanning electron microscope system that was used to collect micrographs of cellulose was the Carl Zeiss Leo 1530 Gemini SEM equipped with an EDAX system for determining sample composition. The samples were dried and gold sputtered before analysis. Magnification up to 100 000x was used in the secondary electron mode.

Dynamic light scattering was completed using a Brookhaven 90plus Particle Size Analyser. The measurement parameters used included a temperature of 25 °C in a water suspension with a probing wavelength of 659 nm at a 90° angle. Two runs were completed lasting a total of 5 minutes each. It was ensured the count rate was approximately 400 kcps (kilocounts per second) to obtain the most significant results.

4.3.2 – Chemical Composition

A pellet consisting of a mixture of about 1% cellulose sample in potassium bromide (KBr) was pressed for each powdered sample to run on the FTIR; vibrational modes for KBr are invisible to infrared absorption. The FTIR used for this study was a Bruker Tensor 27 / Hyperion 2000 FTIR-ATR System.

4.3.3 – Crystallinity

The XRD used for the analysis of the cellulose sources was a Bruker D8 Advance system with a Cu K-α source with wavelength of 1.5404 angstroms. A step size of 0.05 degrees was used over an angle 2θ from 10 to 40°. Powdered samples were prepared by mortar and pestle, vacuum drying, and pressed in an aluminium pan for analysis.

The XRD diffractogram was analysed using Origin peak fit software for peak deconvolution. Six specific peaks were fit using a Gaussian distribution and the area under the curve (AUC) for each peak was determined and used to calculate the crystallinity. The relevance of these peaks was discussed in Chapter 2.

The size of the crystal phase was investigated by incorporating a K factor in the Scherrer equation. Typical literature values for the shape factor, K, for cellulose are 0.97 used by Newman [Newman 1999] and 1.0 used by Garvey [Garvey 2005]. For this study, a shape factor of K=1 will be implemented. Typical crystalline domain sizes for microcrystalline celluloses are in the range of 2.2 to 7.5 nm as documented by Garvey [Garvey 2005].

4.3.4 - Hygroscopic Properties

Approximately 2 g of the cellulose material was conditioned at 24 °C for 40 hours with a relative humidity of 50%. The humidity and temperature were monitored with computer

software, which showed that the temperature remained in the range of 22 to 26 °C and the relative humidity (RH) fell between 30 and 50% during the conditioning processes. After conditioning the cellulose, the moisture content was determined using the OHAUS MB45 Moisture Analyser at a constant temperature of 110 °C. The testing was performed in the same conditions as the conditioning step (24 °C, 50% RH)

4.3.5 – Thermal Stability and Kinetics of Thermal Degradation

The thermogravimetric analysis was completed on a TA Instruments Q50 TGA in air and in nitrogen gas (on separate experiments) with a purge rate of 50 ml/min. The Ozawa-Flynn-Wall method uses the multiple heating rates. The different heating rates used were 5, 10, 20, 30, and 40°C/min and the temperature range covered in these experiments was from 35 to 600°C.

Chapter 5 – Results and Discussion

5.1 - Polymer and Nanocomposite Processing

5.1.1 - Solution Casting

Solution casting was used to prepare a composite solution of nanocellulose and polycarbonate by mixing both components in the same solvent. The objective was to achieve a homogenous solution of polycarbonate with well-dispersed nanocellulose. Two grams of each nanocellulose samples were mixed with 100 g of StarPlastic Polycarbonate in DMF to make a solution, refluxed and then dried as outlined in Section 4.1.1. The mixtures containing NCC-Alb, NCC-FP, and UFC-100 evapourated the majority of their DMF solvent over the first 48 hours in open air and the remaining residual solvent was removed in a vacuum oven at 125 °C over eight hours. The MF 40-10 samples took a noticeably longer time to dry. They were left to dry in air for about 5 days before they reached the same level of apparent dryness as the other four samples; they were then added to the vacuum oven for further drying.

One gram of antioxidant (Irganox 1098) was added to the composite mix to further reduce oxidation by scavenging free radicals. NCC-FP was used as a reference to evaluate the effects of incorporating the antioxidant. The two names that will be used herein for each of the NCC-FP samples will be: 2% NCC-FP / PC, and 2% NCC-FP / PC (no antioxidant or no AO). This naming convention will also be used for each of the other nanocellulose-PC composite samples (i.e. 2% MF 40-10 / PC (dried), 2% MF 40-10 / PC (solution), and 2% UFC-100 / PC. Also note

that, the antioxidant was added to the composite powders after the solution reflux and drying procedures. In future research, each of the other nanocellulose sources should also be tested without the antioxidant, as it may significantly affect the resulting properties. Table 5.1 shows a breakdown of the sample names and their compositions included in this study.

Table 5.1 – Composite component compositions chosen for analysis

Material	Mixing Technique	Anti-Oxidant (g)	PC (g)	Cellulose (g)	Wt-% (%)	Yield (g)
PC	-	-	200.00	-	-	200.00
NCC-Alb	solution	1.00	98.00	1.9626	1.96	97.23
NCC-FP	solution	0.00	96.31	1.9262	1.96	91.30
MF40-10 (a)	solution dry	1.00	100.00	2.0096	1.97	90.40
MF 40-10 (b)	solution DMF	1.00	100.10	2.00	1.96	80.60
NCC-FP	solution mix	1.00	100.50	2.00	1.95	90.34
UFC-100	solution mix	1.00	100.00	2.004	1.96	92.00

After refluxing, the appearance of the composite solution for the 2% NCC-Alb / PC, 2% NCC-FP / PC (no antioxidant), 2% NCC-FP / PC, and 2% UFC-100 / PC samples were a transparent or slightly translucent white. Both 2% MF 40-10 / PC samples made by drying the MF 40-10 fibres and re-dispersing in DMF; as well as exchanging solvent with a roto-evapourator were a yellow-brown colour and contained large visible brown precipitates. The products obtained after solvent evaporation were primarily nanocellulose that formed to the side of the round bottom flask during reflux. The discolouration observed with MF 40-10 composite samples is expected to come from some impurities in the as-received dispersion. An image of the discoloured 2% MF 40-10 / PC (dried) sample with precipitates is included below in Figure 5.1 a). Further confirmation of an impurity is available later in this chapter in the Chemical Composition and Thermal Stability sections.

After air and vacuum drying the composite samples 2% NCC-Alb / PC and 2% UFC-100 /PC, a white powder remained. This can be seen in Figure 5.1 b), which shows the 100 g of dried 2% NCC-Alb / PC. The 2% NCC-FP / PC (no antioxidant) and 2% NCC-FP / PC samples produced more of a hard cake after drying. A reminder that, for both NCC-FP samples, an identical procedure was followed to this point, the antioxidant was added after drying (during

blending). The visual appearance of each composite after drying has been summarized in Table 5.2.

Figure 5.1 – Solution casting of composites a) 2% MF 40-10 / PC (dried), b) 2% NCC-Alb / PC, and c) 2% NCC-FP / PC

Table 5.2 – Visual appearance of cellulose-PC composites following solution casting

Sample	Appearance
Pure PC	Clear solution, white cake
2% NCC-Alb / PC	Clear solution, white cake
2% NCC-FP / PC (no AO)	Clear solution, white cake (cracked after drying)
2% MF40-10 / PC	Noticeable yellowing of solution, brown burnt pieces in powder
2% MF40-10 / PC	Noticeable yellowing of solution, brown burnt pieces in powder
2% NCC-FP / PC	Clear solution, white cake (cracked after drying)
2% UFC-100 / PC	Clear solution, white cake

The material obtained by solution casting was blended in a blender until forming a white powder to facilitate feeding the extruder. The 2% MF 40-10 / PC samples were slightly

discoloured. Figure 5.2 shows the appearance of the as-received StarPlastic Polycarbonate compared to the 2% NCC-Alb / PC sample.

a)   b)
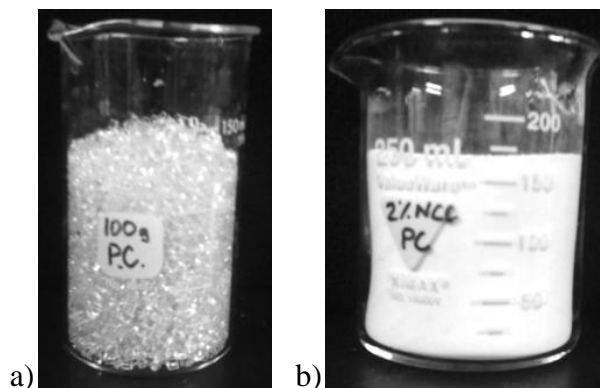
Figure 5.2 – Appearance of a) StarPlastic polycarbonate, b) 2% NCC-Alb / PC

5.1.2 –Melt-Compounding

The melt-compounding was carried out in using the twin-screw micro-extruder. The objective was to melt and mix the power prepared by solution casting. The product of extrusion is called an extrudate. A test of increasing the revolutions per minute of the extruder was completed to determine the optimal rate, where minimal yellowing of the polycarbonate was observed at a temperature of 250 °C. The revolutions per minute of the twin screws that were tested include 50, 75, 100, 150, 200, and 250 rpm. The material processed at 250 rpm was the most translucent polycarbonate obtained and was chosen as the working rate (RPM) as it was close to the maximum setting of the extruder. Increasing the rate (RPM) decreases the residence time, but it also increases the shear rate in the sample. Figure 5.3 shows the PC sample extruded at 50, 75, 100, 150, and 200 rpm. Unfortunately a 250 rpm sample was unavailable at the time of the photo. It is clear that there may be some shear damage to the polycarbonate seen in the yellowing of the extrudates. This is a definite disadvantage of working with temperature restrictions as the material's properties could be severely affected.

Figure 5.3 – Effect of extruder's twin-screw rotation speed on polycarbonate discolouration over 50, 75, 100, 150, and 200 rpm

After extrusion of the composite materials, it was apparent that there was some thermal degradation of the nanocellulose as a result of exposure to temperatures close to the onset of its thermal degradation. It is likely that the addition of the nanocellulose contributed to increasing the viscosity or melt flow index. Increasing the viscosity of the sample would lead to further increase in shear stress, thus further contributing to degradation of the nanocellulose or polycarbonate. This was seen as yellowing or browning of the samples colour. Particularly, the 2% NCC-Alb / PC, 2% MF 40-10 / PC (dried), 2% MF 40-10 / PC (solution), and 2% NCC-FP composites had very increased melt flow rates which lead to thinning and beading of the extrudates. The 2% NCC-FP / PC (no antioxidant) and 2% UFC-100 / PC composite samples seemed similar in melt flow index to the StarPlastic PC. The quantitative analysis of the melt flow rates of the composites is available later in the Processability section to further understand and discuss this phenomenon.

Figure 5.4 – Noticeable browning of composite samples after extrusion and pelletizing From LR: PC, 2% NCC-Alb / PC, 2% NCC-FP / PC (no antioxidant), 2% MF 40-10 / PC (dried), 2% MF 40-10 (solution), 2% NCC-FP / PC, and 2% UFC-100 / PC.

5.1.3 – Compression Moulding

The extrudate was cut in smaller pieces (approximately 1 cm long) and used for preparation of specimens by compression moulding. These rectangular specimen bars were prepared for mechanical testing according to ASTM's D256, D790 and D1708 for impact flexural and tensile tests, respectively. Due to the lower temperature of 220 °C that the compression moulder was controlled, the additional discolouration of the material was negligible. Figure 5.5 depicts three of the composite samples after pressed into D256 and D790 size specimen bars.
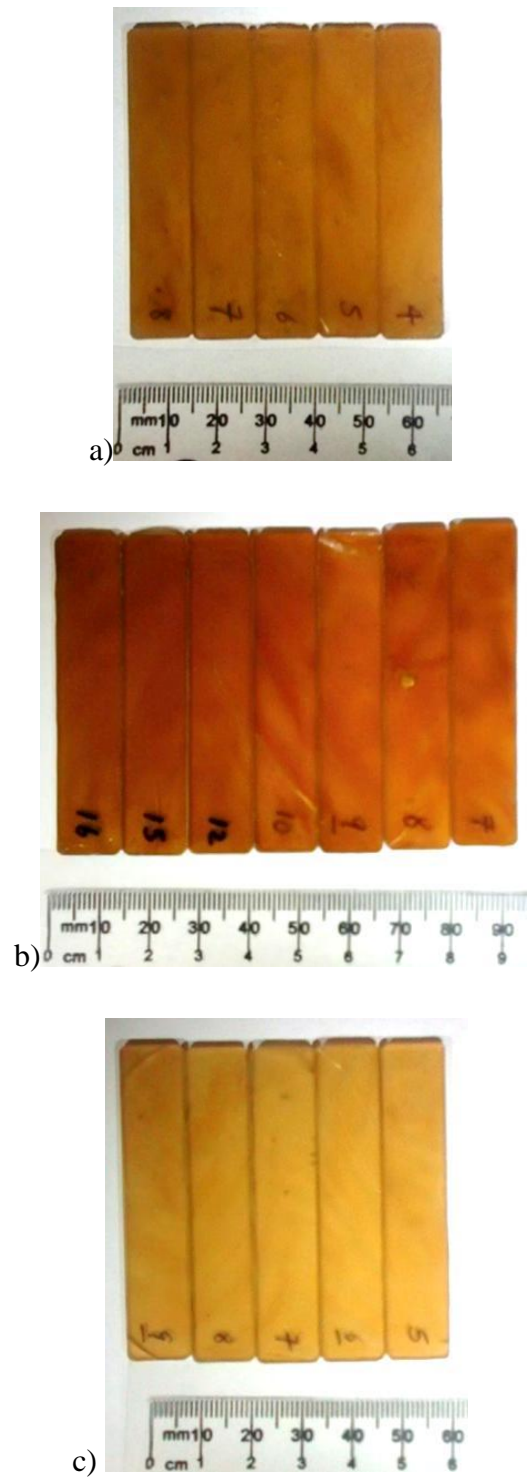
Figure 5.5 – Appearance of a) 2% NCC-Alb / PC, and b) 2% NCC-FP / PC (no AO), and c) 2% NCC-FP / PC ASTM D256 and D790 specimen bars

5.2 - Polymer Characterization

5.2.1 – Mechanical Properties

The mechanical properties for StarPlastic polycarbonate were determined from the tensile and flexural stress-strain curves following ASTM methods: D1708 for microtensile and D790 for flexural testing. The average slope of the elastic region of each tensile and flexural curve was determined as the modulus of the material. The average maximum stress achieved in the tensile and flexural tests was also calculated as the yield strength of the polycarbonate. The standard deviation was calculated using the testing of 5 specimen bars. The tensile modulus for polycarbonate was 372 MPa with a standard deviation of 40.2 MPa. The flexural modulus was 1419 MPa with a standard deviation of 101.66 MPa. The specification sheet for the grade of StarPlastic Polycarbonate that was used here had tensile and flexural moduli of 2410 MPa.

A number of factors may have contributed to this deviation in mechanical properties compared to specification, including the presence of moisture, internal stresses during moulding or cooling of the moulds, or some plasticization caused by the mould release agent (WD40). For the sake of comparison, it is assumed that these differences are consistent among the different composite materials and these values will work well as a baseline comparison. Additionally, the yield strengths for the StarPlastic polycarbonate are 58.7 ($\pm$3.68) and 75.06 ($\pm$4.4) MPa respectively; this is compared to the materials specification of 62.1 and 89.6 MPa for tensile and flexural yield strength, respectively. The tensile and flexural stress strain curves for StarPlastic polycarbonate specimens are included in Figure 5.6.

a)
b)
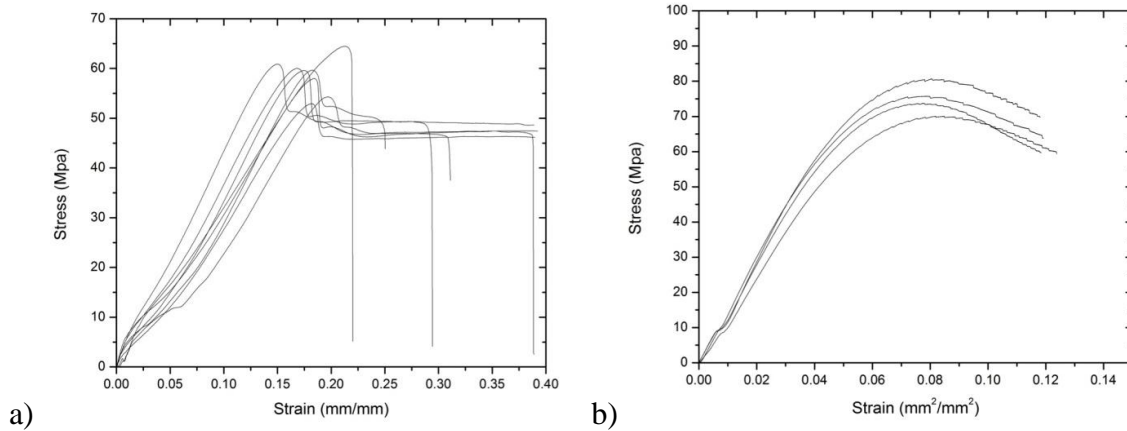
Figure 5.6 – Stress-Strain curves for a) tensile and b) flexural tests performed for StarPlastic polycarbonate

The impact resistance for StarPlastic polycarbonate was determined from the notched Izod impact test following ASTM method D256. The resulting impact resistance for the polycarbonate was 776.65 ($\pm$17.34) J/m, comparing well to 801 J/m data on the material specification sheet and with literature [Allen 1973]. The specification sheets for the general material and the specific batch used have been included in Appendix 1. All of the mechanical properties for StarPlastic polycarbonate material and its specification data have been collected in Table 5.3.

Table 5.3 – Mechanical properties for tensile, flexural, and impact tests performed for StarPlastic polycarbonate

	Property	Measured Value	Standard Deviation	Specification	Units
Tensile	Tensile Strength	58.72	3.68	62.1	[MPa]
	Tensile Modulus	372.22	40.26	2410	[MPa]
	Extension at break	0.330	0.070	-	[mm/mm]
Flexural	Flexural Strength	75.06	4.42	89.6	[MPa]
	Flexural Modulus	1419.08	101.66	2410	[MPa]
	Extension at break	0.120	0.003	-	[mm]
Impact	Impact Resistance	776.65	17.34	801	[J/m]

5.2.2 – Thermal Properties

The thermal properties of the StarPlastic polycarbonate were measured using thermal gravimetric analysis (TGA) and differential scanning calorimetry (DSC): including glass transition, melting point, and onset of degradation. The glass transition temperature is the point

of inflection at the top of the DSC thermogram, appearing at 142 ºC. The melting point of the sample appears as a valley or inflection on the bottom of the curve when the endothermic is plotted towards the bottom of the graphic. The melting point in our sample of polycarbonate is difficult to locate, but is somewhere around 238 ºC suggesting that the crystallinity in the sample is low. The second heating ramp was used to analyse the sample after erasing the thermal history affected by processing (moulding). In the second heating ramp the melting point is no longer visible, thus suggesting that crystallinity was during processing by moulding. Also, although the material has a melting point of 238 ºC, the material begins to flow somewhere around 150 ºC. The low amount of crystallinity is further confirmed by the fact that the polymer is very transparent due to a highly amorphous structure; with increased crystallinity it would become more hazy or opaque due to molecular arrangement within the material. The DSC and TGA curves for StarPlastic polycarbonate are in Figure 5.7. [Wissler 1980]

a)

b)
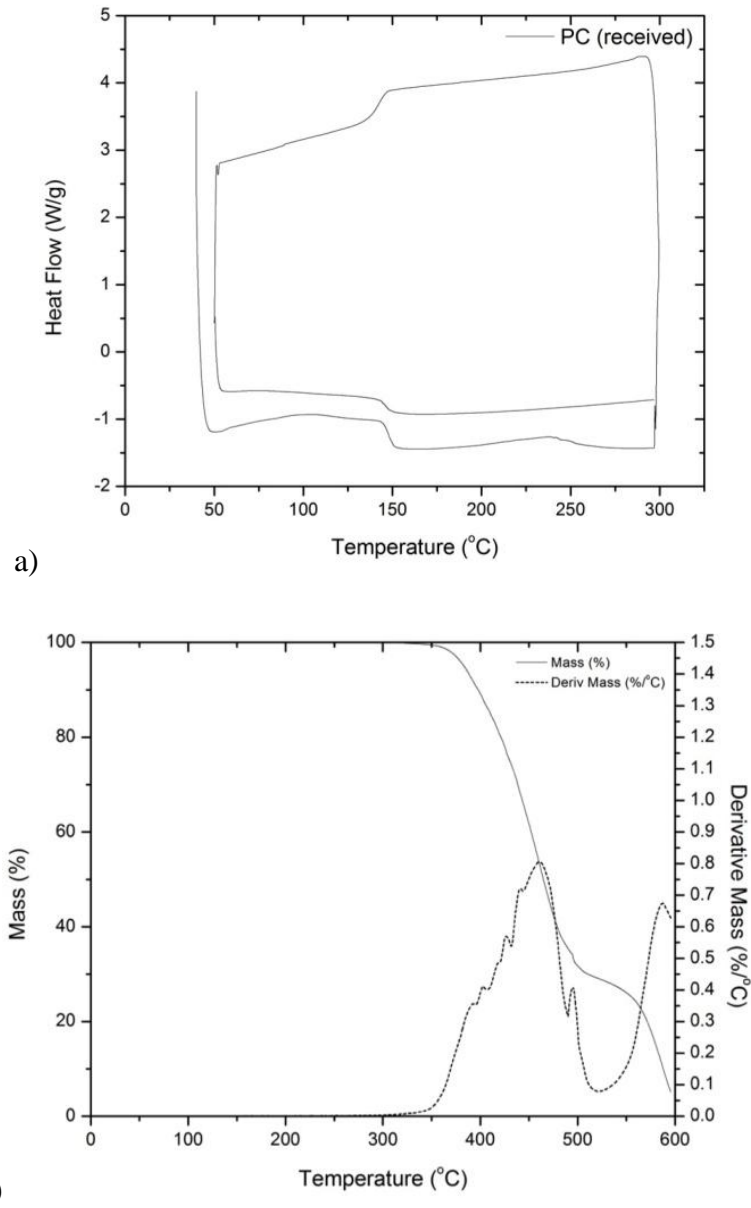
Figure 5.7 – a) DSC and b) TGA thermograms for StarPlastic polycarbonate

The onset of degradation was determined by finding the temperature corresponding to 1 wt-% degradation of the material. In the case of the polycarbonate, the onset of degradation is at 361 ºC. The different thermal properties for StarPlastic polycarbonate are included below in Table 5.4.

Table 5.4 – Thermal properties for StarPlastic polycarbonate

Thermal Property (Polycarbonate)	Temperature (°C)
Onset of Degradation	361.73
Glass Transition	142.22
Melting Point	238.32

This initial characterization of polycarbonate thermal properties was completed to determine feasible working temperatures for our solution casting, extrusion and compression moulding techniques. The ease at which the polycarbonate can flow, or the melt flow index, will be quantified for a set of different temperatures next in Processing Properties.

5.2.3 – Processing Properties

The melt flow index (MFI) for polycarbonate was determined over a set of expected working temperatures to better understand the viscosity, or processing properties, the material will have. This is a standard ASTM procedure, D1238, and has specific parameters for polycarbonate materials – applying a 1.2 kg load at 300 °C. The StarPlastic PC specification sheet gives an MFI of 12.0 g/10min; this was verified in the lab and also tested for other temperatures and weights. At 300°C, the melt flow index found for the StarPlastic PC was 13.41 g/10min, or slightly above the expected 12.0 g/10min recorded on the specification sheet. The higher melt flow index measured in the laboratory hints at some moisture or impurity acting as a plasticizer incorporated in the material either during or post-processing. The MFI drops as the temperature is reduced; below 270 °C a heavier load was used. The collected data is tabulated in Table 5.5 and graphically represented in Figure 5.8.

Table 5.5 – Melt flow indices for StarPlastic polycarbonate over various temperatures and loads

Temperature (°C)	MFI (g/10min)	
	[2.16kg]	[1.2kg]
250	3.86	1.98
260	6.53	-
270	9.26	-
280	-	7.374
290	-	10.025
300	-	13.41
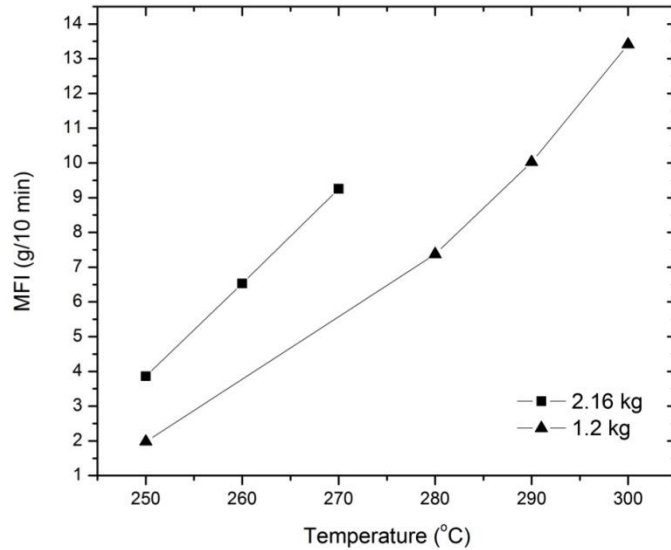
Figure 5.8 – Melt flow indices for StarPlastic polycarbonate over various temperatures and loads

5.2.4 – Chemical Properties

Table 5.6 lists some bonds characteristic to polycarbonate as well as the corresponding infrared absorption wavenumber. The FTIR spectra includes peaks corresponding to CH_3, CO, C-C, C=C, and part of the carbonate bond, C-O-C. The FTIR spectrum for StarPlastic polycarbonate is included in Figure 5.9. The FTIR was recorded in relatively thick and thin films to allow identification of peaks in different regions of the spectrum. [Griffiths 2007]

Table 5.6 – Some characteristic FTIR peaks associated with StarPlastic polycarbonate and the corresponding wavenumbers

Peak Wavenumber (cm^-1)	Corresponding Chemical Bond
3528	OH
2971	CH3
1791	CO
1602	CC
1514	CC
1019	C-O-C

a)

b)
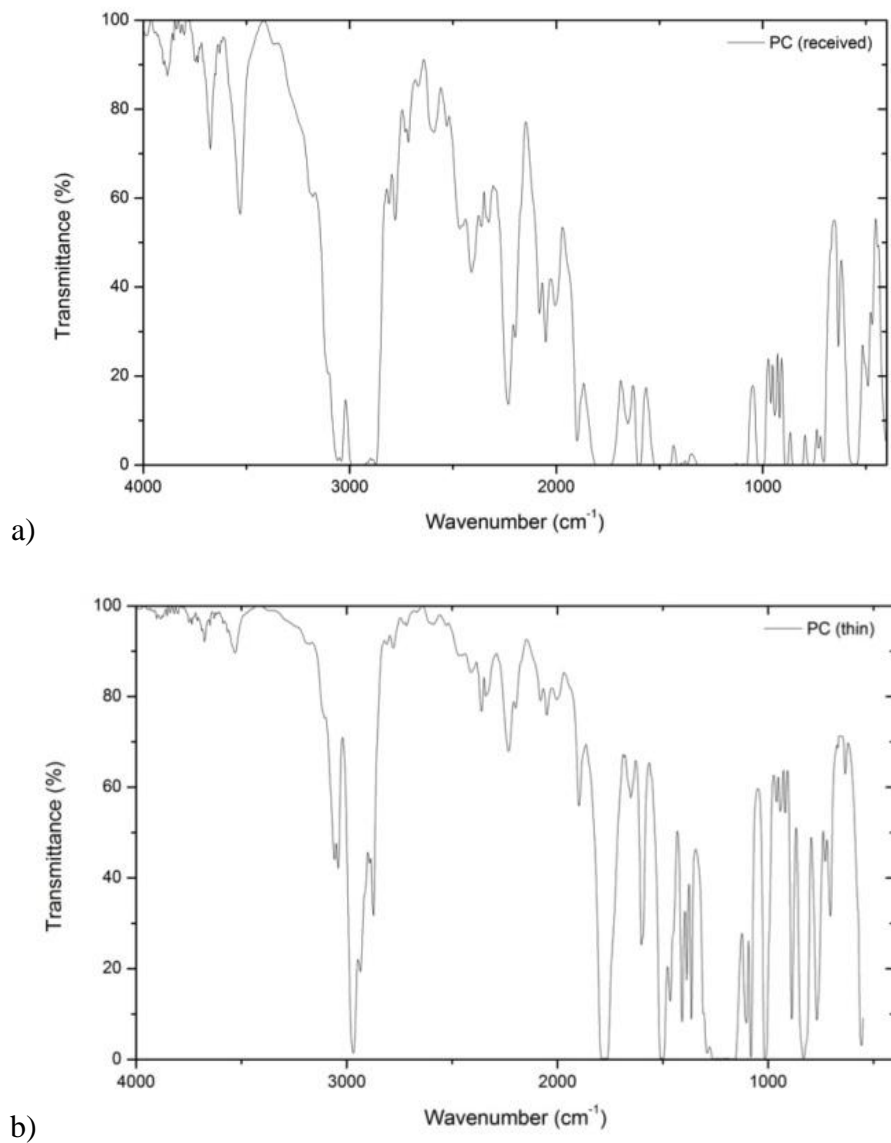
Figure 5.9 – FTIR spectrum of a) relatively thick film and b) relatively thin film of StarPlastic polycarbonate

5.3 – Nanocellulose Characterization

5.3.1 – Surface Morphology

Scanning electron microscopy (SEM) was used for investigation of the surface morphology of the nanocellulose samples.   For each sample the powder was affixed to the sample stub using carbon tape. After drying in vacuum, the SEM sample stubs were sputtered with a thin film of gold to increase conductivity. This thin film of gold is approximately 10 to 20 nm thick based on

the 120 s exposure time in the gold plasma. Two micrographs of each sample have been included: one that attempts to depict micro-scale features typical to a microfibril source, and another that shows identifiable features at the nano-scale.

Images are shown for three Sigma-Aldrich cellulose sources: Cellulose, fibrous, medium; SigmaCell Type 50; and SigmaCell Type 101. The purpose of imaging the Sigma-Aldrich sources is to give an idea of what is to be expected for a micro-fibrillated cellulose source before analysing the morphology of the nanocrystalline cellulose.

Figure 5.10 shows two micrographs of Cellulose, fibrous, medium from Sigma-Aldrich. It can clearly be seen in the first micrograph that the source is very fibre-like, with high aspect ratio fibres. Judging by the differences in diameter of the two visible fibres, a wide distribution of fibre sizes and aspect ratios may exist in the sample. It also appears that the cellulose fibres are over 10's of micrometres in diameter, and possibly nearing a hundred micrometres long, confirming that there are no nanofibrils present in the sample. As the magnification increases, nano-scale features appear on the surface and at the ends of the microfibril, however they were not isolated from the microfibril source.
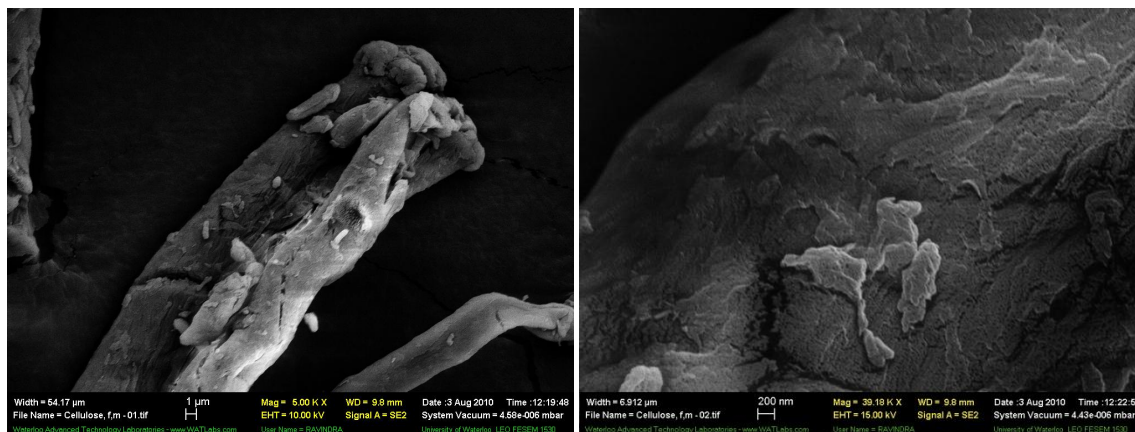
Figure 5.10 – SEM micrographs of Sigma Cellulose Powder, Fibrous, medium

Figure 5.11 shows two micrographs of SigmaCell Type 50 (SC50). It can clearly be seen in the first micrograph that the source is not very fibrilar, with a low aspect ratio particle. This cellulose source is known to have a particle size distribution centred on 50 μm (spanning 21-125 μm) [Kaziltas 2008]. As the magnification is increased, nano-scale features can be clearly seen.

In sample SC50, the surface structure appears fibrous, with the tips of some nanofibril bundles peeling away from the surface. Again, these nano-scale fibres or fibrils were not isolated.
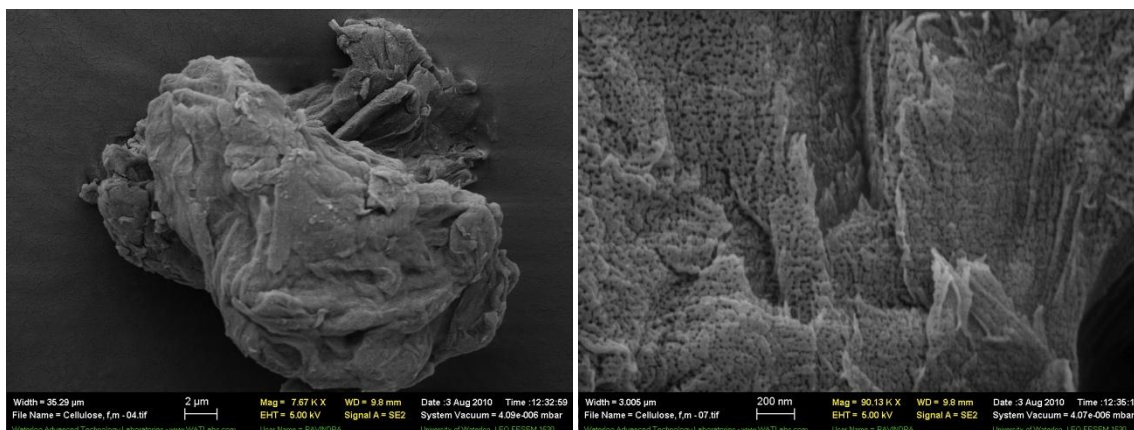
Figure 5.11 – SEM micrographs of Sigma SigmaCell® (Cellulose) Type 50

Figure 5.12 shows two micrographs of SigmaCell Type 101 (SC101). It can clearly be seen in the first micrograph that the source is somewhat fibrilar, with some aspect ratio to the particles. The known particle distribution of SC101 is 15.02 ± 0.91 μm [Dourado 1998]. As the magnification is increased, clear nanofibrils made up of dozens of cellulose chains are apparent at the surface of the fibre, also appearing more isolated from the surface compared to Cellulose, fib, med. and SC50. It appears that among the three Sigma-Aldrich samples, the different methods used for preparation of these materials have been employed, resulting in particles of about 100+ μm, 50 μm, and 15 μm for Cellulose, fib, med, SC50 and SC101, respectively. Information about the method used for preparation of these samples is not available from Sigma-Aldrich.
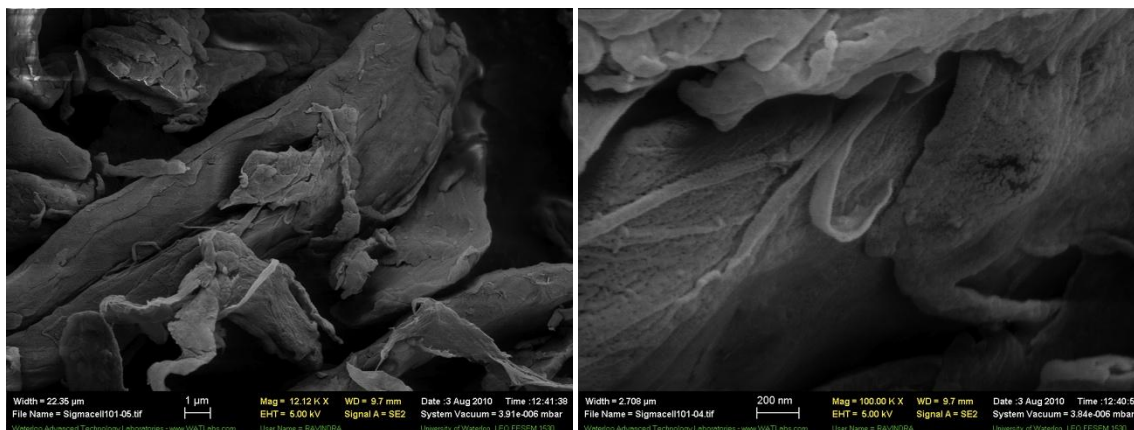
Figure 5.12 – SEM micrographs of Sigma SigmaCell® (Cellulose) Type 101

As it was discussed in Chapter 2, several methodologies including chemical and enzymatic treatments can be used to continue to reduce the cellulose fibre particle size. This work includes samples from three companies working on developing this technique: JRS Inc. of Germany, Alberta Innovates-Technology Futures, and FP Innovations in Canada. Two JRS Inc. samples are MF 40-10 and UFC-100; the Alberta Innovate-Technology Futures sample is NCC-Alb; and the FP Innovation sample is NCC-FP.

Figure 5.13 shows two micrographs of JRS Arbocel NANO MF 40-10 (MF40-10) nano disperse cellulose. It can clearly be seen in the first micrograph that this sample is very whisker-like. The aspect ratio of this nanocellulose ranks around medium when compared to the other samples. According to the specification sheet, the medium particle diameter is less than 1 μm and it was designed for the paper coatings industry. The particle distribution appears very narrow, and the presence of some impurity between the particles is apparent. Being designed as a coating, surfactants or other additives may have been incorporated to aid in its original design purpose. Increasing the magnification of the sample, there are in fact some nano-scale features on the surface of the fibre, including what appears to be a very porous surface likely caused by degassing during the drying process of the dispersion.
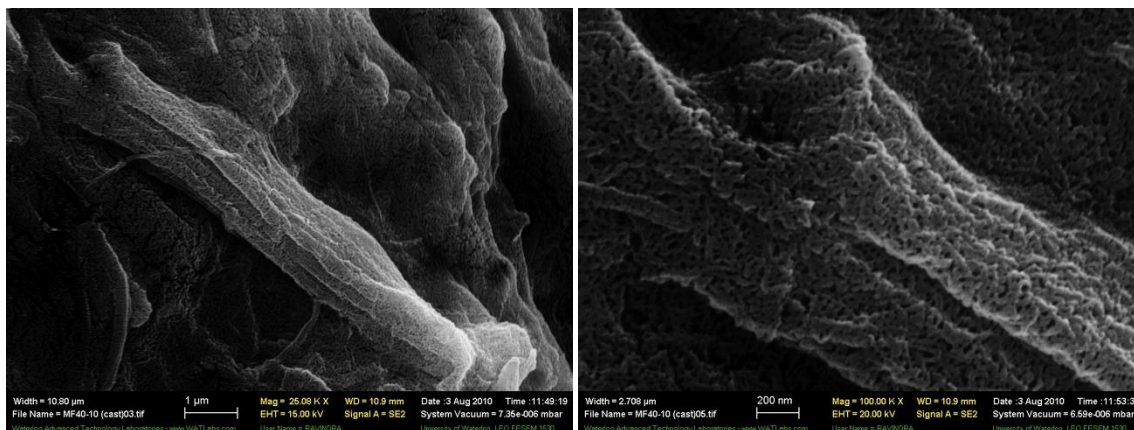
Figure 5.13 – SEM micrographs of JRS Arbocel® NANO MF 40-10 Nano Disperse Cellulose

Figure 5.14 shows two micrographs of JRS Arbocel UltraFine Cellulose 100 (UFC-100). It can clearly be seen in the first micrograph that the source is very fibrilar, with high aspect ratio fibres. The distribution of the fibres size and aspect ratio appears large but according to literature it is 1 μm. As the magnification is increased, nano-fibrils can be seen bundled together at the end of a larger microfibril.
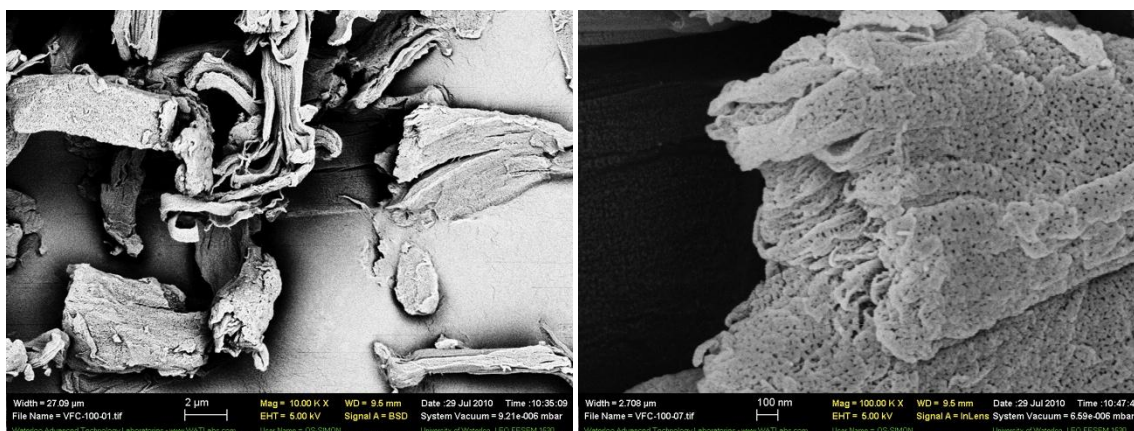
Figure 5.14 – SEM micrographs of JRS Arbocel® UFC-100 Ultrafine Cellulose

Figures 5.15 and 5.16 show two micrographs each of Nanocrystalline Cellulose from Alberta Innovates-Technology Futures (NCC-Alb) and FP Innovations (NCC-FP), respectively. These two cellulose sources are the most refined and processed of all the sources tested. Each of these samples arrived as a translucent flaky material as if the final processing step consisted of some solvent removal via compression or filtration. The low magnification images for the NCC sources depict the smooth surface of the cellulose flakes as well as the roughness observed at a

crack or edge of the materials. Small fibrous extrusions are observed, similar to the edge of a ripped piece of paper. As the magnification is increased small fibres with lengths of about 100 to 200 nm were observed as if they had agglomerated during processing.
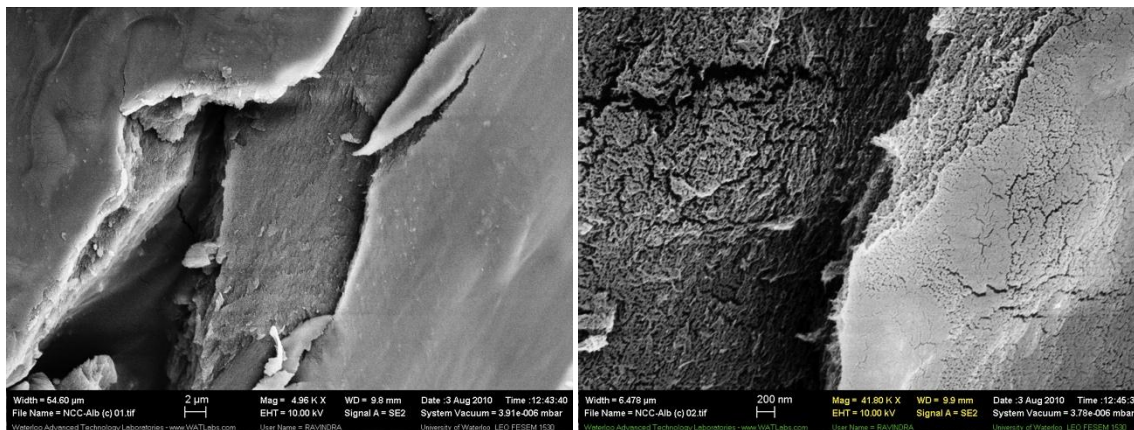
Figure 5.15 – SEM micrographs of Alberta Innovates – Technology Futures Nanocrystalline Cellulose
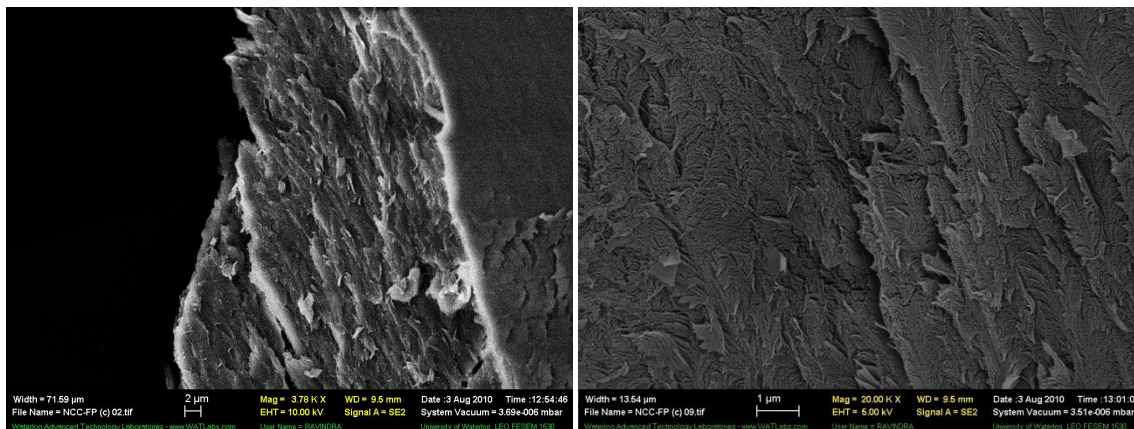
Figure 5.16 – SEM micrographs of FP Innovations Nanocrystalline Cellulose

Using Dynamic Light Scattering (DLS) techniques, the particle sizes for NCC-Alb and NCC-FP were found to be about 103.4 and 222.9 nm in length respectively, dispersed in water. The DLS analysis has been included in Appendix 2.

It is apparent that the source of the cellulose is critical to the particle size and morphology and it does indeed vary widely from source to source. This is expected, as the cellulose may have been isolated from different trees or crops. Because of the complexity and variety of isolation and pulping techniques (introduced earlier in Chapter 2), it too is expected that the

quality of the resulting fibres be different and diverse. This is an important point to be considered when evaluating the physical properties of the nanocellulose samples and their composites.

5.3.2 – Chemical Composition

The chemical composition for cellulose was investigated through FTIR analysis. Different from the FTIR sample preparation for the Polycarbonate, the cellulose samples were mixed with KBr powder and pressed into a pellet. KBr is transparent in the IR range and the resulting spectrum is characteristic of the cellulose sample only that is contained within. Table 5.7 lists some of the IR peaks characteristic of cellulose. The large band between 4,000 and 2,995 cm^{-1} corresponds with the OH stretching within bound water molecules and at the cellulose surface. The band around 1,635-1,638cm^{-1} corresponds to OH bending. The peak at 2,971cm^{-1} is characteristic of CH stretching, 1,430 cm^{-1} is characteristic of HCH and OCH in plane bending, 1,375 cm^{-1} corresponds to CH deformation vibrations, and at 900 cm^{-1} there are effects from COC, CCO, and CCH deformation.

Table 5.7 – Some expected FTIR peaks associated with typical cellulose sources and the corresponding wavenumbers [Griffiths 2007]

Peak Wavenumber (cm^{-1})	Corresponding Chemical Bond
4,000 - 2,995	OH (stretching)
2,971	CH (stretching)
1,971	CH$_3$
1,791	CO
1,638 – 1,635	OH (bending)
1,602	CC
1,514	CC
1,430	HCH, OCH (plane bending)
1,375	CH (deformation)
1,019	COC
900	COC, CCO, CCH (deformation)

Figure 5.17 a) shows a stacked FTIR spectrum of each of the cellulose materials. Figure 5.17 b) shows an overlay FTIR spectrum of each of the cellulose materials. Figure 5.17 c) shows

a detailed stacked FTIR spectrum of the region 1,800 to 800 cm^{-1} of each of the cellulose materials. Figure 5.17 d) shows a detailed overlay FTIR spectrum of the region 1800 to 800 cm^{-1} of each of the cellulose materials.

Individual FTIR spectrographs for each of the cellulose sources are available in Appendix 3.

a)

b)
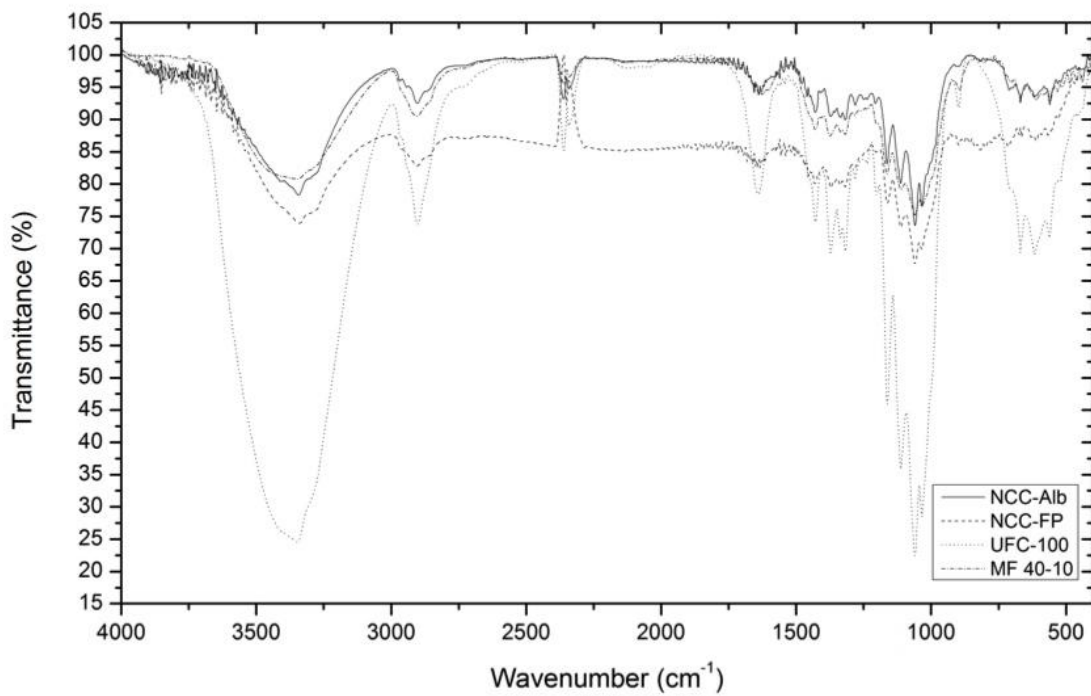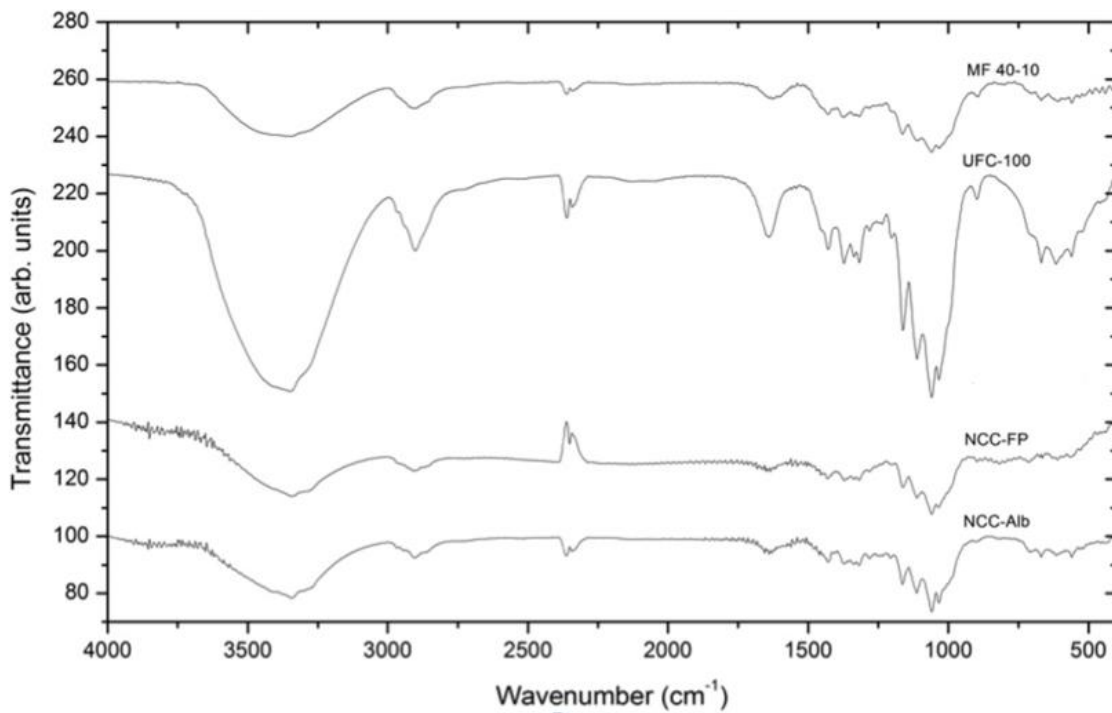
Figure 5.17 – a) Stacked plot, b) overlay plot, c) detailed stacked plot, and d) detailed overlay plot of each nanocellulose source FTIR spectrum as prepared by KBr pellet
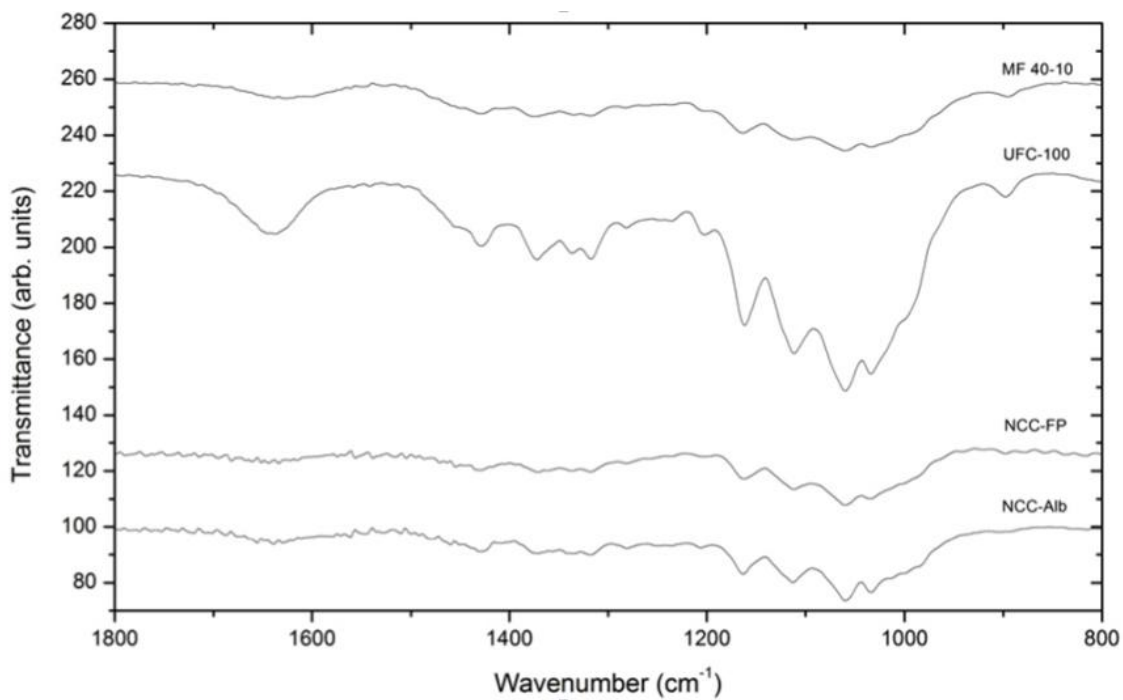
c)
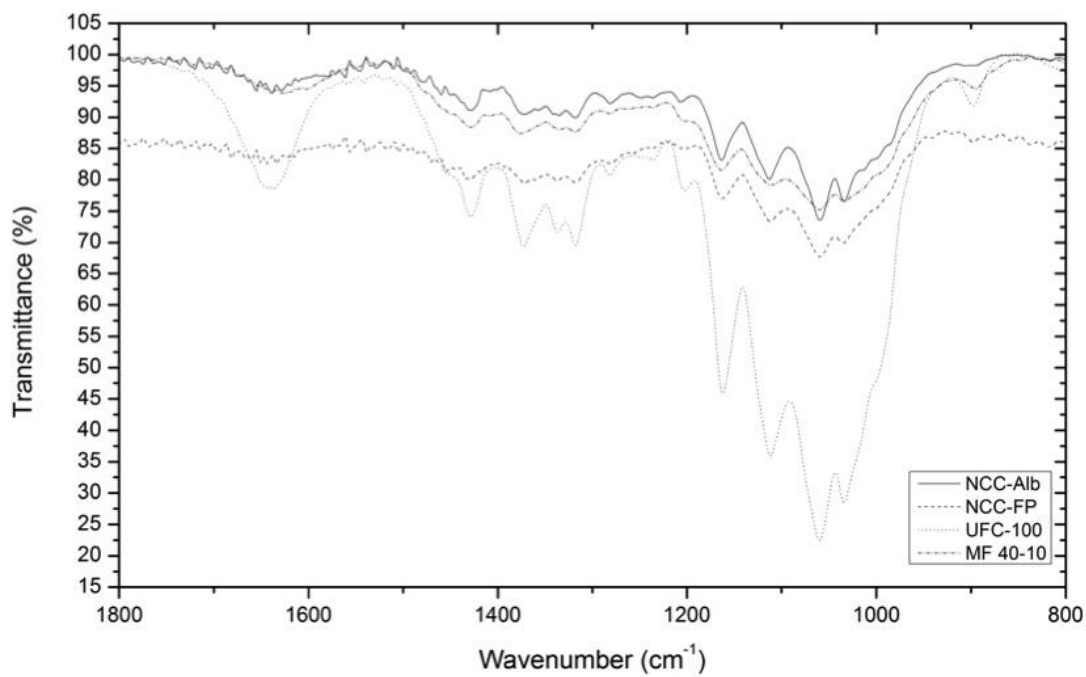
d)

Figure 5.17 (continued) – a) Stacked plot, b) overlay plot, c) detailed stacked plot, and d) detailed overlay plot of each nanocellulose source FTIR spectrum as prepared by KBr pellet

5.3.3 – Crystallinity

The crystallinity index of the cellulose sources was determined using X-ray diffraction techniques. The XRD diffractogram for each of the cellulose samples is included in Figure 5.18; more detailed XRD diffractograms for each sample including the modelled curves (result of deconvolution) are included in Appendix 4.
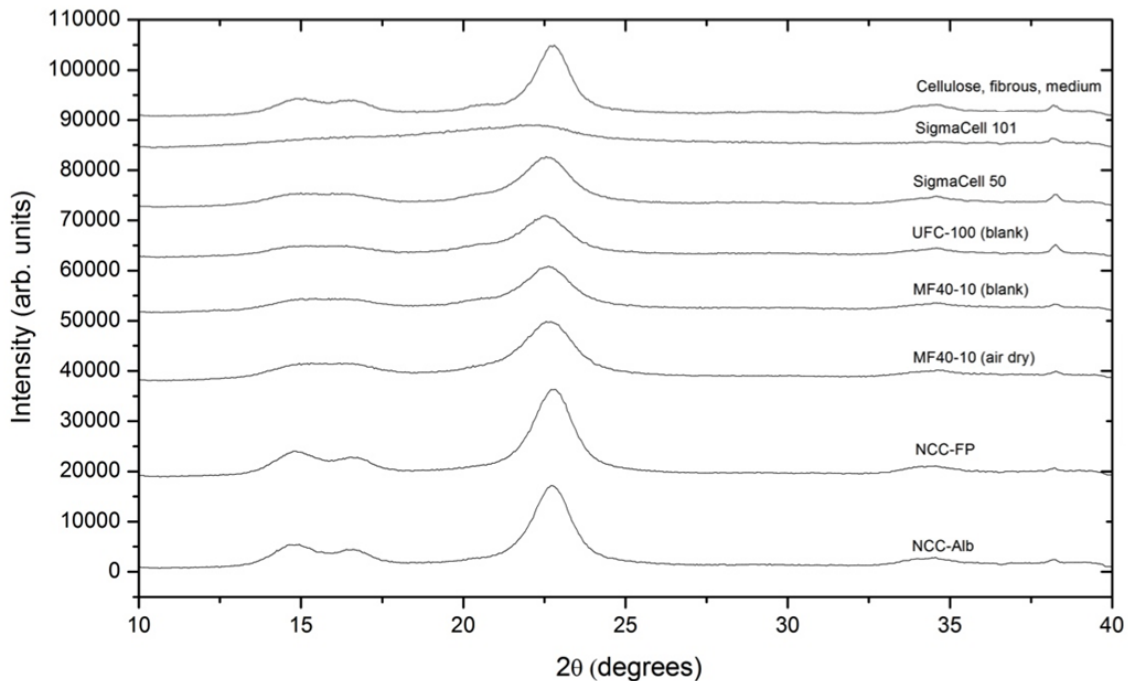
Figure 5.18 – XRD diffractogram for each cellulose source

Using Origin plotting software's peak deconvolution tool, the characteristic peaks for (101), (10-1), (021), (002), and (040) reflection planes were modelled as separate Gaussian distributions. After dividing the area under the curve of the peaks corresponding to crystalline regions by the entire area under the curve, % CI was calculated. Table 5.8 shows the determined crystallinity index for each cellulose source and the R-squared value for the fitted curve after peak deconvolution. Individual XRD diffractograms and the fitted curves are included in Appendix 4.

Table 5.8 – a) Miller indices and corresponding 2θ value for crystalline mirror planes and b) crystallinity index of cellulose sources received

a)

Miller Index	2θ
(101)	14.83
(10-1)	16.46
(021)	20.98
(002)	22.67
(040)	34.48

b)

Sample	%CI	R-squared
UFC-100	71.02	0.99053
NCC-FP	78.82	0.99077
NCC-Alb	80.23	0.99035
NCC-Alb (Blank)	89.79	0.98394

UFC-100 had a %CI of 71%, NCC-FP was 79%, NCC-Alb was 80%, and after an ethanol washing this NCC-Alb sample increased to 90%. It is expected the increase in NCC-Alb's %CI can be attributed to the removal of some of the impurities observed in the TGA analysis. The crystallinity index of the cellulose tested fell between 70% and 90% and corresponds somewhat with literature values reported by Sunkyu Park et al in his reference on, "Cellulose crystallinity index: measurement techniques and their impact on interpreting cellulase performance." Park reports %CI from 50% to 70% for microfiber cellulose sources via the XRD peak deconvolution technique. Park also makes comparisons to different XRD and NMR techniques for determining %CI. The further refining and processing to purify the sources used in this study likely improved the crystallinity index as amorphous material is being removed from the crystalline phases. [Park 2010, Rowe 1994]

Also, by finding the full-width at half-maximum (FWHM) of each of the de-convoluted peaks and plugging into the Scherrer equation (K=1) gives an approximate value of the grain size of the cellulose in that mirror direction. The grain sizes measured in four of the five crystalline directions have been included in Table 5.9, most of the grain sizes fall within the range of 5-9 nm. This corresponds with the size of bundled crystalline regions of cellulose chains within a nanofibril as discussed earlier to be 3 to 10 nm. This also matches with literature values of 4 to 7 nm reported by Teeaar et al. in "Crystallinity of cellulose, as determined by CP/MAS NMR and XRD methods," and 2.2 to 7.5 nm reported by Garvey et al.[Teeaar 1987, Garvey 2005]

Table 5.9 – Crystallite or grain size measured in each reflection plane direction

Sample	Reflection			
	(101) d (nm)	(10-1) d (nm)	(021) d (nm)	(002) d (nm)
UFC-100	5.75	6.09	6.02	5.16
NCC-FP	6.06	7.05	8.65	6.34
NCC-Alb	6.12	7.18	7.02	6.51
NCC-Alb (Blank)	6.82	7.57	5.68	6.71

5.3.4 - Hygroscopic Properties

The inherent moisture content of the cellulose sources was tested to determine not only the amount of moisture contained within the sample, but also to see how well the moisture was bound to the surface of the cellulose. This was done with an isothermal heating of 110 °C until the mass change was negligible. By determining the time required to reach no mass change gives a good indication of the necessary drying time before mixing.

The final moisture content was calculated over four replicates for each sample. The samples were conditioned at ambient temperature and humidity (23±2 °C and 50±10 % Relative Humidity) for at least 48 hours before drying. The order of cellulose sources, from the most to least moisture content is: 1) SigmaCell 101, 2) NCC-FP, 3) UFC-100, 4) MF 40-10, 5) SigmaCell 50, 6) NCC-Alb, and 7) Cellulose, fib, med. The moisture content ranged from close to 10% down to around 4%. The standard deviation was relatively high for sample MF 40-10. Coincidently, the MF 40-10 sample was the only one of the group that was received as dispersion in water and required drying before %MC analysis.

All of the moisture content tests were finished in less than 10 minutes, suggesting that one hour of drying at temperatures above 110 °C should be more than sufficient before solution casting to eliminate moisture contamination. Table 5.10 lists the moisture content of each of the cellulose samples and the standard deviation over 4 replicates. Figure 5.19 depicts the moisture content of each sample in a bar graph with error bars.

Table 5.10 – Moisture content by weight of each cellulose source at ambient conditions (23 °C, 50% RH)

Sample	Moisture Content (%)	Standard Deviation (%)
Cell., fib, med	4.17	0.74
MF 40-10	5.66	2.19
NCC-Alb	4.89	0.56
NCC-FP	6.37	0.45
SigmaCell 101	9.83	0.47
SigmaCell 50	5.59	0.69
UFC-100	6.31	0.40
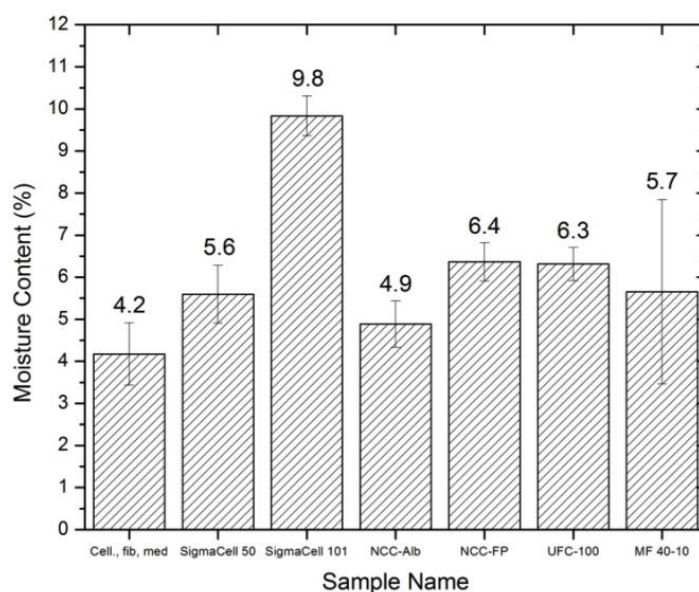
Figure 5.19 – Moisture content by weight of each cellulose source at ambient conditions (23 °C, 50% RH)

The NCC samples reached their stabilized mass faster than the other samples, but each took less than 10 minutes to dry. The impurities in the non-NCC samples may hold the moisture longer than the more crystalline NCC samples. The moisture content analysis curves for each individual source and test are available in Appendix 5.

5.3.5–Thermal Stability

The thermal stability of the NCC samples is very important since the processing with polycarbonate is done at a relatively high temperature. Typical processing temperatures for polycarbonate can be as high as 310 ^{o}C. The information on the thermal stability of nanocellulose samples is seldom reported in the literature. Moreover, it is difficult to compare the data from different reports in the literature; because sometimes, the investigations were carried out in different conditions (type of method, sample preparation, type of gas, temperatures scanning rate, etc.).

Here, the thermal stability of the cellulose was investigated using thermal gravimetric analysis. The plots for the non-isothermal thermogravimetric analysis of the Sigma-Aldrich cellulose samples in both air and nitrogen at a heating rate of 10 ℃ per minute are presented in Figure 5.20. This includes Cellulose, fib, med, SigmaCell 50, and SigmaCell 101. These are HPLC grade cellulose fibres; they should be high in purity and contain little or no impurities. The purpose of analyzing these Sigma-Aldrich samples is to familiarize with the typical profile of pure cellulose for later comparison to the cellulose sources in this study.
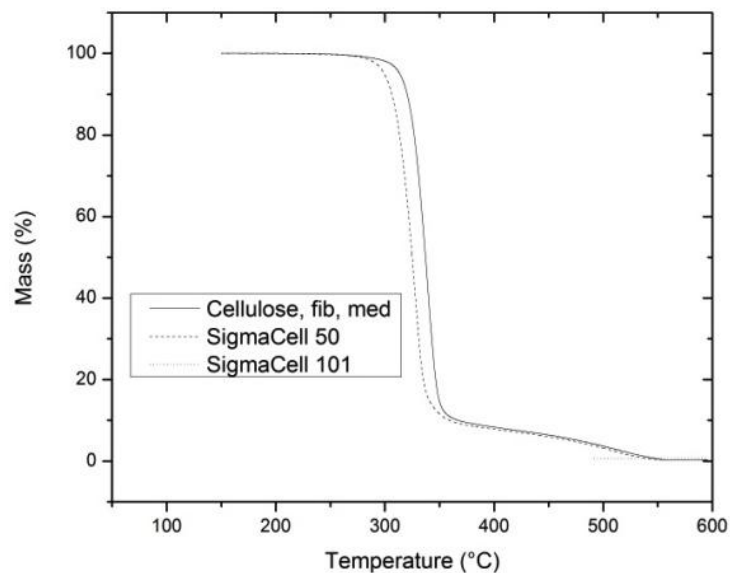
a)
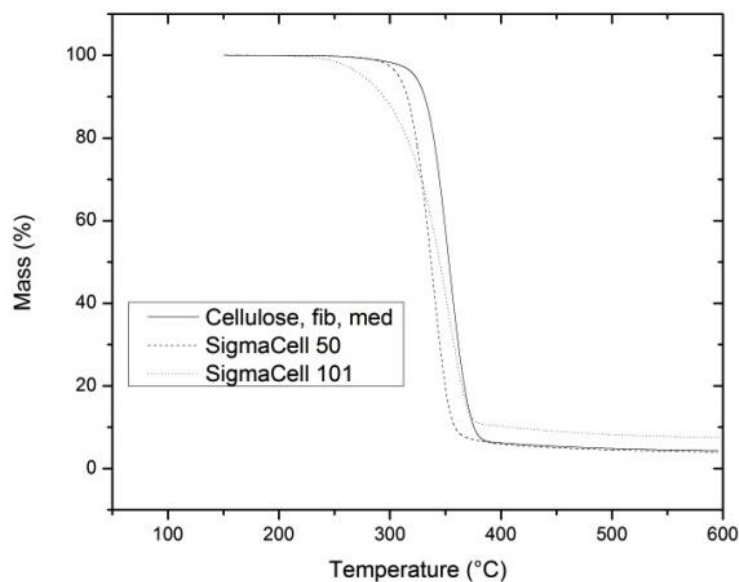
b)

Figure 5.20 – Non-isothermal TGA of three different cellulose materials from Sigma-Aldrich in a) air and b) nitrogen at 10°C/min

It can be seen that the mass of the cellulose sample decreases in mass as the temperature increases. It can also be seen that the onset of degradation for samples heated in air occurs slightly earlier than samples in nitrogen. For example, 10ºC per minute in air SigmaCell 50 sample has an onset of 279 ºC with the onset 5 ºC higher in nitrogen. The onset temperatures for

each heating rate and gas for each of the three Sigma-Aldrich samples has been tabulated in Table 5.11.

Four different regions can be observed in each thermogram separated by a large change in rate of degradation. Initially in the first region, the mass decreases at a very slow rate between 150 ℃ and approximately 300 ℃. In the second region between approximately 300 ℃ and 350 ℃, the rate of mass loss increases significantly and about 90% of the mass is lost in this short time. The temperature at which the rate of mass loss increases significantly is the *onset of degradation temperature* of the material; here a 1 wt-% conversion is used to quantify the onset.

In the third region, the degradation rate decreases significantly. In nitrogen, the rate is much lower than in air as the lack of oxygen is likely hindering some oxidation of the remaining residue. The final region of the thermograms is quite different depending on the purge gas. In air, the cellulose once again increases in the rate of mass loss until it plateaus at a very small mass (residual ash) around 550 ℃. In nitrogen, the rate of mass loss decreases and continues to fall slightly until 600 ℃, the end of the test. The reason for this difference is the complete versus incomplete combustion between the oxygen-rich air and oxygen-free nitrogen. The residues remaining at the conclusion of each TGA run (600℃) have been included in Table 5.11 for reference.

Table 5.11 – Thermal stability parameters for three different cellulose samples from Sigma-Aldrich

Fibre (gas)	Heating Rate (°C/min)	Onset Temperature (°C)	Mass Loss at 600°C (%)	Residue at 600°C (%)
Cellulose Powder				
(Air)	10	285	99.72	0.28
(Nitrogen)	10	284	95.70	4.30
SigmaCell 50				
(Air)	10	279	99.76	0.24
(Nitrogen)	10	284	96.00	4.00
SigmaCell 101				
(Air)	10	241	99.35	0.65
(Nitrogen)	10	243	92.50	7.50

The plots for the thermogravimetric analysis of the Nanocrystalline Cellulose from Alberta Innovates – Technology Futures (NCC-Alb) in both air and nitrogen at heating rates of 5, 10, 20, 30, and 40℃ per minute are presented in Figure 5.21. As observed, a slower heating rate means

an earlier degradation than at a faster heating rate. In air, the onset of degradation for the 5ºC per minute heating rate is 249ºC, whereas for 40ºC per minute the onset is higher at 277ºC, a 28ºC increase. It can also be seen that the onset of degradation for samples heated in air occurs slightly earlier than samples in nitrogen. For example, 20ºC per minute in air has an onset of 268ºC with the onset 2ºC higher for nitrogen. The onset temperatures for each heating rate and gas for NCC-Alb sample have been tabulated below in Table 5.12 for easy reference.

a)

b)
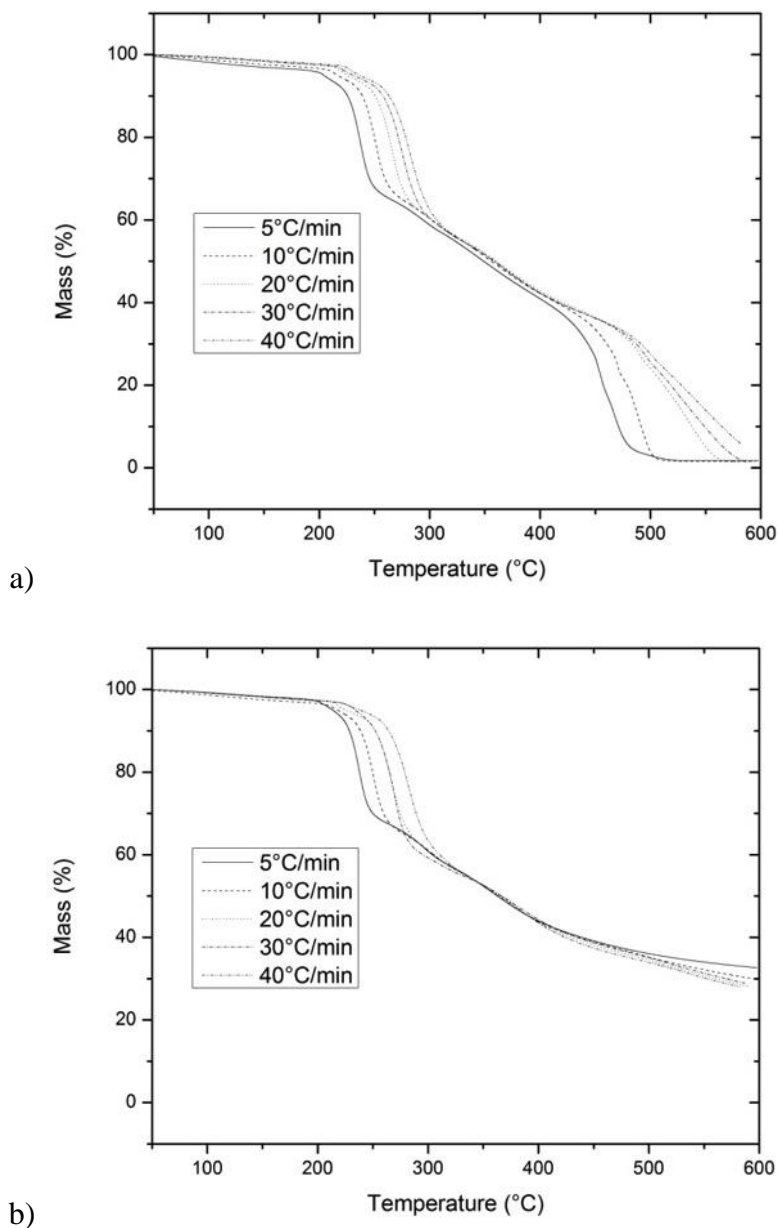
Figure 5.21 – Non-isothermal TGA of Nanocrystalline Cellulose from Alberta Innovates – Technology Futures in a) air and b) nitrogen at five heating rates 5, 10, 20, 30, and 40°C/min

The drop observed in the second region of the curve is about 30%, much lower than the 90% observed with the pure Sigma-Aldrich sources. There is also some observable slope in the first region of the curve, this may be attributed somewhat to moisture, but this is unlikely as there is not a sharp drop at 100 ºC (boiling point of water). It is reported in the literature that this degradation profile is actually characteristic of the presence of some lignin in the sample due to incomplete purification during processing of the cotton fibres [Ramiah 1970, Abidi 2007].

Table 5.12 – Thermal stability parameters for Nanocrystalline Cellulose from Alberta Innovates

Fibre (gas)	Heating Rate (°C/min)	Onset Temperature (°C)	Mass Loss at 600°C (%)	Residue at 600°C (%)
NCC-Alb (Air)	5	249	98.28	1.72
	10	256	98.47	1.53
	20	268	98.56	1.44
	30	274	98.48	1.52
	40	277	94.29	5.71
NCC-Alb (Nitrogen)	5	251	67.38	32.62
	10	258	70.08	29.92
	20	270	72.06	27.94
	30	274	71.13	28.87
	40	275	72.02	27.98

The Ozawa-Flynn-Wall (OFW) method was used for determining the activation energy of thermal decomposition. The data required for application of this method is obtained from TGA curves. For NCC-Alb conversions of 5, 10, 20, and 30% were used to complete the OFW analysis. The region of 5% to 30% was chosen as it is in second region described above where the initial majority of mass loss occurs and is of most interest to the current study. Processing cellulose within a polymer matrix will typically require temperatures at or below the onset of degradation temperature and it can be assumed that mass loss will come primarily from region 2 during processing. The activation energies in air at 5, 10, 20 and 30% conversion were found to be 139.1, 124.2, 111.9, and 113.0 kJ/mol respectively, with an average 122.1 kJ/mol. The activation energies in nitrogen at 5, 10, 20 and 30% conversion are 155.0, 128.2, 116.7, and 125.3 kJ/mol respectively, with an average 131.3 kJ/mol. The complete results are tabulated in Table 5.16 for easy comparison.

The TGA thermograms for NCC-FP are included in Figure 5.22. It can be seen that the thermal degradation profile for NCC-FP is quite different than that of NCC-Alb and closer to the

Sigma-Aldrich samples. For NCC-FP, the moisture content loss around 100 ℃ was a clean step drop for each sample, unlike NCC-Alb. The mass loss due to moisture content was then truncated from the thermogram, as this was previously determined using a different methodology, and each thermogram for NCC-FP was normalized to the mass of the sample at 150 ℃. This was done for all samples excluding NCC-Alb. It is likely that the NCC-FP has fewer impurities than NCC-Alb, as there is no mass loss soon after the water is removed as illustrated by a flat line with no slope in region 1.

a)

b)
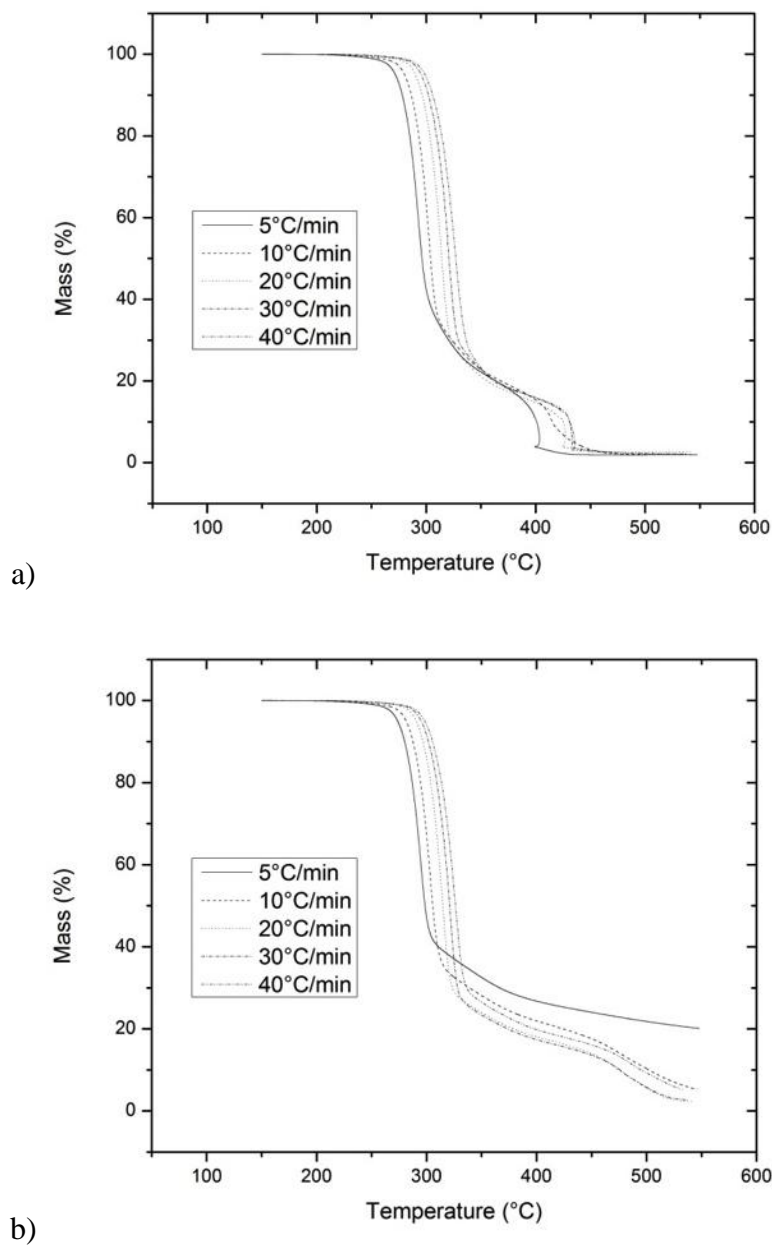
Figure 5.22 – Non-isothermal TGA of Nanocrystalline Cellulose from FP Innovations in a) air and b) nitrogen at five heating rates 5, 10, 20, 30, and 40°C/min

Region 2 for NCC-FP once again shows a similar trend as NCC-Alb where the slower heating rates have an earlier onset of degradation and the air purge gas onset occurs before the corresponding nitrogen sample. In air, the onset for a 5°C per minute heating rate is 249°C, whereas for 40°C per minute it is 277°C, a 28°C increase in onset. It can also be seen that the onset for samples heated in air occurs slightly earlier than in nitrogen. For example, 20°C per

minute in air has an onset of 268ºC with the onset 2ºC higher for nitrogen. The onset temperatures for each heating rate and gas for NCC-FP sample have been tabulated in Table 5.13 for convenience. The onset temperatures found for NCC-FP were calculated at a 1 wt-% conversion.

Another observation about region 2 is that the mass loss drop here is much larger than the 30% for NCC-Alb reaching about 60% or 70% mass loss before an inflection. This is another hint that NCC-FP has fewer impurities as a larger proportion of the sample lost mass at the same temperature than did for the NCC-Alb samples indicating a more homogeneous material. Region 3 and 4 for NCC-FP are similar to NCC-Alb although with less mass; in air the mass quickly drops to a residual ash mass and in nitrogen it slowly decreases until the end of the run at 550 ºC. The mass loss observed in Figure 5.22 for NCC-FP in air around 400 ºC was caused by insufficient temperature control in the TGA unit in that temperature range (this is typical when fast and exothermic reactions causing the temperature to be above the set point for a brief moment).

Table 5.13 – Thermal stability parameters for Nanocrystalline Cellulose from FP Innovations

Fibre (gas)	Heating Rate (°C/min)	Onset Temperature (°C)	Mass Loss at 550°C (%)	Residue at 550°C (%)
NCC-FP	5	249	98.07	1.93
(Air)	10	256	98.04	1.96
	20	268	97.31	2.69
	30	274	97.89	2.11
	40	277	97.92	2.08
NCC-FP	5	251	79.91	20.09
(Nitrogen)	10	258	94.80	5.20
	20	270	97.72	2.28
	30	274	97.33	2.67
	40	275	94.86	5.14

After collecting the thermograms, the Ozawa-Flynn-Wall method for determining the activation energy of thermal decomposition was implemented. For NCC-FP conversions of 5, 10, 20, 30 and 40% were used to complete the analysis. The activation energies in air at 5, 10, 20, 30 and 40% conversion are 186.1, 185.0, 183.2, 180.8, and 180.5 kJ/mol respectively, with an average 183.1 kJ/mol. The activation energies in nitrogen at 5, 10, 20, 30 and 40%

conversion are 204.7, 204.5, 199.3, 202.3, and 198.4 kJ/mol respectively, with an average 201.9 kJ/mol. The complete results are tabulated in Table 5.16.

The thermograms for UFC-100 are included in Figure 5.23. It can be seen that the thermal degradation profile is nearly identical to the Sigma-Aldrich samples. A drop to less than 5% of the original mass, even lower than the Sigma samples, this is likely attributed to extra processing beyond Sigma removing more impurities; seen earlier the UFC-100 particle size was much smaller than Sigma-Aldrich's. The onset of degradation and residue remaining at 600 ℃ are tabulated in Table 5.14.

Table 5.14 – Thermal stability parameters for UltraFine Cellulose (UFC-100) from JRS

Fibre (gas)	Heating Rate (°C/min)	Onset Temperature (°C)	Mass Loss at 600°C (%)	Residue at 600°C (%)
UFC-100 (Air)	5	256	99.80	0.20
	10	260	99.89	0.11
	20	276	99.83	0.17
	30	281	99.69	0.31
	40	286	99.15	0.85
UFC-100 (Nitrogen)	5	256	96.73	3.27
	10	261	98.11	1.89
	20	274	97.19	2.81
	30	281	97.29	2.71
	40	288	96.90	3.10
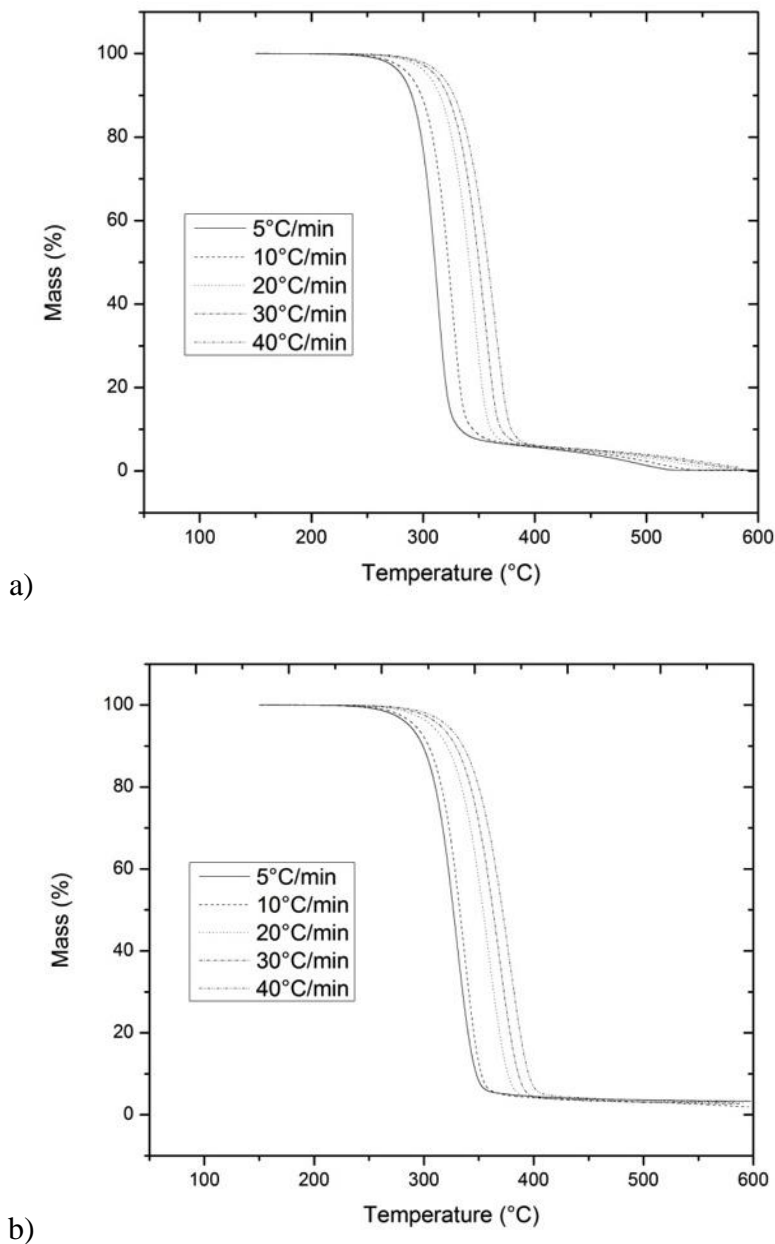
Figure 5.23 – Non-isothermal TGA of UltraFine Cellulose (UFC-100) from JRS in a) air and b) nitrogen at five heating rates 5, 10, 20, 30, and 40°C/min

After collecting the thermograms, the Ozawa-Flynn-Wall method for determining the activation energy of thermal decomposition was implemented. For UFC-100, conversions of 5, 10, 20, 30 and 40% were used to complete the analysis. The activation energies in air at 5, 10, 20, 30 and 40% conversion are 142.4, 140.0, 134.9, 130.8, and 128.6 kJ/mol respectively, with an average 135.3 kJ/mol. The activation energies in nitrogen at 5, 10, 20, 30 and 40%

conversion are 148.0, 145.9, 140.0, 136.2, and 133.6 kJ/mol respectively, with an average 140.8 kJ/mol. The complete results are tabulated in Table 5.16.

The thermograms for MF 40-10 after drying are included in Figure 5.24. It can be seen that the thermal degradation profile is of some resemblance to the Sigma-Aldrich samples, but the drop is not near as steep. The onset of degradation also occurs much earlier, near 230 ℃. This is most definitely attributed to some impurity that leads to mass loss at 40 ℃ earlier than the other cellulose sources. It is not clear at this moment if the mass loss is associated with a physical process (volatilization, evaporation) or with a chemical process (chemical reaction whereas the products are gases). The onset of degradation and residue remaining at 600 ℃ for MF 40-10 are tabulated in Table 5.15.

Table 5.15 – Thermal stability parameters for MF 40-10 from JRS

Fibre (gas)	Heating Rate (°C/min)	Onset Temperature (°C)	Mass Loss at 600°C (%)	Residue at 600°C (%)
MF 40-10 (Air)	5	224	99.57	0.43
	10	232	99.57	0.43
	20	244	100.00	0.00
	30	245	99.55	0.45
	40	249	99.57	0.43
MF 40-10 (Nitrogen)	5	224	85.22	14.78
	10	232	86.78	13.22
	20	242	89.76	10.24
	30	247	88.65	11.35
	40	251	88.64	11.36

a)

b)
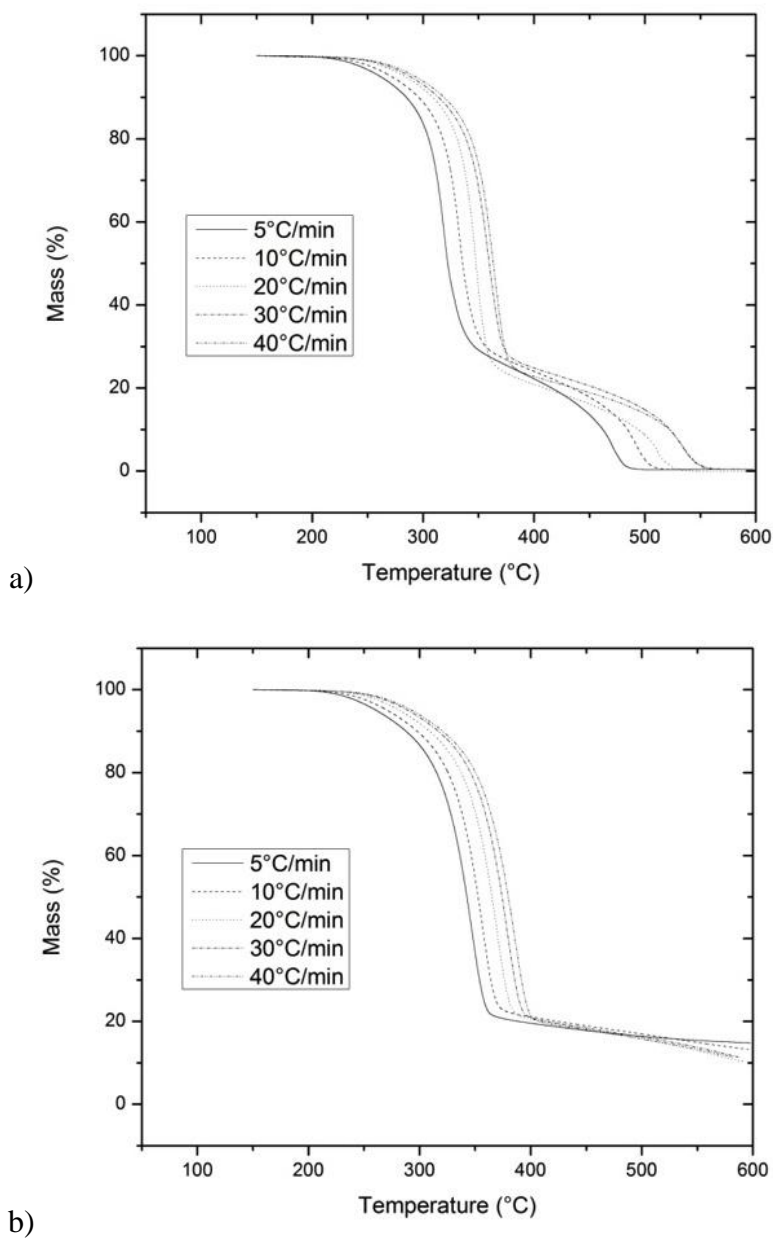
Figure 5.24 – Non-isothermal TGA of MF 40-10 from JRS in a) air and b) nitrogen at five heating rates 5, 10, 20, 30, and 40°C/min

After collecting the thermograms, the Ozawa-Flynn-Wall method for determining the activation energy of thermal decomposition was implemented. For MF 40-10 conversions of 5, 10, 20, 30 and 40% were used to complete the analysis. The activation energies in air at 5, 10, 20, 30 and 40% conversion are 155.4, 157.7, 151.3, 148.7, and 146.8 kJ/mol respectively, with an average 152.0 kJ/mol. The activation energies in nitrogen at 5, 10, 20, 30 and 40%

conversion are 151.2, 162.1, 168.3, 171.5, and 173.5 kJ/mol respectively, with an average 165.3 kJ/mol. The complete results are tabulated in Table 5.16.

Initially, looking through the data it can be seen that the nanocellulose sources have higher activation energy in nitrogen than in air; this difference is around 20 KJ/mol. This is understandable as a nitrogen atmosphere is less favourable to oxidization than oxygen rich air. Because the lines are nearly parallel, it confirms that the activation energies are relatively consistent and do not depend on previous conversion. Therefore, it can be concluded that the mechanism of thermal degradation remains the same for the temperature range where the activation energy is constant. The activation energies are tabulated in Table 5.16 for each conversion value in both air and nitrogen. This data is also plotted in Figure 5.25 up to a conversion of 40%. The main focus of this work is to better understand the onset of thermal degradation; therefore the conversions investigated here are limited to 40%. The log β versus 1/RT plots for determining the activation energy are included in Appendix 6.

The activation energy varies greatly depending on the source of nanocellulose. NCC-FP has the highest activation energy followed by MF 40-10, UFC-100, and NCC-Alb. The activation energies varied from 204.7 to 111.9 KJ/mol between the NCC-FP and NCC-Alb samples respectively. It was later found that a solvent wash of the NCC-Alb sample changes its TGA curve to be more similar of samples with higher activation energy. This topic was not further explored here and it is left as a suggestion for future work. It is assumed that the inconsistency and lower magnitude for NCC-Alb can be associated to inclusions of lignin or hemi-cellulose.
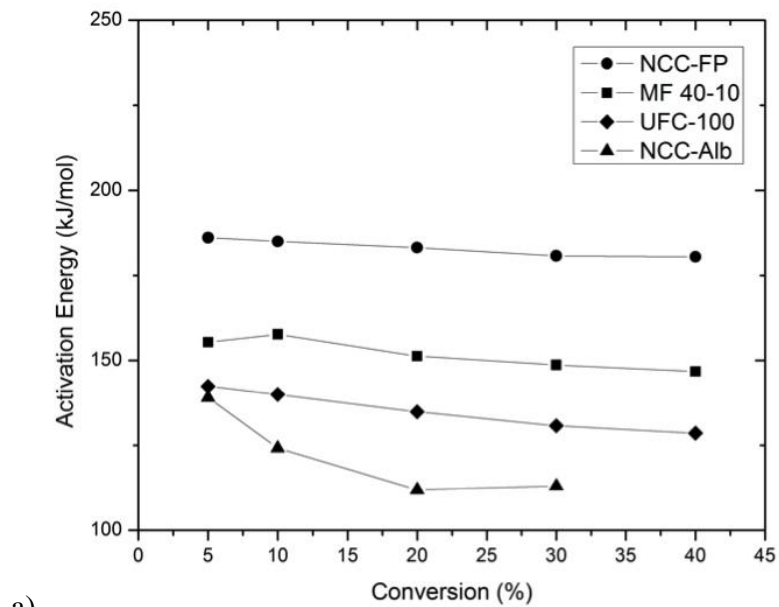
a)
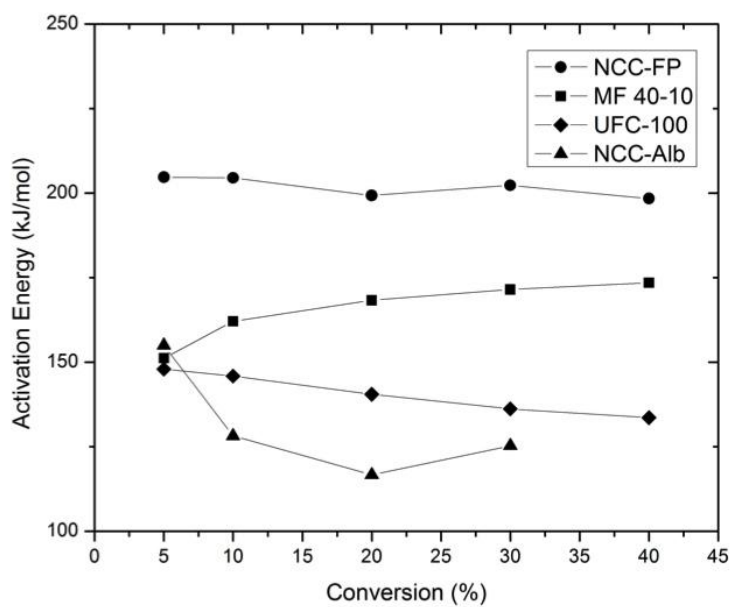
b)

Figure 5.25 – Comparison of activation energies at different conversions for as received Cellulose materials in a)

air and b) nitrogen

Table 5.16 – Activation energy calculated at different conversions for each cellulose sample

Fiber (gas)	Conversion (%)	R-Squared (OFW Line Fit)	Activation Energy (Ea) (KJ/mol)	Average Ea (KJ/mol)	St. Dev. Ea (KJ/mol)
NCC-FP (as received) (Air)	5	0.998	186.39		
	10	0.999	185.13		
	20	0.998	183.57		
	30	0.997	181.29		
	40	0.995	181.14	183.5	2.3
NCC-FP (as received) (Nitrogen)	5	0.998	205.08		
	10	0.999	204.69		
	20	0.998	202.61		
	30	0.997	199.83		
	40	0.995	199.29	202.3	2.7
NCC-Alb (as received) (Air)	5	0.993	139.82		
	10	1.000	124.19		
	20	0.999	111.98		
	30	0.995	113.44	122.4	12.9
NCC-Alb (as received) (Nitrogen)	5	0.935	164.15		
	10	0.997	122.93		
	20	0.998	111.81		
	30	0.991	120.96	130.0	23.3
UFC-100 (as received) (Air)	5	0.977	144.91		
	10	0.987	141.36		
	20	0.992	135.74		
	30	0.994	131.50		
	40	0.994	128.49	136.4	6.8
UFC-100 (as received) (Nitrogen)	5	0.963	152.27		
	10	0.962	150.08		
	20	0.961	144.82		
	30	0.960	140.36		
	40	0.958	137.88	145.1	6.1
MF40-10 (air dried) (Air)	5	0.995	155.96		
	10	0.996	158.11		
	20	0.999	151.43		
	30	0.998	148.96		
	40	0.996	147.25	152.3	4.6
MF40-10 (air dried) (Nitrogen)	5	0.999	151.33		
	10	0.998	162.33		
	20	0.998	168.58		
	30	0.997	171.89		
	40	0.996	173.94	165.6	9.1

5.4 - Nanocomposite Characterization Results and Discussion

5.4.1 – Mechanical Properties

The mechanical properties for the different cellulose-PC composites were determined from the tensile and flexural stress-strain curves following ASTM methods D1708 for microtensile and D790 for flexural testing. The average slope of the elastic region of each curve was determined as the modulus of the material. The average maximum stress achieved was also calculated as the yield strength of the composite material.

The tensile modulus for the 2% NCC-Alb / PC composite was 263 MPa with a standard deviation of 94.6 MPa over 5 specimen bars. The flexural modulus was calculated to be 2136 MPa with a standard deviation of 101 MPa.

The yield strengths for the 2% NCC-Alb / PC composite was 17.4 ($\pm$3.56) and 39.2 ($\pm$6.54) MPa respectively. The tensile and flexural stress strain curves for 2% NCC-Alb / PC composite are included in Figure 5.26.

a)   b)
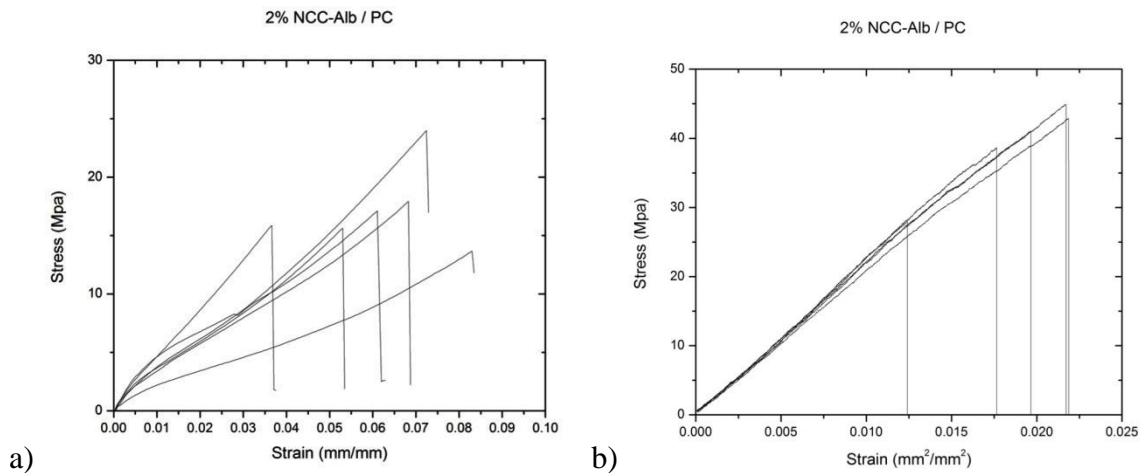
Figure 5.26 – Stress-strain curves for a) tensile and b) flexural tests performed for 2% NCC-Alb / PC

The impact resistance for 2% NCC-Alb / PC composite was determined from the notched Izod impact test following ASTM method D256. The impact resistance for the 2% NCC-Alb / PC composite was 5.73 J/m ($\pm$2.97), or extremely brittle in comparison to pure PC. All of the mechanical properties for 2% NCC-Alb / PC composite have been collected in Table 5.17.

Table 5.17 – Mechanical properties for tensile, flexural, and impact tests performed for 2% NCC-Alb / PC

	Property	Magnitude	Standard Deviation	Units
Tensile	Tensile Strength	17.36	3.56	[MPa]
	Tensile Modulus	263.13	94.64	[MPa]
	Extension at break	0.0632	0.0161	[mm]
Flexural	Flexural Strength	39.16	6.54	[MPa]
	Flexural Modulus	2136.62	101.66	[MPa]
	Extension at break	0.0187	0.0039	[mm]
Impact	Impact Resistance	5.73	2.97	[J/m]

The tensile modulus for 2% NCC-FP / PC (no antioxidant) composite was 345 MPa with a standard deviation of 95.1 MPa over 5 specimen bars. The flexural modulus was calculated to be 2136 MPa with a standard deviation of 161 MPa.

The yield strengths for the 2% NCC-FP / PC (no antioxidant) composite were 33.3 (±9.86) and 44.0 (±5.87) MPa respectively. The tensile and flexural stress strain curves for 2% NCC-FP / PC (no antioxidant) composite are included in Figure 5.27.
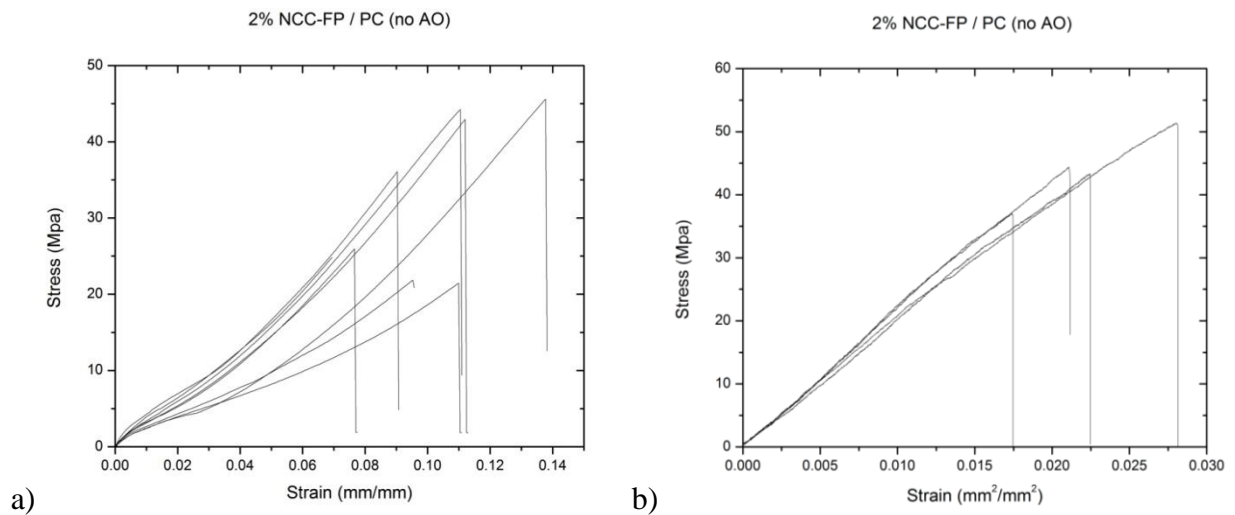
Figure 5.27 – Stress-strain curves for a) tensile and b) flexural tests performed for2% NCC-FP / PC (no AO)

The impact resistance for the 2% NCC-FP / PC (no antioxidant) composite was 41.5 (±8.26) J/m. All of the mechanical properties for 2% NCC-FP / PC (no antioxidant) composite have been collected in Table 5.18.

Table 5.18 – Mechanical properties for tensile, flexural, and impact tests performed for 2% NCC-FP / PC (no AO)

	Property	Magnitude	Standard Deviation	Units
Tensile	Tensile Strength	33.26	9.86	[MPa]
	Tensile Modulus	345.19	95.06	[MPa]
	Extension at break	0.0951	0.0186	[mm]
Flexural	Flexural Strength	44.04	5.89	[MPa]
	Flexural Modulus	2023.20	161.15	[MPa]
	Extension at break	0.0244	0.0047	[mm]
Impact	Impact Resistance	41.54	8.26	[J/m]

The determined tensile modulus for 2% NCC-FP / PC composite was 377.7 MPa with a standard deviation of 64.6 MPa over 5 specimen bars. The flexural modulus was calculated to be 1934 MPa with a standard deviation of 191 MPa.

The yield strengths for the 2% NCC-FP / PC composite were 56.3 ($\pm$2.67) and 25.4 ($\pm$6.47) MPa respectively. The tensile and flexural stress strain curves for 2% NCC-FP / PC composite are included in Figure 5.28.

a)   b)
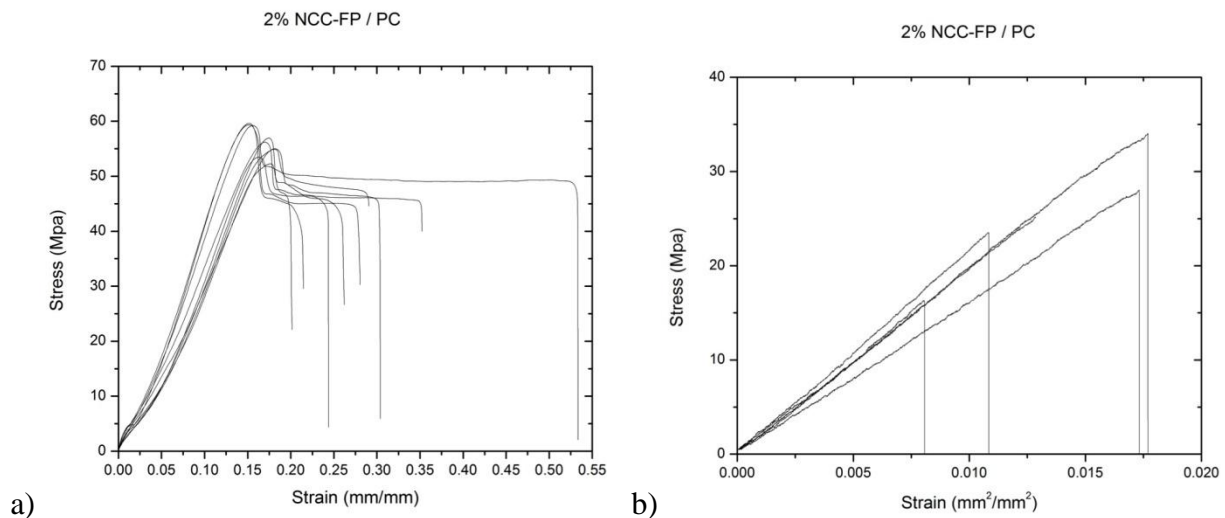
Figure 5.28 – Stress-strain curves for a) tensile and b) flexural tests performed for 2% NCC-FP / PC

The impact resistance for the 2% NCC-FP / PC composite was 5.38 ($\pm$1.13) J/m. All of the mechanical properties for 2% NCC-FP / PC composite have been collected in Table 5.19.

Table 5.19 – Mechanical properties for tensile, flexural, and impact tests performed for 2% NCC-FP / PC

	Property	Magnitude	Standard Deviation	Units
Tensile	Tensile Strength	56.33	2.67	[MPa]
	Tensile Modulus	377.74	64.63	[MPa]
	Extension at break	0.2982	0.0995	[mm]
Flexural	Flexural Strength	25.44	6.47	[MPa]
	Flexural Modulus	1933.66	191.39	[MPa]
	Extension at break	0.0134	0.0042	[mm]
Impact	Impact Resistance	5.38	1.13	[J/m]

The tensile modulus for 2% UFC-100 / PC composite was 436 MPa with a standard deviation of 66.8 MPa over 5 specimen bars. The flexural modulus was calculated to be 1924 MPa with a standard deviation of 83.2 MPa.

The yield strengths for the 2% UFC-100 / PC composite were 58.39 (±2.3) and 80.38 (±5.78) MPa respectively. The tensile and flexural stress strain curves for 2% UFC-100 / PC composite are included in Figure 5.29.


a) b)
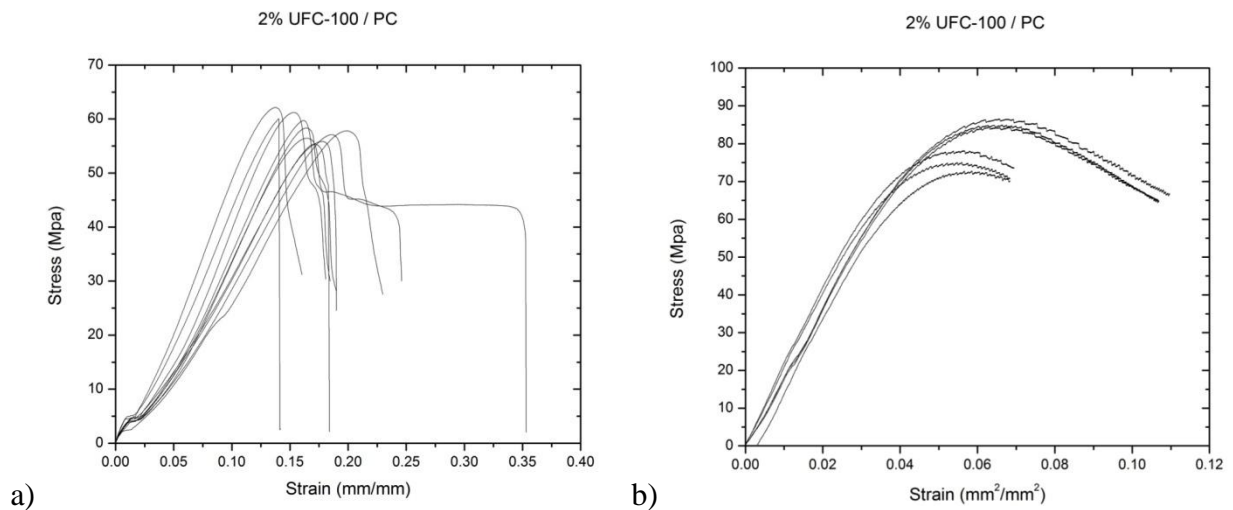
*Figure 5.29 – Stress-strain curves for a) tensile and b) flexural tests performed for 2% UFC-100 / PC*

The impact resistance for the 2% UFC-100 / PC composite was 118.5 (±19.5) J/m. All of the mechanical properties for 2% UFC-100 / PC composite have been collected in Table 5.20.

Table 5.20 – Mechanical properties for tensile, flexural, and impact tests performed for 2% UFC-100 / PC

	Property	Magnitude	Standard Deviation	Units
Tensile	Tensile Strength	58.39	2.30	[MPa]
	Tensile Modulus	436.50	66.79	[MPa]
	Extension at break	0.215	0.0841	[mm]
Flexural	Flexural Strength	80.38	5.78	[MPa]
	Flexural Modulus	1924.08	83.16	[MPa]
	Extension at break	0.0923	0.0213	[mm]
Impact	Impact Resistance	118.47	19.47	[J/m]

From the tensile and flexural data it can be seen that the incorporation of 2% UFC-100 resulted in similar strengths to the StarPlastic PC. Also, in tensile the NCC-FP samples showed only a slight drop in strength, more significant in flexural than tensile. The NCC-Alb sample shows a significant drop in both tensile and flexural strength.

Figure 5.30 shows a comparison of the tensile strengths and moduli of each of the composites with StarPlastic polycarbonate.

a)

b)
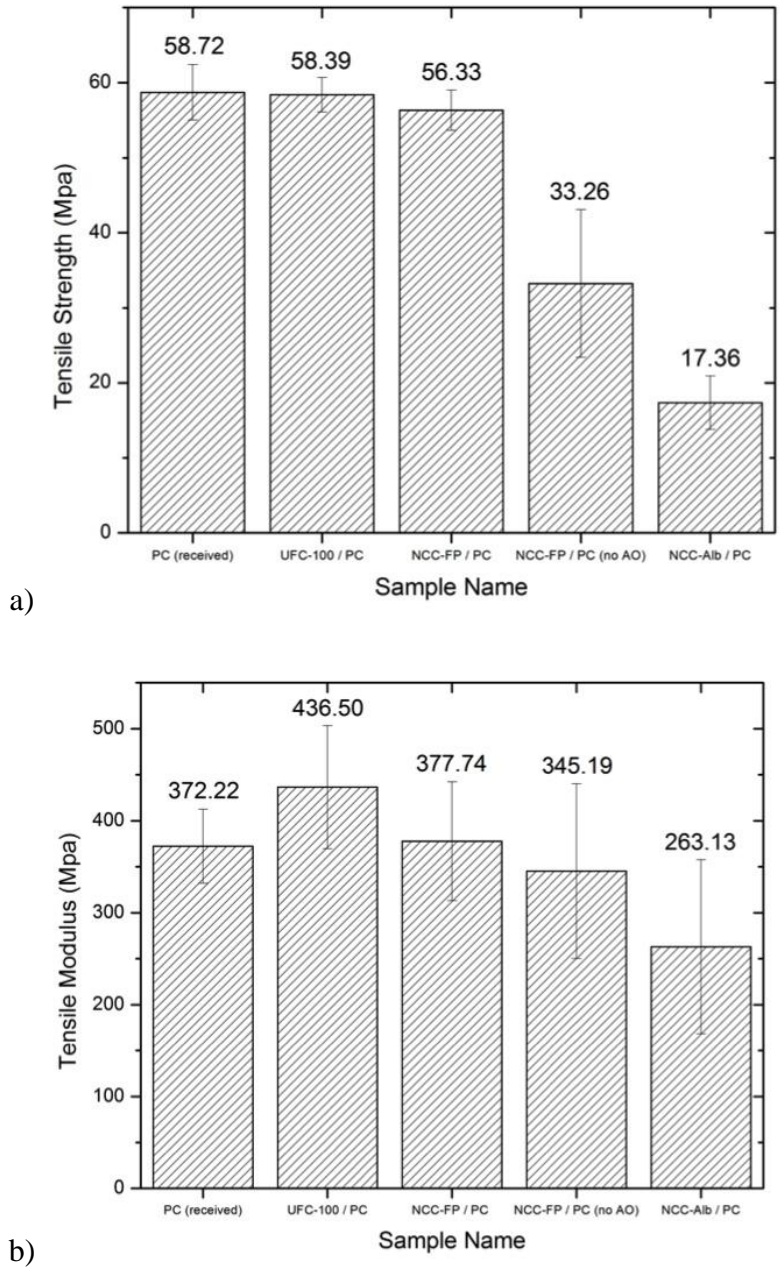
Figure 5.30 – Comparison of a) tensile strength and b) modulus for each cellulose-PC sample

The tensile modulus for 2% UFC-100 / PC saw an increase of 17% where as 2% NCC-FP with and without antioxidant were in agreement within error of the StarPlastic PC. A drop of nearly 30% in the tensile modulus was seen for the 2% NCC-Alb / PC sample.

Figure 5.31 shows a comparison of the flexural strengths and moduli of each of the composites with StarPlastic polycarbonate.
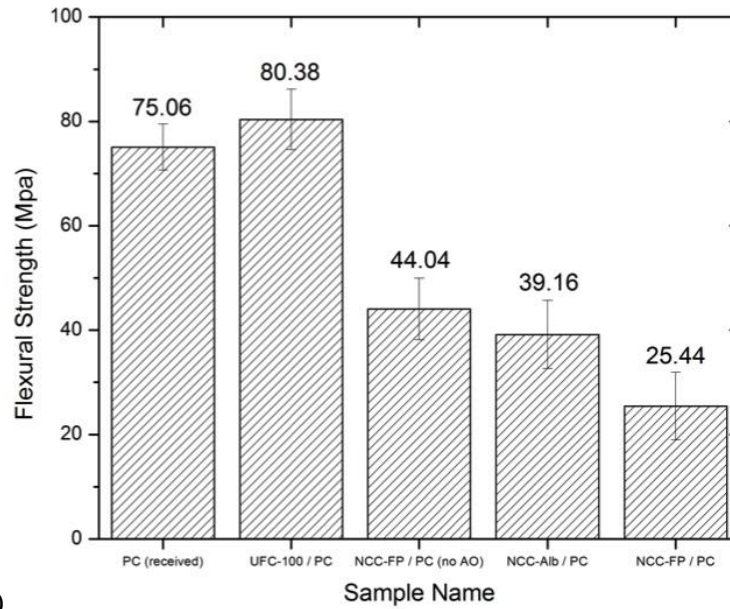
a)
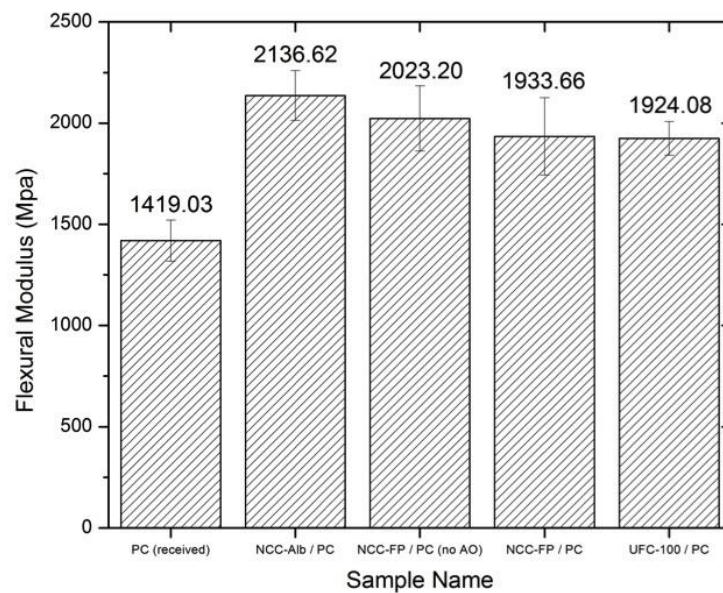
b)

Figure 5.31 – Comparison of a) flexural strength and b) modulus for each cellulose-PC sample

For the flexural modulus, each composite material saw an increase of at least 36% over the StarPlastic PC, with 2% UFC-100 / PC showing the largest increase at 2136 MPa, or a 51% increase.

The impact resistance of the composite materials saw the largest change, as depicted in Figure 5.32. Incorporating 2% UFC-100 resulted in an impact resistance of only 15% of

StarPlastic PC. The sample 2% NCC-FP / PC (no AO) was at only 5% of PC. 2% NCC-Alb / PC and 2% NCC-FP /PC were very brittle with an impact resistance less than 1% of the original polycarbonate. It would be nice to try a 2% UFC-100 / PC sample without antioxidant as it seems it plays some role in the mechanical properties of the composite.
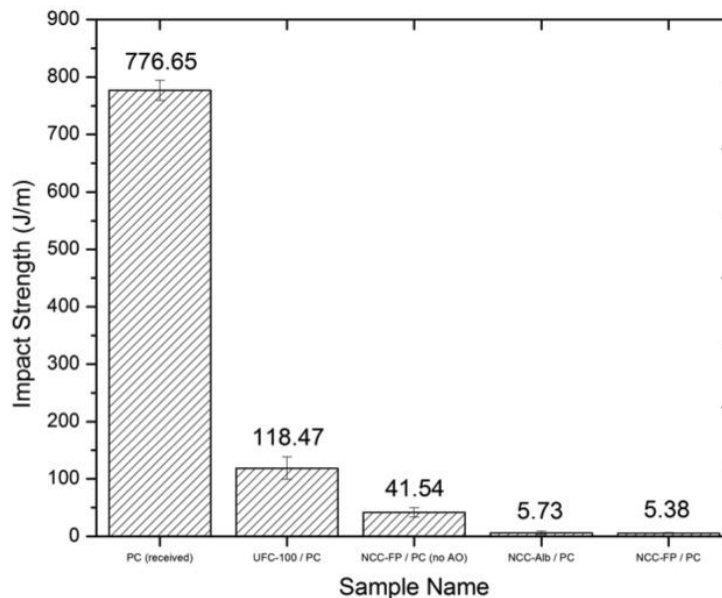
Figure 5.32 – Comparison of impact resistance for each cellulose-PC sample

5.4.2 – Thermal Properties

Differential scanning calorimetry was used for measurement of glass transition and melting point, and thermal gravimetric analysis was used for measurement of onset temperature of degradation. The glass transition temperature is the point of inflection at the top of the DSC thermogram, appearing at around 140 ℃. It may vary a great deal depending on the crystallinity and intermolecular forces acting in the composite. The melting point of the sample appears as a valley on the bottom portion of the curve (exo. up). The melting point in our composites were difficult to locate but is somewhere around 238 ℃, again suggesting variability of the crystallinity in the sample due to processing.

The DSC and TGA thermograms for the 2% NCC-Alb / PC composite are included in Figure 5.33. The onset of degradation occurs at 244 ℃, the glass transition temperature at 131

ºC, and the melting point at 243 ºC. The thermal properties for the 2% NCC-Alb / PC composite are tabulated in Table 5.21.

Table 5.21 – Thermal properties for 2% NCC-Alb / PC

Thermal Property 2% NCC-Alb / PC	Temperature (°C)
Onset of Degradation	244.29
Glass Transition	130.69
Melting Point	242.55

a)

b)
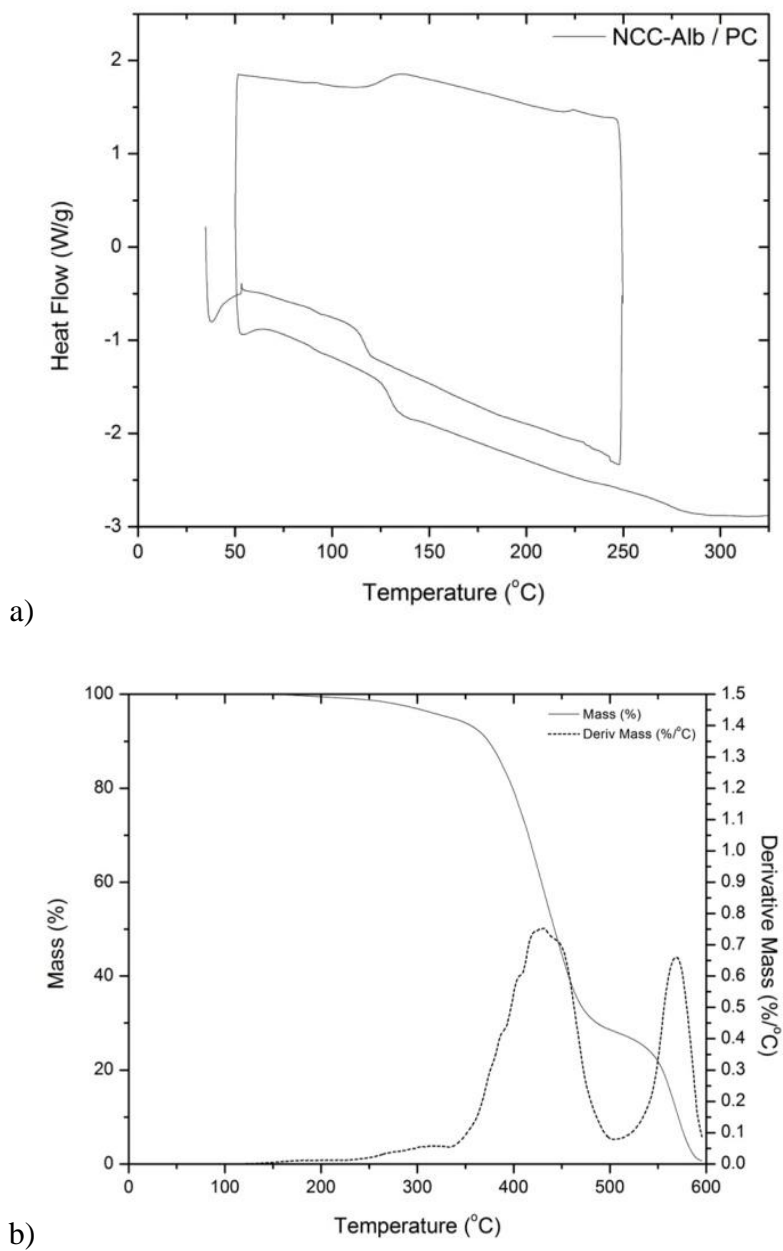
Figure 5.33 – a) DSC and b) TGA thermograms for 2% NCC-Alb / PC

The DSC and TGA thermograms for the 2% NCC-FP / PC (no antioxidant) composite are included in Figure 5.34. The onset of degradation occurs at 247 ℃, the glass transition temperature at 130 ℃, and the melting point at 238 ℃. The thermal properties for the 2% NCC-FP / PC (no antioxidant) composite are tabulated in Table 5.22.

Table 5.22 – Thermal properties for 2% NCC-FP / PC (no AO)

Thermal Property (2% NCC-FP / PC (no AO))	Temperature (°C)
Onset of Degradation	246.82
Glass Transition	125.71
Melting Point	237.82

a)

b)
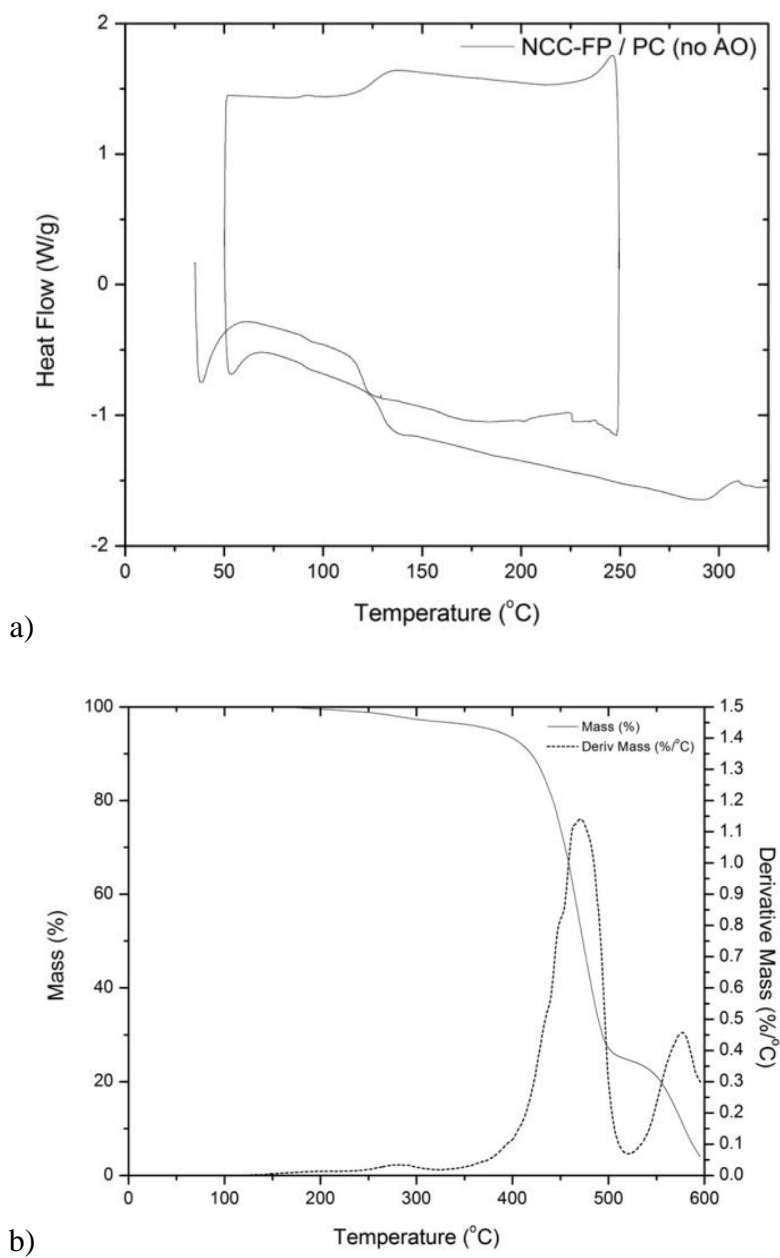
Figure 5.34 – a) DSC and b) TGA thermograms for2% NCC-FP / PC (no AO)

The DSC and TGA thermograms for the 2% NCC-FP / PC composite are included in Figure 5.35. The onset of degradation occurs at 287 ºC, the glass transition temperature at 126 ºC, and the melting point is not visible. The thermal properties for the 2% NCC-FP / PC composite are tabulated in Table 5.23.

Table 5.23 – Thermal properties for 2% NCC-FP / PC

Thermal Property (2% NCC-FP / PC)	Temperature (°C)
Onset of Degradation	286.81
Glass Transition	126.23
Melting Point	na

a)

b)
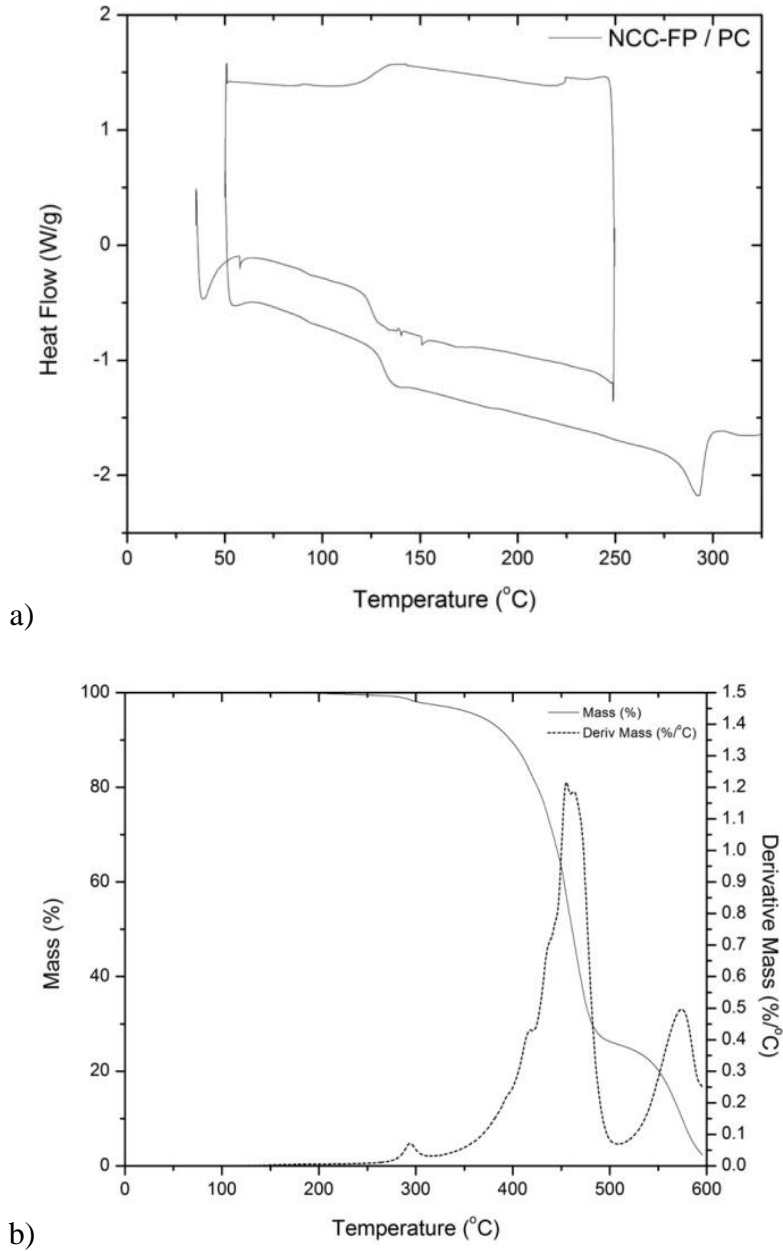
Figure 5.35 – a) DSC and b) TGA thermograms for2% NCC-FP / PC

The DSC and TGA thermograms for the 2% UFC-100 / PC composite are included in Figure 5.36. The onset of degradation occurs at 338 ºC, the glass transition temperature at 138 ºC, and the melting point is 237 ºC. The thermal properties for the 2% UFC-100 / PC composite are tabulated in Table 5.24.

Table 5.24 – Thermal properties for 2% UFC-100 / PC

Thermal Property (2% UFC-100 / PC)	Temperature (°C)
Onset of Degradation	337.66
Glass Transition	137.79
Melting Point	236.86

a)

b)
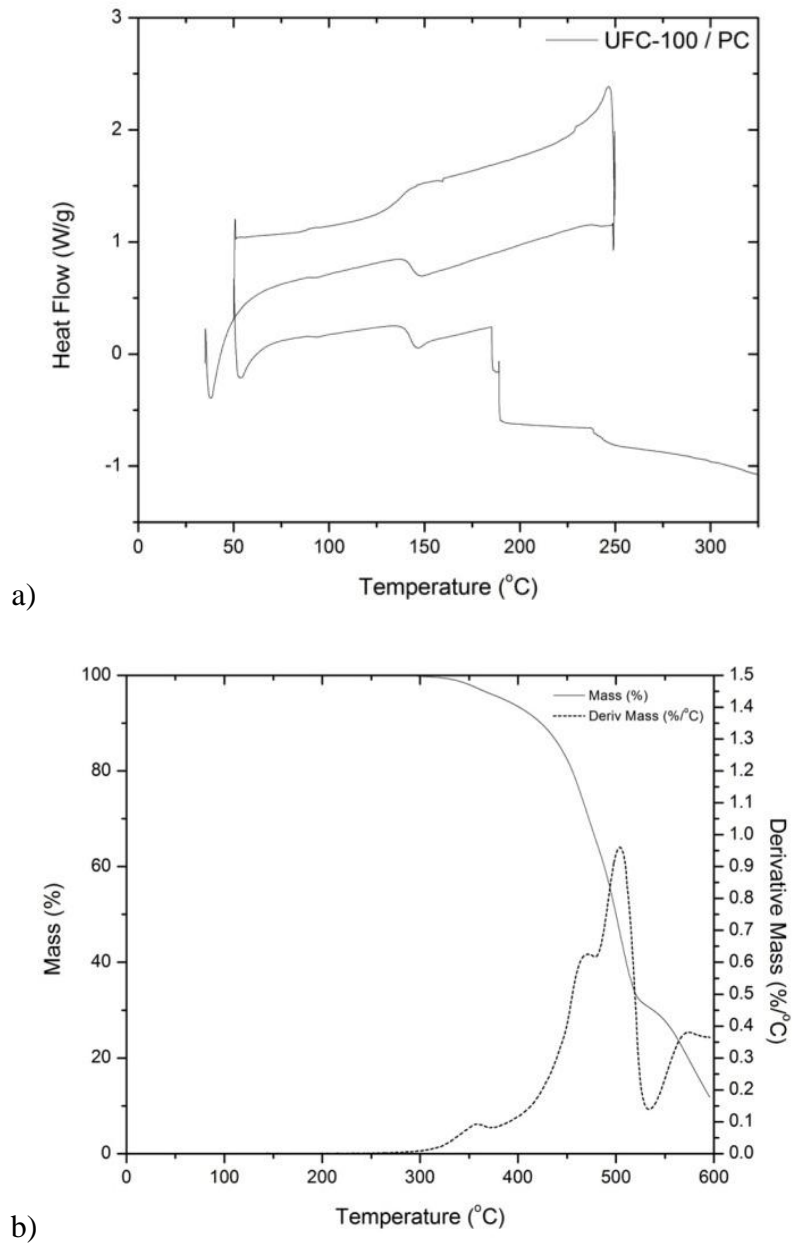
Figure 5.36 – a) DSC and b) TGA thermograms for 2% UFC-100 / PC

After the first heating ramp pass of the material in each case, the melting point became unapparent. That is because there was some inherent stress caused by the incorporation of cellulose or by the processing techniques employed. This was removed after a slow heating cycle.

The glass transition temperature (T_g) decreased in each case. For StarPlastic PC, the glass transition was 142 °C. The T_g fell to 138 °C for UFC-100, 131 °C for NCC-Alb, and 126 °C for both NCC-FP composites. It appears that the incorporation of the antioxidant affected the glass transition of the material, but the cellulose source had a significant effect.

5.4.3 – Processing Properties

The melt flow index (MFI) for the cellulose-PC composites were determined to better understand the viscosity, or the processability, the material will have. This is a standard ASTM procedure, D123, and has specific parameters for polycarbonate materials, applying a 1.2 kg load at 300 °C. However, to avoid thermal degradation, a lower temperature of 250 °C was used. This lower temperature was also further facilitated by the plasticization effects caused by the cellulose fibres, antioxidant, and perhaps moisture incorporated in the composite. The melt flow indices for each of the cellulose-PC samples are listed in Table 5.25.

Table 5.25 – Melt flow indices of each composite sample at 250ºC and 1.2kg

Sample (mass in kg)	MFI at 250°C (g/10min)	Standard Deviation (g/10min)
Pure PC [2.16]	3.86	0.085
Pure PC [1.2]	1.98	0.035
2% NCC-Alb / PC [1.2]	26.65	4.822
2% NCC-FP / PC (no AO) [1.2]	22.47	0.462
2% MF40-10 / PC [1.2]	115.40*	18.84*
2% MF40-10 / PC [1.2]	203.03*	14.72*
2% NCC-FP / PC [1.2]	32.39	2.232
2% UFC-100 / PC [1.2]	4.79	0.219

The different cellulose-PC composites varied greatly in melt flow index. At 250 °C polycarbonate has an MFI of 1.98 g/10min. The nanocrystalline cellulose samples, 2% NCC-Alb / PC, NCC-FP / PC (no AO) and 2% NCC-FP / PC, had an MFI of 27, 22, and 32 g/10 min respectively, a considerable increase over 2 g/10min. The two composites that incorporated MF

40-10 - 2% MF 40-10 / PC (dried), and 2% MF 40-10 / PC (solution) – had extremely high MFI values, 115 and 203 g/10min respectively. The MF 40-10 results cannot be fully trusted as there was a large amount of degassing during the process, which is not accepted according to the ASTM guidelines. This degassing could was very likely caused by impurities and moisture incorporated in the sample. The 2% UFC 100 / PC composite sample had an MFI of 4.8 g/10min.

The MFIs have also been plotted in a bar graph in Figure 5.37 to show a comparison between them; the MF 40-10 samples were removed for a better scale.
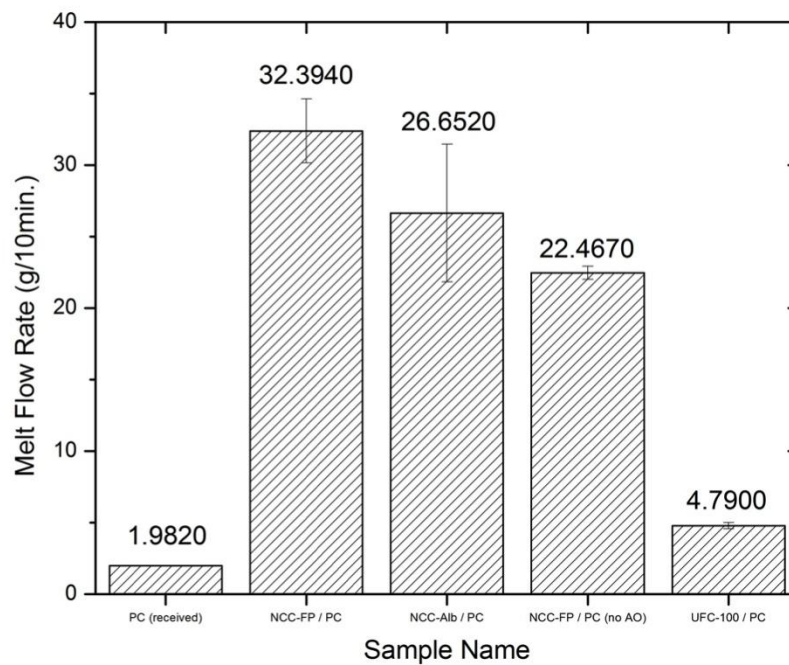
Figure 5.37 – Melt flow indices of each composite sample at 250ºC and 1.2kg

The increased MFI of the NCC-FP and NCC-Alb samples suggests that they may be able to be processed at lower temperatures or lower rpm.

5.4.4 – Chemical Properties

Taking the FTIR spectrograph of each of the composite components, as well as the final composite material, will allow validation of the inclusion of cellulose within the final composite.

Peaks characteristic to cellulose and not polycarbonate visible in the final composite spectrograph will indicate the presence of cellulose.

Table 5.26 – Thickness of composite films tested on FTIR and UV-Vis

Sample	Film Thickness (µm)
StarPlastic PC (thick)	274
StarPlastic PC (thin)	82
NCC-Alb	58
NCC-FP (no AO)	80
MF-40-10 A	234
MF 40-10 B	254
NCC-FP	86
UFC-100	82

Figure 5.38 a) shows a stacked FTIR spectrum of each of the composite materials with StarPlastic PC included for reference. Figure 5.38 b) shows an overlay FTIR spectrum of each of the composite materials with StarPlastic PC. Figure 5.38 c) shows a detailed stacked FTIR spectrum of the region 1800 to 800 cm^{-1} of each of the composite materials with StarPlastic PC. Figure 5.38 d) shows a detailed overlay FTIR spectrum of the region 1800 to 800 cm^{-1} of each of the composite materials with StarPlastic PC.

a)

b)
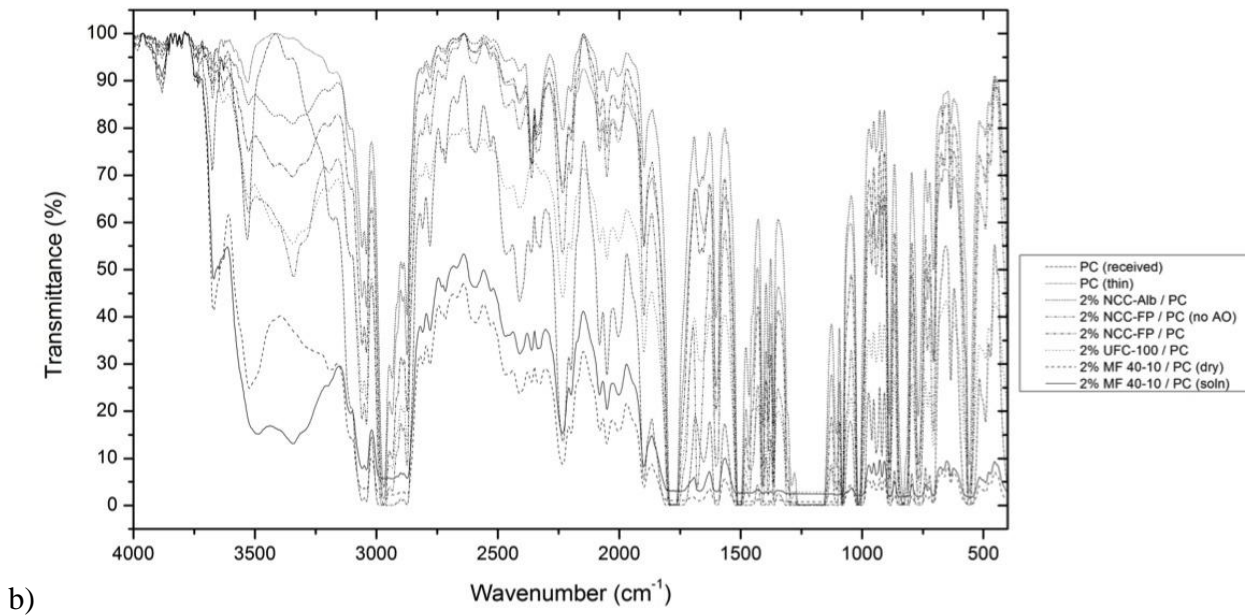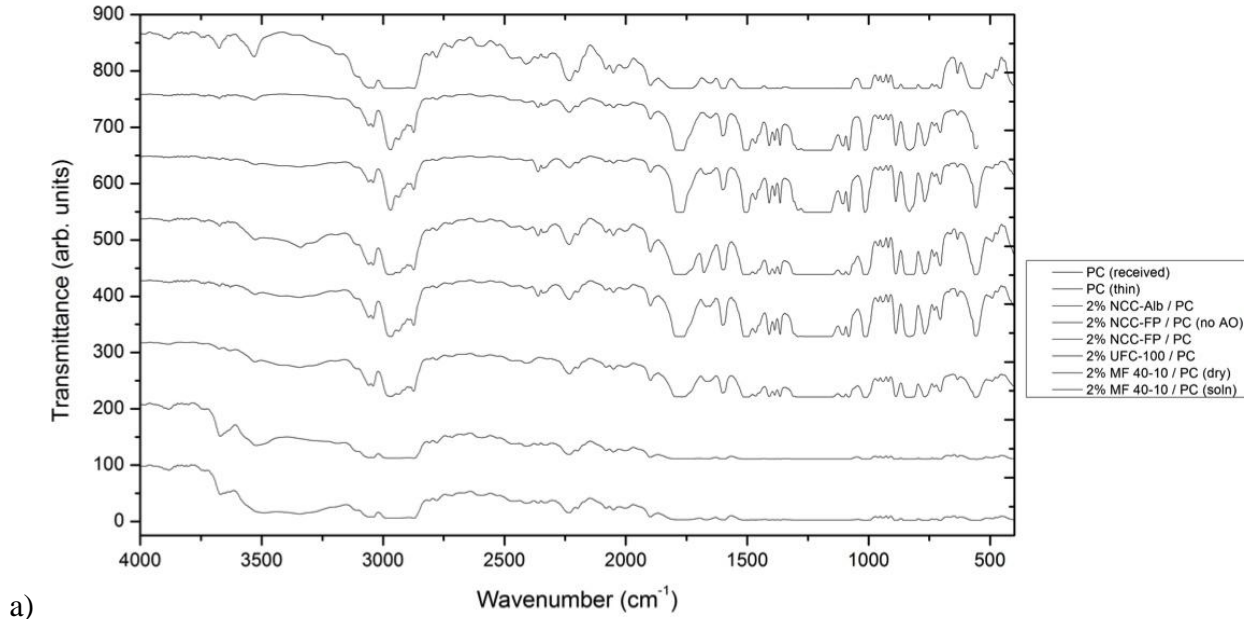
Figure 5.38 – a) Stacked plot, b) overlay plot, c) detailed stacked plot, and d) detailed overlay plot of each cellulose-PC composite FTIR spectrum as prepared by transparent film

116
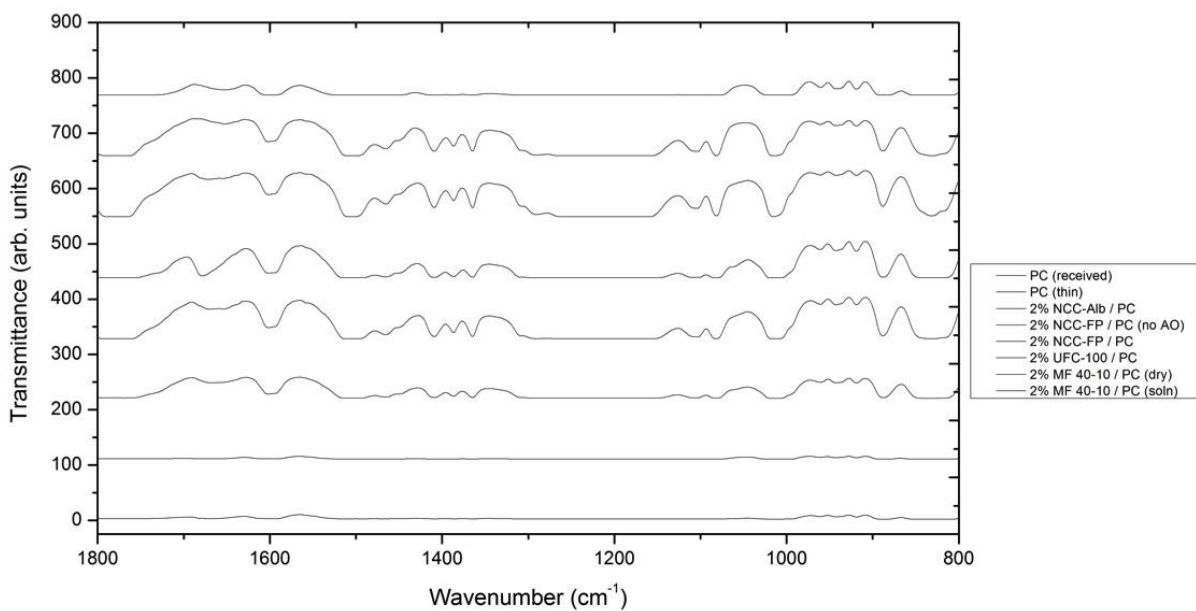
c)
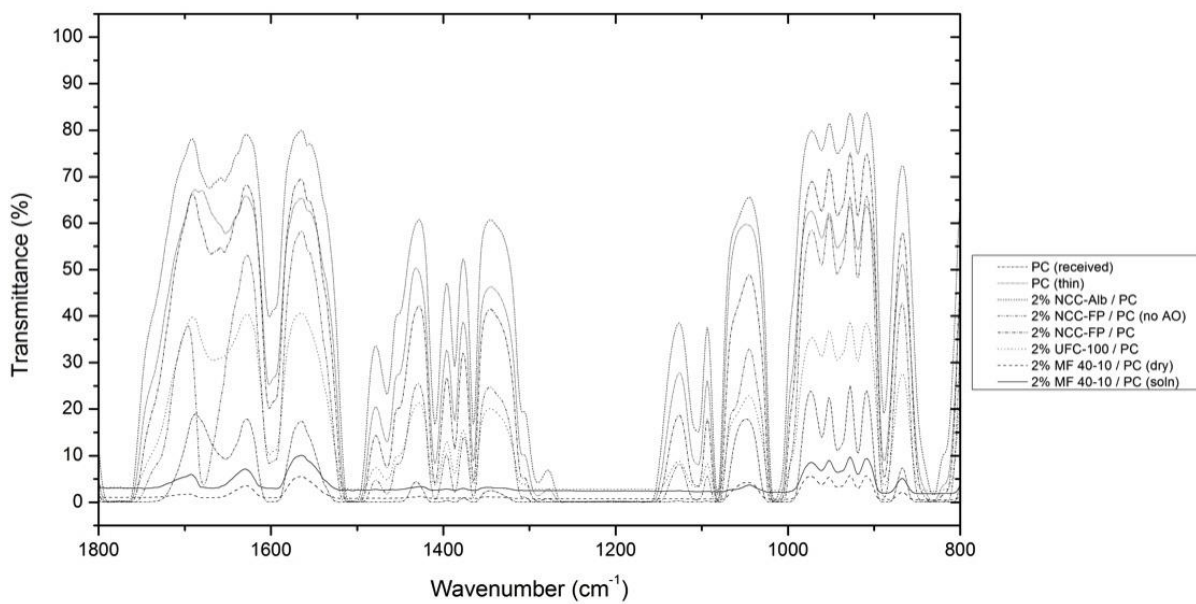
d)

Figure 5.38 (continued) – a) Stacked plot, b) overlay plot, c) detailed stacked plot, and d) detailed overlay plot of each cellulose-PC composite FTIR spectrum as prepared by transparent film

It is difficult to identify any peaks that indicate the incorporation of cellulose in the composite. Unfortunately, this is because of the overlapping in the peaks and the relatively low concentration of cellulose in the composite. The MF 40-10 composite samples appear almost as a flat line; this is because of the thickness of the specimens tested and the moisture within. Thinner samples could not be fabricated due to the extreme brittleness of the specimens.

Individual FTIR spectrographs for each of the cellulose-PC composites are available in Appendix 7.

The UV-Vis spectrograph of each composite was obtained in order to quantify the transparency of the material in the visible spectrum, seen in Figure 5.39. A wavelength of 532 nm was chosen to classify the transparency in the visible region. The thicknesses of the films tested are included in Table 5.26. At 532 nm pure PC had a transmittance of 64%, 2% NCC-Alb / PC was 46%, 2% UFC-100 was 42%, 2% MF 40-10 (dry) / PC was also 42%, 2% NCC-FP / PC was 39%, 2% NCC-FP / PC was 25%, and 2% MF 40-10 (solution) / PC was 14%. The values for %Transmittance at 532 nm are listed in Table 5.27.

Table 5.27 – Transparency of composite samples at 532 nm

Sample	Transmittance at 532nm (%)
pure PC	64.0
2% NCC-Alb / PC	46.3
2% UFC-100 / PC	41.7
2% MF 40-10 (dry) / PC	41.6
2% NCC-FP / PC	38.6
2% NCC-FP (no AO) / PC	24.7
2% MF 40-10 (soln) / PC	14.0
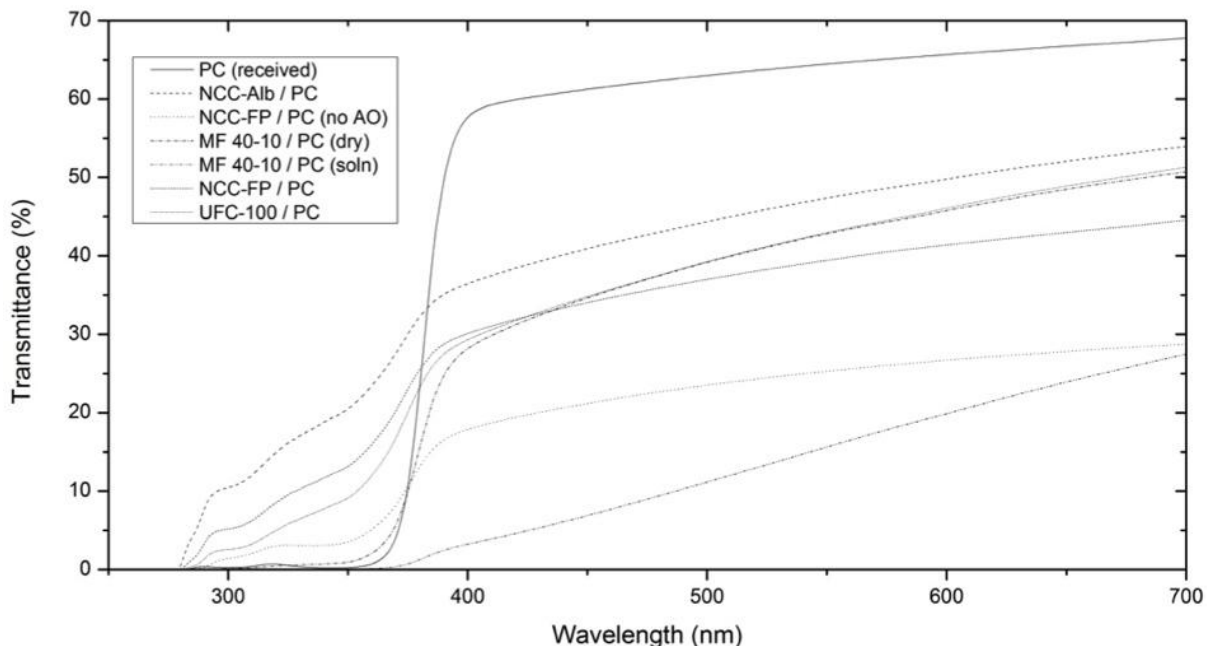
Figure 5.39 – Overlay plot of each cellulose-PC composite UV-Vis spectrum as prepared by a pressed film

It is seen that the use of cellulose, especially NCC, is feasible and with improved dispersion and reduced thermal degradation may be on par with PC in the visible spectrum. It is also interesting that with the incorporation of cellulose there is more transmission in the ultraviolet region (<350 nm). This could be attributed to the damage or loss of the UV stabilizer present in the StarPlastic PC.

Chapter 6 – Conclusions

6.1 – Summary and Contributions

Four new cellulose-polycarbonate nanocomposites were investigated with the main objective of developing new alternatives for applications in automotive windows. Specifically, focus was on the material design and characterization of polycarbonate (PC) based nanocomposite with nanocrystalline cellulose (NCC). One polycarbonate source and 4 new nanocellulose sources were studied. This is the first study in the field, since at the present moment there is no literature available for high-temperature processing of cellulose-thermoplastic nanocomposites based on polycarbonate and nanocellulose.

Chapter Two covered relevant background information from literature that helped understand and justify the study and design of Nanocrystalline Cellulose-Polycarbonate nanocomposites. The concept of a nanocomposite was introduced and each component phase, the matrix and reinforcements, are carefully defined to help the reader understand how they can come together to create a new material with desired properties like mechanical strength and optical transmission. The use of plant fibres as polymer additives was discussed with focus on the automotive industry, as well as the preparation and structure of nanocellulose micro and nano structure, and nanocrystalline cellulose isolation techniques.

The characterization techniques used to study the properties of polycarbonate, nanocrystalline cellulose, and the NCC-PC nanocomposites were introduced, including the

theoretical background. Since the pure polycarbonate and the NCC-PC nanocomposites were of similar polymer morphology, they were characterized in the same fashion allowing direct comparison of properties. The polymer and composite characterization covered: mechanical tests including tensile, flexural, and impact testing; thermal testing including DSC for glass transition and TGA for thermal stability; processing property tests including MFI for flow index; FTIR spectroscopy for composition and UV-Vis spectroscopy for transparency. The cellulose characterization covered: SEM for particle size and morphology; XRD for crystallinity index and crystallite size; moisture content analysis for moisture in the sample; and TGA for thermal stability including activation energy of burning.

The different processing techniques for polycarbonate and the NCC-PC nanocomposite were discussed. The composite processing methods included: solution casting; melt-compounding by extrusion; and compression moulding of specimen bars.

Chapter 3 covered all of the polycarbonate and cellulose sources used in the preparation and design of the nanocomposites, including supplier and any known properties. The polycarbonate used was moulding grade resin from StarPlastic Inc. The cellulose sources included: NCC-Alb from Alberta Innovates-Technology Futures; NCC-FP from FP Innovations Inc.; and MF 40-10 and UFC-100 from JRS Inc. Three sources of cellulose from Sigma-Aldrich were also discussed as they were used for comparison purposes. The solvent used was dimethylformamide and the antioxidant was Irganox 1098.

Chapter 4 covered in detail, the methodology and procedures for polymer processing and each characterization technique used for polycarbonate, nanocrystalline cellulose, and the NCC-PC composite materials.

In Chapter 5, the results of the preparation and the characterization processes were presented. A discussion of the data and results was presented, including justifications, theoretical calculations and other references to the literature.

6.2 – Main Conclusions

The processing techniques used to make the cellulose-polycarbonate nanocomposites were developed. The solution casting procedure was successful for most of the cellulose sources; issues were encountered with the MF 40-10 sample but this was attributed to the composition of the source and the fact it was intended for coating applications. Melt-compounding via extrusion further processed the resulting composite powders. This was done to further mix the composite components and produce pellet extrudates for compression moulding. Compression moulding using a hot-press was completed to create mechanical and chemical testing specimens.

The properties of polycarbonate were measured. The tensile modulus for polycarbonate was 372 MPa and the flexural modulus was 1419 MPa. The tensile and flexural strength for the polycarbonate were 58 and 75 MPa, respectively. The resulting impact resistance for the polycarbonate was 777 J/m. The results were accepted for comparison purposes. The glass transition for polycarbonate was 142 ℃, the melting point was 238 ℃, and the onset of degradation was 361 ℃. It was noted that the melting point for this grade of transparent polycarbonate was almost unapparent due to the inherent amorphous intermolecular structure. The melt flow index was found to be 13 g/10min at 300 ℃ but dropped significantly to 2 g/10min at 250 ℃. The chemical structure was also analysed using FTIR to later verify cellulose incorporation in the composite materials.

Scanning electron microscopy was used for investigation of the surface morphology and particle size of the nanocellulose samples: MF 40-10, UFC-100, NCC-Alb, and NCC-FP. Sample MF 40-10 had a whisker shape structure with low to medium aspect ratio. The particle size had a narrow distribution around 1 μm, but some possible impurity was observed between the fibres after drying the as received cellulose paste. Sample UFC-100 had a fibrous morphology with a wide distribution of aspect ratio and size of fibres around 1 μm. Samples NCC-Alb and NCC-FP were the most refined and processed of all the sources tested with a flaky appearance before dispersion in solvent. Along the edges of the NCCs, small fibrils were visible with dimensions on the nano-scale. With dynamic light scattering (DLS) the particle size was determined to be about 100 and 220 nm for NCC-Alb and NCC-FP, respectively.

Three Sigma-Aldrich cellulose samples were also analysed by SEM for comparison. The Cellulose, fibrous, medium sample was seen to have fibre or whisker-like shape with a medium to large aspect ratio. The particle size was large with a diameter over 10s of nm and length in the 100s of nm. SigmaCell 50 was less fibrilar with a lower aspect ratio than Cellulose, fibrous, medium. The particle size for SC50 spans a wide distribution around 50 μm. SigmaCell 101 was fibrilar with a particle size around 15 μm.

The chemical structure was also analysed using FTIR to verify cellulose incorporation in the composite materials.

X-Ray diffraction of the nanocellulose samples was used to measure the crystallinity index (%CI) and crystallite size of each of the cellulose sources. UFC-100 had a %CI of 71% and NCC-FP was 79% crystalline. NCC-Alb had an 80% crystallinity index, and after an ethanol washing this increased to 90%. It is expected the increase in NCC-Alb's %CI can be attributed to removal of some of the impurities observed in the TGA analysis. The crystallite sizes for all the samples fell between 5 and 9 nm in each of the crystalline reflection directions that is consistent in size with the crystalline region in a nanofibril. The NCC samples also appear to have significant crystallinity increase over the larger cellulose source, UFC-100; this is expected through the additional processing to the nano-scale fibrils removing impurities.

The moisture content of each sample was determined. The moisture content was somewhat consistent across the three Sigma-Aldrich samples and four nanocellulose sources. The moisture content was between 4 and 10 wt-%, with SC101 having the highest %MC. The NCC samples reached their stabilized mass faster than the other samples, but each took less than 10 minutes to dry. The impurities in the non-NCC samples may hold the moisture longer than the more crystalline NCC samples. This analysis justified one hour of drying time before processing.

The thermal stability was analysed through TGA and OFW activation energy analysis. The TGA thermograms were discussed for each material, comparing and discussing the thermal degradation of nanocellulose samples. OFW methods were employed to calculate the activation energy for the thermal degradation of nanocellulose. This would help understand any issues with high temperature processing. It is worth noting that this type of study has not been reported in the literature yet.

It was seen that the nanocellulose sources had higher activation energy in nitrogen than in air, this difference was around 20 KJ/mol. This is understandable as a nitrogen atmosphere is less favourable to oxidization than oxygen rich air. The activation energy varies greatly depending on the source of nanocellulose. Sample NCC-FP had the highest activation energy followed by samples MF 40-10, UFC-100, and NCC-Alb. The activation energies varied from 205 to 112 KJ/mol between the NCC-FP and NCC-Alb samples respectively.

The mechanical properties of the composite materials were discussed next. From the tensile and flexural data it was seen that the incorporation of 2% UFC-100 resulted in similar strengths to the StarPlastic PC. Also, in tensile tests the NCC-FP samples showed only a slight drop in strength, more significant in flexural than tensile. The NCC-Alb sample showed a significant drop in both tensile and flexural strength.

The tensile modulus for 2% UFC-100 / PC increased 17% whereas 2% NCC-FP with and without antioxidant were in agreement within error of the StarPlastic PC. A drop of nearly 30% in the tensile modulus was seen for the 2% NCC-Alb / PC sample.

For the flexural modulus, each composite material saw an increase of at least 36% over the StarPlastic PC, with 2% UFC-100 / PC showing the largest increase at 2136 MPa, or a 51% increase.

The impact resistance of the composite materials saw the largest change. Incorporating 2% UFC-100 resulted in an impact resistance of only 15% of StarPlastic PC. The sample 2% NCC-FP / PC (no AO) was at only 5% of PC. 2% NCC-Alb / PC and 2% NCC-FP /PC were very brittle with an impact resistance less than 1% of the original polycarbonate.

After a first heating ramp pass of the material in each case, the melting point became unapparent. That is attributed to inherent stress caused by the incorporation of cellulose or by the processing techniques employed. The glass transition temperature (T_g) decreased in each case. For StarPlastic PC the glass transition was 142 °C. The T_g fell to 138 °C for UFC-100, 131 °C for NCC-Alb, and 126 °C for both NCC-FP composites. It appears that the incorporation of the antioxidant affected the glass transition of the material, but the nanocellulose also source had a significant effect. The onset of degradation agreed with the order of degradation of the fibres

themselves: 2% NCC-Alb / PC, 2% NCC-FP / PC, and 2% UFC-100 PC. It was also seen the inclusion of cellulose decreased the onset, as well antioxidant decreased the onset by around 40 °C. There may have been some degradation of the antioxidant leading to decreased or undesired properties.

The different cellulose-PC composites varied greatly in melt flow index. At 250 °C polycarbonate has an MFI of 1.98 g/10min. The nanocrystalline cellulose samples, 2% NCC-Alb / PC, NCC-FP / PC (no AO) and 2% NCC-FP / PC, had an MFI of 27, 22, and 32 g/10 min respectively, a considerable increase over 2 g/10min. The two composites that incorporated MF 40-10 - 2% MF 40-10 / PC (dried), and 2% MF 40-10 / PC (solution) – had extremely high MFI values, 115 and 203 g/10min. These results cannot be fully trusted as there was a large amount of degassing during the process, which is not accepted according to ASTM. This degassing could was very likely caused by impurities and moisture incorporated in the sample. The 2% UFC 100 / PC composite sample had an MFI of 4.8 g/10min.

Finally the chemical properties were analysed using FTIR and UV-Vis. The FTIR was unable to confirm the inclusion of the cellulose in each of the final composite materials. This was due to the overlapping of similar peaks and the relatively low concentration of NCC.

The UV-Vis spectrograph of each composite was obtained in order to quantify the transparency of the material in the visible spectrum. The order of transparency from most transparent in the visible spectrum to least is: StarPlastic PC, NCC-Alb, NCC-FP (no AO), MF 40-10 (dry), MF 40-10 (solution), NCC-FP, and UFC-100. It is seen that the use of cellulose, especially NCC, is feasible and with improved dispersion and reduced thermal degradation may be on par with PC.

6.3 – Recommendations & Future Work

6.3.1 – Recommendations

It was concluded that there is the potential for using these new fibres as reinforcing additives in polycarbonate and other high temperature processing thermoplastics. This does not mean that the process is yet ideal or scalable. Design issues were encountered and not all were addressed

properly at the time of experimentation. A set of recommendations, or next steps if you will, has been developed for the current study. This includes:

- Use of the cellulose FTIR data to calculate the crystallinity index to validate the %CI determined with XRD [Baldinger 2005];

- Further exploration of the cellulose TGA data to determine more thermal stability kinetic parameters like order of reaction and the pre-exponential factor. Having all of these parameters with the activation energy will allow modelling of the cellulose degradation for the sources tested [Mirsa 1987];

- SEM analysis of break and fracture analysis to observe the mechanisms of crack propagation with hopes to determine the cause of loss of strength and modulus in some of the cellulose-PC composites;

- An analysis of the molecular weight distribution of the polycarbonate before and after each processing step to see if any damage has been caused. In particular, it will help to observe any PC chain scission caused by solvent, heat, or shear;

- Along with the different composite materials and pure polycarbonate, a blank polycarbonate sample should be analysed. This would be a sample experiencing the same solvent reflux and extrusion processes as the composites, but with no cellulose incorporation. This sample could act as a better baseline for comparison to the composites;

- Ideally, seeing that the antioxidant plays a large role on the mechanical and thermal properties of the composite, a composite without Irganox 1098 should be made and analysed for those samples that were not tested in this study;

- More exploration of the effect of extrusion temperature and revolutions per minute should be examined to better understand the effects they play on final composite properties;

- Hardness or abrasion resistance should be tested as this was one of the drawbacks of traditional polycarbonate in automotive applications; abrasion could be tested using a five-finger scratch testing method;

- Polarized light microscopy could be used to analyse any flocculation or agglomeration in the samples which would lead to mechanical and optical properties less than ideal [Paralikar 2008];

- Sensitivity analysis or design of experiment focusing on each of the parameters that were deemed to be important in this study. This could include cellulose incorporation (wt-%), processing temperature, and refluxing time among others; and

- Cellulose surface chemical modification that could increase the processing temperature of the reinforcements. More discussion on this recommendation is included in Section 6.3.2. [Belgacem 2005]

6.3.2 – Chemical Additives and Modifications

The surface functional groups of the cellulose nanofibrils may allow for an increased thermal stability. This means that the onset of degradation can be increased for the cellulose samples. This would decrease the yellowing of cellulose-PC composites. It would also open the reinforcing fibres to new high temperature applications. [George 2001, Baiardo 2002]

The hydroxyl groups of the cellulose surface can be directly reacted to form derivative surfaces; common cellulose surface reactions include esterification and silanation for creating a more organophilic filler. It is crucial to maintain the original strength and crystallinity of the cellulose fibres throughout any modification process. It has also been seen that the degree of functionalization of the hydroxyl groups can be tailored to maximize physical properties like modulus of elasticity, strength to breakage, or impact resistance. Depending on the final application of the nanocomposite, the right balance of flexibility and rigidity should be considered and proper modification techniques developed [Jacob 2005, Biswal 2004].

Silane derivitization to cellulosic fibres is a common technique for creating a silicon-covered surface with good heat-deflection properties [Abdelmouleh 2002]. A wide range of Silane based chemicals can be used to modify a cellulosic surface, resulting in numerous possible functional groups in place of the original hydroxyl groups [Lu 2000]. Many researchers have used silanation to modify cellulosic fibres for use in composite and nanocomposite materials [Gousse 2004, Roman 2006, Panaitescu 2007].

Castellano proposed the mechanism of silanation coupling in 2004. In the absence of water, the SiOR groups will not react with the hydroxyl groups of the cellulose. In the presence of moisture, the silane becomes partially hydrolysed, making it possible to react with the hydroxyl groups at sufficient temperatures. Roman and Winter (2006) have shown that silylated cellulosic nanocrystals affect the crystallinity of the polymer matrix and give an increase in the composite stiffness. It is not yet realized if the derivitization technique for modifying a nano-filler surface like cellulose will prove cost-effective at larger scales, requiring additional work applying macro-scale cellulosic modification techniques to the nanocrystals.

References

M. Abdelmouleh, S. Boufi, A. ben Salah, M.N. Belgacem, and A. Gandini, "Interaction of silane coupling agents with cellulose," *Langmuir*, vol. 18, Apr. 2002, pp. 3203-3208.

N. Abidi and E. Hequet, "Characterization of cotton fibers using TGA and FTIR," *The World Cotton Research Conference 4*, Lubbock, TX: The World Cotton Research Conference, 2007.

G. Allen, D.C.W. Morley, and T. Williams, "The impact strength of polycarbonate," *Journal of Materials Science*, vol. 8, Oct. 1973, pp. 1449-1452.

D.F. Arseneau, "Competitive reactions in the thermal decomposition of cellulose," *Canadian Journal of Chemistry*, vol. 49, 1971, pp. 632-638.

ASTM, *D790-10: Standard test methods for flexural properties of unreinforced and reinforced plastics and electrical insulating materials*, 2010.

ASTM, *D883-08: Standard terminology relating to plastics*, 2008.

ASTM, *D638-10: Standard test method for tensile properties of plastics*, 2010.

ASTM, *E698-05: Standard test method for Arrhenius kinetic constants for thermally unstable materials*, 2005.

ASTM, *D618-08: Standard practice for conditioning plastics for testing*, 2008.

ASTM, *D1238-10: Standard test method for melt flow rates of thermoplastics by extrusion plastometer*, 2010.

ASTM, *D1708-10: Standard test method for tensile properties of plastics by use of microtensile specimens*, 2010.

ASTM, *D4000-10a: Standard classification system for specifying plastic materials*, 2010.

ASTM, *D570-98(2010)e1: Standard test method for water absorption of plastics*, 1998.

ASTM, *D3935-09: Standard specification for polycarbonate (PC) unfilled and reinforced material*, 2009.

M.A.S. Azizi Samir, F. Alloin, and A. Dufresne, "Review of recent research into cellulosic whiskers, their properties and their application in nanocomposite field," *Biomacromolecules*, vol. 6, Jan. 2005, pp. 612-26.

W. Bai, J. Holbery, and K. Li, "A technique for production of nanocrystalline cellulose with a narrow size distribution," *Cellulose*, vol. 16, Feb. 2009, pp. 455-465.

M. Baiardo, G. Frisoni, M. Scandola, and A. Licciardello, "Surface chemical modification of natural cellulose fibers," *Journal of Applied Polymer Science*, vol. 83, Jan. 2002, pp. 38-45.

T. Baldinger, J. Moosbauer, and H. Sixta, "Supermolecular structure of cellulosic materials by Fourier transform infrared spectroscopy (FT-IR) calibrated by WAXS and 13C NMR," *Internal report from LENZING AG, A- 4860*, 2005.

D. Bansal, "Automotive Textiles – Changed Perspective," *Text on TEXTILES*, 2010.

M.N. Belgacem and A. Gandini, "Surface modification of cellulose fibres," *Polímeros*, vol. 15, Jun. 2005, pp. 114-121.

A.A. Berlin, S.A. Volfson, N.S. Enikolopian, and S.S. Negmatov, *Principles of polymer composites*, Berlin: Springer-Verlag, 1986.

A. Bhatnagar, "Processing of cellulose nanofiber-reinforced composites," *Journal of Reinforced Plastics and Composites*, vol. 24, Aug. 2005, pp. 1259-1268.

BioVision, "Bio Vision Technology." 2011.

D. Biswal, "Characterisation of carboxymethyl cellulose and polyacrylamide graft copolymer," *Carbohydrate Polymers*, vol. 57, Sep. 2004, pp. 379-387.

A. Bledzki, "Composites reinforced with cellulose based fibres," *Progress in Polymer Science*, vol. 24, May. 1999, pp. 221-274.

J. Bolton, "The potential of plant fibres as crops for industrial use," *Outlook on Agriculture*, vol. 24, 1995, pp. 85-89.

D. Bondeson, A. Mathew, and K. Oksman, "Optimization of the isolation of nanocrystals from microcrystalline cellulose by acid hydrolysis," *Cellulose*, vol. 13, Apr. 2006, pp. 171-180.

L. Bragg, *The development of X-ray analysis*, London: G. Bell and Sons Ltd, 1975.

R.M.J. Brown and I.M. Saxena, eds., *Cellulose: Molecular and Structural Biology*, Dordrecht, Netherlands: Springer, 2007

A. Chakraborty, M. Sain, and M. Kortschot, "Cellulose microfibrils: A novel method of preparation using high shear refining and cryocrushing," *Holzforschung*, vol. 59, Jan. 2005, pp. 102-107.

P.K. Chatterjee and C.M. Conrad, "Thermogravimetric analysis of cellulose," *Journal of Polymer Science Part A: Polymer Chemistry*, vol. 6, Dec. 1968, pp. 3217-3233.

P.K. Chatterjee and C.M. Conrad, "Kinetics of the pyrolysis of cotton cellulose," *Textile Research Journal*, vol. 36, Jun. 1966, pp. 487-494.

]L. Chen, X. Pang, and Z. Yu, "Study on polycarbonate/multi-walled carbon nanotubes composite produced by melt processing," *Materials Science and Engineering: A*, vol. 457, May. 2007, pp. 287-291.

Y.K. Choi, K.I. Sugimoto, S.M. Song, and M. Endo, "Production and characterization of polycarbonate composite sheets reinforced with vapor grown carbon fiber," *Composites Part A: Applied Science and Manufacturing*, vol. 37, Nov. 2006, pp. 1944-1951.

J. Conesa, "Analysis of different kinetic models in the dynamic pyrolysis of cellulose," *Thermochimica Acta*, vol. 254, Apr. 1995, pp. 175-192.

E. Corradini, E.M. Teixeira, P.D. Paladin, J.A. Agnelli, O.R.R.F. Silva, and L.H.C. Mattoso, "Thermal stability and degradation kinetic study of white and colored cotton fibers by thermogravimetric analysis," *Journal of Thermal Analysis and Calorimetry*, vol. 97, Apr. 2009, pp. 415-419.

S.P. Davis, M.C. Abrams, and J.W. Brault, *Fourier transform spectroscopy*, San Diego: Academic Press, 2001.

D.P. Delmer and Y. Amor, "Cellulose biosynthesis," *Plant Cell*, vol. 7, 1995, pp. 987-1000.

M.M. de Souza Lima and R. Borsali, "Rodlike cellulose microcrystals: Structure, properties, and applications," *Macromolecular Rapid Communications*, vol. 25, Apr. 2004, pp. 771-787.

Domtar, "Domtar and FP Innovations to jointly develop innovative fiber-based nanotechnologies at new demonstration plant," *NanoWerk.com*, 2010.

F. Dourado, F.M. Gama, E. Chibowski, and M. Mota, "Characterization of cellulose surface free energy," *Journal of adhesion science and technology*, vol. 12, 1998, pp. 1081-1090.

A. Dufresne, "Polysaccharide nano crystal reinforced nanocomposites," *Canadian Journal of Chemistry*, vol. 86, 2008, p. 11.

C.F. Fan, T. Cagin, Z.M. Chen, and K.A. Smith, "Molecular modeling of polycarbonate. 1. Force field, static structure, and mechanical properties," *Macromolecules*, vol. 27, Apr. 1994, pp. 2383-2391.

A.C. Finkle, *Thermal degradation of nanocrystalline cellulose*, Waterloo, Canada: 2010.

A.C. Finkle, *WKRPT400: Nanocrystalline cellulose - polycarbonate nanocomposite*, Waterloo, Canada: 2009.

A.C. Finkle, C.R. Reddy, and L.C. Simon, "Thermal stability of nanocrystalline cellulose," *Biocomp 2010: 10th Pacific Rim Bio-Based Composites Symposium*, Banff, Canada: BioComp 2010, 2010.

J.H. Flynn and L.A. Wall, "A quick, direct method for the determination of activation energy from thermogravimetric data," *Journal of Polymer Science Part B: Polymer Letters*, vol. 4, May. 1966, pp. 323-328.

FP Innovations Inc., *Nanocrystalline Cellulose - "Green" Nanoparticles*, Pointe-Claire, PQ: 2008.

Freedonia, "Polycarbonate demand to increase 5.2 percent annually," *The IAPD Magazine*, 2003.

D.J. Gardner, G.S. Oporto, R. Mills, and M.A.S. Azizi Samir, "Adhesion and surface issues in cellulose and nanocellulose," *Journal of Adhesion Science and Technology*, vol. 22, 2008, p. 545–56.

C.J. Garvey, I.H. Parker, and G.P. Simon, "On the Interpretation of X-Ray Diffraction Powder Patterns in Terms of the Nanostructure of Cellulose I Fibres," *Macromolecular Chemistry and Physics*, vol. 206, Aug. 2005, pp. 1568-1575.

J. George, M.S. Sreekala, and S. Thomas, "A review on interface modification and characterization of natural fiber reinforced plastic composites," *Polymer Engineering & Science*, vol. 41, Sep. 2001, pp. 1471-1485.

C. Gousse, H. Chanzy, M. Cerrada, and E. Fleury, "Surface silylation of cellulose microfibrils: preparation and rheological properties," *Polymer*, vol. 45, Mar. 2004, pp. 1569-1575.

D.G. Gray, "Transcrystallization of polypropylene at cellulose nanocrystal surfaces," *Cellulose*, vol. 15, Sep. 2007, pp. 297-301.

P.R. Griffiths, J.A. DeHaseth, and N.J. Hoboken, *Fourier transform infrared spectroscopy*, Wiley-Interscience, 2007.

M.A. Hubbe, O.J. Rojas, L.A. Lucia, and M. Sain, "Cellulosic nanocomposites: A Review," *BioResources*, vol. 3, 2008, pp. 929-980.

S. Iwamoto, A.N. Nakagaito, and H. Yano, "Nano-fibrillation of pulp fibers for the processing of transparent nanocomposites," *Applied Physics A*, vol. 89, Jul. 2007, pp. 461-466.

A. Iwatake, M. Nogi, and H. Yano, "Cellulose nanofiber-reinforced polylactic acid," *Composites Science and Technology*, vol. 68, Jul. 2008, pp. 2103-2106.

M. Jacob, S. Joseph, L.A. Pothan, and S. Thomas, "A study of advances in characterization of interfaces and fiber surfaces in lignocellulosic fiber-reinforced composites," *Composite Interfaces*, vol. 12, Jan. 2005, pp. 95-124.

D. Jagadeesh, A. Varada Rajulu, and B.R. Guduri, "Tensile Properties of Polycarbonate-Coated Natural Fabric Hildegardia populifolia," *Journal of Reinforced Plastics and Composites*, vol. 27, Nov. 2008, pp. 1833-1838.

S. Janardhnan and M. Sain, "Isolation of cellulose microfibrils - An enzymatic approach," *BioResources*, vol. 1, 2006, pp. 176-188.

B. Jang and C. Wilkie, "The thermal degradation of bisphenol A polycarbonate in air," *Thermochimica Acta*, vol. 426, Feb. 2005, pp. 73-84.

J.A. Jansen, "The Properties and Failure of Polycarbonate," The Madison Group, 2011.

J.L. Kardos, F.S. Cheng, and T.L. Tolbert, "Tailoring the interface in graphite-reinforced polycarbonate," *Polymer Engineering and Science*, vol. 13, Nov. 1973, pp. 455-461.

A. Kiziltas, D.J. Gardner, Y.S. Han, C. West, and H.S. Yang, "Thermoplastic Nanocomposite Based on Cellulose Nanocrystals and PET/PTT Blends," *International Conference on Nanotechnology for the F.P.I.*, St. Louis: University of Maine, 2008.

D. Klemm, D. Schumann, F. Kramer, N. Heßler, M. Hornung, H.-P. Schmauder, and S. Marsch, "Nanocelluloses as innovative polymers in research and application," *Polysaccharides II: Advances in Polymer Science*, D. Klemm, ed., Springer Berlin Heidelberg, 2006, pp. 49-96.

I. Kvien and K. Oksman, "Orientation of cellulose nanowhiskers in polyvinyl alcohol," *Applied Physics A*, vol. 87, Feb. 2007, pp. 641-643.

J. Laskar, F. Vidal, O. Fichet, C. Gauthier, and D. Teyssie, "Synthesis and characterization of interpenetrating networks from polycarbonate and cellulose acetate butyrate," *Polymer*, vol. 45, Jul. 2004, pp. 5047-5055.

J. Leitner, B. Hinterstoisser, M. Wastyn, J. Keckes, and W. Gindl, "Sugar beet cellulose nanofibril-reinforced composites," *Cellulose*, vol. 14, Jun. 2007, pp. 419-425.

A. Leão, "'Green' cars could be made from pineapples and bananas," *American Chemical Society*, 2011.

J.Z. Lu, W. Qinglin, and H.S. McNabb, "Chemical coupling in wood fiber and polymer composites : A review of coupling agents and treatments," *Wood and fiber science*, vol. 32, 2000, pp. 88-104.

A.P. Mathew, A. Chakraborty, K. Oksman, and M. Sain, *Cellulose nanocomposites*, Washington, DC: American Chemical Society, 2006.

MatWeb, "Star Plastics PC743 Molding Grade PC," *MatWeb: Material Property Data*.

I. Milosavljevic and E.M. Suuberg, "Cellulose thermal decomposition kinetics: Global mass loss kinetics," *Industrial & Engineering Chemistry Research*, vol. 34, Apr. 1995, pp. 1081-1091.

D.K. Misra, "Cereal straw, secondary fibers and nonwood pulping," *Pulp and Paper Manufacture*, B.L. and M.J.K. F. Hamilton, ed., Montreal, Canada: Joint Textbook Committee of the Paper Industry TAPPI-CPPA, 1987, pp. 82-93.

M. Mitsunaga, Y. Ito, S.S. Ray, M. Okamoto, and K. Hironaka, "Intercalated polycarbonate/clay nanocomposites: Nanostructure control and foam processing," *Macromolecular Materials and Engineering*, vol. 288, Jul. 2003, pp. 543-548.

V. Mittal, ed., *Polymer Nanotube Nanocomposites: Synthesis, Properties, and Applications*, Salem: Wiley, 2010.

J.I. Morán, V.A. Alvarez, V.P. Cyras, and A. Vázquez, "Extraction of cellulose and preparation of nanocellulose from sisal fibers," *Cellulose*, vol. 15, Aug. 2007, pp. 149-159.

A.N. Nakagaito and H. Yano, "Novel high-strength biocomposites based on microfibrillated cellulose having nano-order-unit web-like network structure," *Applied Physics A*, vol. 80, Jul. 2003, pp. 155-159.

A.N. Nakagaito, S. Iwamoto, and H. Yano, "Bacterial cellulose: the ultimate nano-scalar cellulose morphology for the production of high-strength composites," *Applied Physics A*, vol. 80, Jul. 2004a, pp. 93-97.

A.N. Nakagaito and H. Yano, "The effect of morphological changes from pulp fiber towards nano-scale fibrillated cellulose on the mechanical properties of high-strength plant fiber based composites," *Applied Physics A*, vol. 78, Mar. 2004b, pp. 547-552.

A.N. Nakagaito and H. Yano, "The effect of fiber content on the mechanical and thermal expansion properties of biocomposites based on microfibrillated cellulose," *Cellulose*, vol. 15, Mar. 2008, pp. 555-559.

K. Nevalainen, J. Vuorinen, V. Villman, R. Suihkonen, P. Järvelä, J. Sundelin, and T. Lepistö, "Characterization of twin-screw-extruder-compounded polycarbonate nanoclay composites," *Polymer Engineering & Science*, vol. 49, Apr. 2009, pp. 631-640.

R. Newman, "Estimation of the lateral dimensions of cellulose crystallites using 13C NMR signal strengths," *Solid State Nuclear Magnetic Resonance*, vol. 15, Oct. 1999, pp. 21-29.

T. Nishino, I. Matsuda, and K. Hirao, "All-cellulose composite," *Macromolecules*, vol. 37, Oct. 2004, pp. 7683-7687.

OICA, *OICA 2009 World Motor Vehicle Production Statistics*, 2009.

K. Oksman, A. Mathew, D. Bondeson, and I. Kvien, "Manufacturing process of cellulose whiskers/polylactic acid nanocomposites," *Composites Science and Technology*, vol. 66, Dec. 2006, pp. 2776-2784.

W.J. Orts, J. Shey, S.H. Imam, G.M. Glenn, M.E. Guttman, and J.-F. Revol, "Application of cellulose microfibrils in polymer nanocomposites," *Journal of Polymers and the Environment*, vol. 13, Oct. 2005, pp. 301-306.

T. Ozawa, "Kinetic analysis of derivative curves in thermal analysis," *Journal of Thermal Analysis*, vol. 2, Sep. 1970, pp. 301-324.

T. Ozawa, "Estimation of activation energy by isoconversion methods," *Thermochimica Acta*, vol. 203, Jul. 1992, pp. 159-165.

T. Ozawa, "Non-isothermal kinetics and generalized time," *Thermochimica Acta*, vol. 100, May. 1986, pp. 109-118.

M. Ozgurseydibeyoglu and K. Oksman, "Novel nanocomposites based on polyurethane and micro fibrillated cellulose," *Composites Science and Technology*, vol. 68, Mar. 2008, pp. 908-914.

D.M. Panaitescu, D. Donescu, C. Bercu, D.M. Vuluga, M. Iorga, and M. Ghiurea, "Polymer composites with cellulose microfibrils," *Polymer Engineering & Science*, vol. 47, Aug. 2007, pp. 1228-1234.

J.K. Pandey, W.S. Chu, C.S. Kim, C.S. Lee, and S.H. Ahn, "Bio-nano reinforcement of environmentally degradable polymer matrix by cellulose whiskers from grass," *Composites Part B: Engineering*, vol. 40, Oct. 2009, pp. 676-680.

S.A. Paralikar, J. Simonsen, and J. Lombardi, "Poly(vinyl alcohol)/cellulose nanocrystal barrier membranes," *Journal of Membrane Science*, vol. 320, Jul. 2008, pp. 248-258.

S. Park, J.O. Baker, M.E. Himmel, P.A. Parilla, and D.K. Johnson, "Cellulose crystallinity index: measurement techniques and their impact on interpreting cellulase performance.," *Biotechnology for biofuels*, vol. 3, May. 2010, p. 10.

A. Patterson, "The Scherrer Formula for X-Ray Particle Size Determination," *Physical Review*, vol. 56, Nov. 1939, pp. 978-982.

L. Petersson and K. Oksman, *Cellulose nanocomposites*, Washington, DC: American Chemical Society, 2006.

Q. Ping, Z. LiPing, D. JiuFang, and C. Yu, "Study on micro-nano cellulose/poly (lactic acid) composite.," *Symposium on Chemistry and Engineering of Forestry Biomass, Nanjing, China.*, Editorial Board of Chemistry and Industry of Forest Products, 2009, pp. 179-182, 186.

T. Pullawan, A.N. Wilkinson, and S.J. Eichhorn, "Discrimination of matrix–fibre interactions in all-cellulose nanocomposites," *Composites Science and Technology*, vol. 70, Dec. 2010, pp. 2325-2330.

A. Rai and C.N. Jha, *Natural fibre composites and its potential as building materials*, New Delhi: 2010.

M.V. Ramiah, "Thermogravimetric and differential thermal analysis of cellulose, hemicellulose, and lignin," *Journal of Applied Polymer Science*, vol. 14, May. 1970, pp. 1323-1337.

M. Roman and W.T. Winter, "Effect of sulfate groups from sulfuric acid hydrolysis on the thermal degradation behavior of bacterial cellulose.," *Biomacromolecules*, vol. 5, Jan. 2004, pp. 1671-7.

M. Roman and W.T. Winter, "Cellulose nanocrystals for thermoplastic reinforcement: Effect of filler surface chemistry on composite properties," *Cellulose Nanocomposites*, K. Oksman and M. Sain, eds., Washington, DC: American Chemical Society, 2006, pp. 99-113.

R. Rowe, A. McKillop, and D. Bray, "The effect of batch and source variation on the crystallinity of microcrystalline cellulose," *International Journal of Pharmaceutics*, vol. 101, Jan. 1994, pp. 169-172.

R.A. Ryntz and D. Britz, "Scratch resistance behavior of automotive plastic coatings," *Journal of Coatings Technology*, vol. 74, Feb. 2002, pp. 77-81.

E. Small and D. Marcus, "Hemp: A new crop with new uses for North America," *Trends in new crops and new uses. ASHS Press, Alexandria, VA*, 2002, pp. 284-326.

C. Smith, "Plastics News - Bayer shows one-piece polycarbonate tailgate," *European Plastics News*, 2010.

C. Smith, "Bugatti's supercar gets a transparent PC roof," *European Plastics News*, 2010.

D. Smock, "More composites for cars?," *Design News*, 2010.

J. Sottys, Z. Listowski, and J. Knapczyk, "X-ray diffraction study of the crystallinity index and the structure of the microcrystalline cellulose," *Acta Pharmaceutica Technologica*, vol. 30, 1984, pp. 174-181.

J. Soulestin, N. Quiévy, M. Sclavons, and J. Devaux, "Polyolefins–biofibre composites: A new way for an industrial production," *Polymer Engineering & Science*, vol. 47, Apr. 2007, pp. 467-476.

M. Tajvidi and A. Takemura, "Thermal degradation of natural fiber-reinforced polypropylene composites," *Journal of Thermoplastic Composite Materials*, vol. 23, Sep. 2009, pp. 281-298.

M.K. Tam, "Class Notes." *NE 335: Macromolecular Science 2,* 2008.

I.A. Tarchevsky and G.N. Marchenko, *Cellulose: Biosynthesis and structure*, Berlin: Springer-Verlag, 1991.

N.G. Taylor, "Cellulose biosynthesis and deposition in higher plants.," *The New Phytologist*, vol. 178, Jan. 2008, pp. 239-52.

R. Teeaar, R. Serimaa, and T. Paakkarl, "Crystallinity of cellulose, as determined by CP/MAS NMR and XRD methods," *Polymer Bulletin*, vol. 17, Mar. 1987, pp. 231-237.

J. Tetreau, *Impact of nanotechnology in Alberta: Nanocrystalline cellulose*, Edmonton: 2010.

Tullo, "c,mm,n - open source mobility."

D. Viet, S. Beck-Candanedo, and D.G. Gray, "Dispersion of cellulose nanocrystals in polar organic solvents," *Cellulose*, vol. 14, Oct. 2006, pp. 109-113.

D. Vink in Neuss, "K2010: SPE Award for PC roof panel from Webasto," *European Plastics News*, 2010.

B. Wang, M. Sain, and K. Oksman, "Study of structural morphology of hemp fiber from the micro to the nanoscale," *Applied Composite Materials*, vol. 14, Jan. 2007, pp. 89-103.

I.M. Watt, *The principles and practice of electron microscopy*, Cambridge: Cambridge University Press, 1985.

G.E. Wissler and B. Crist, "Glass transition in semicrystalline polycarbonate," *Journal of Polymer Science: Polymer Physics Edition*, vol. 18, Jun. 1980, pp. 1257-1270.

P. Yoon, "Polycarbonate nanocomposites: Part 2. Degradation and color formation," *Polymer*, vol. 44, Aug. 2003, pp. 5341-5354.

P. Yoon, "Polycarbonate nanocomposites. Part 1. Effect of organoclay structure on morphology and properties," *Polymer*, vol. 44, Aug. 2003, pp. 5323-5339.

P. Zadorecki and A.J. Michell, "Future prospects for wood cellulose as reinforcement in organic polymer composites," *Polymer Composites*, vol. 10, Apr. 1989, pp. 69-77.

H. Zhao, J. Kwak, Z. Conradzhang, H. Brown, B. Arey, and J. Holladay, "Studying cellulose fiber structure by SEM, XRD, NMR and acid hydrolysis," *Carbohydrate Polymers*, vol. 68, Mar. 2007, pp. 235-241.

Appendix 1 – Material Specification Sheets

Certificate Of Analysis

Star Plastics Inc
Jackson County Industrial Center
Millwood WV 25262
Phone: (304) 273-0352
Fax: (304) 273-3326

Customer Name : POLYONE
Product : PC743R-CLS112
Lot : 62896
Date : 6/18/2009

Izod Impact, Notched 73F .125"	ASTM D256A	17.1 9125/m	Ft-Lb/In
Melt Flow 300C/1.2kg	ASTM D1238	12.0	Grams/10Min.
UL Vertical Burn @ 0.060"	UL Standard 94	94V2	Pass

Certified By: Mickey Ballard
              Quality Assurance Rep.

An ISO 9001:2000 Registered Company

Figure A.1.1 – PC743R specification sheet for Batch 62896

138

Star Plastics PC743 Molding Grade PC

Categories: Polymer; Thermoplastic; Polycarbonate; Polycarbonate, Molded

Material Notes:	Information provided by Star Plastics, Inc.
Vendors:	No vendors are listed for this material. Please click here if you are a supplier and would like information on how to add your listing to this material.

Printer friendly version   Download as PDF   Download to Excel (requires Excel and Windows)

Export data to your CAD/FEA program   Add to Folder: ☐ My Folder ▲▼ **0/0**

Physical Properties	Metric	English	Comments
Specific Gravity	1.20 g/cc	1.20 g/cc	ASTM D792
Maximum Moisture Content	0.0200	0.0200	
Linear Mold Shrinkage	0.00500 - 0.00700 cm/cm	0.00500 - 0.00700 in/in	ASTM D955
Melt Flow	11.0 g/10 min @Load 1.20 kg, Temperature 300 °C	11.0 g/10 min @Load 2.65 lb, Temperature 572 °F	ASTM D1248

Mechanical Properties	Metric	English	Comments
Tensile Strength, Yield	62.1 MPa	9000 psi	ASTM D638
Tensile Modulus	2.41 GPa	350 ksi	ASTM D638
Flexural Modulus	2.41 GPa	350 ksi	ASTM D790
Flexural Yield Strength	89.6 MPa	13000 psi	ASTM D790
Izod Impact, Notched	8.01 J/cm	15.0 ft-lb/in	73°F, 0.125 in.; ASTM D256

Thermal Properties	Metric	English	Comments
Deflection Temperature at 1.8 MPa (264 psi)	129 °C	265 °F	unannealed, .125in; ASTM D648
Flammability, UL94	HB	HB	.045in
	V-2	V-2	.062in

Processing Properties	Metric	English	Comments
Rear Barrel Temperature	271 - 288 °C	520 - 550 °F	
Middle Barrel Temperature	277 - 299 °C	530 - 570 °F	
Front Barrel Temperature	288 - 316 °C	550 - 600 °F	
Nozzle Temperature	288 - 316 °C	550 - 600 °F	
Melt Temperature	288 - 316 °C	550 - 600 °F	
Mold Temperature	76.7 - 104 °C	170 - 220 °F	
Drying Temperature	121 °C	250 °F	
Dry Time	4 hour	4 hour	
Back Pressure	0.345 - 0.689 MPa	50.0 - 100 psi	
Screw Speed	40.0 - 75.0 rpm	40.0 - 75.0 rpm	

Some of the values displayed above may have been converted from their original units and/or rounded in order to display the information in a consistent format. Users requiring more precise data for scientific or engineering calculations can click on the property value to see the original value as well as raw conversions to equivalent units. We advise that you only use the original value or one of its raw conversions in your calculations to minimize rounding error. We also ask that you refer to MatWeb's terms of use regarding this information. Click here to view all the property values for this datasheet as they were originally entered into MatWeb.

Figure A.1.2 – PC743R specification sheet from MatWeb.com

ARBOCEL®

Ultrafine Cellulose

Basic raw material

highly pure cellulose

Characteristic

ultrafine white powder, in water dispersible, insoluble

Physical and chemical properties

cellulose content	approx.	99,5 %
average particle size	approx.	1 µm
bulk density	approx.	160 g/l
whiteness (absolute value at 461 nm)		> 85 %
residue on ignition (850 °C, 4 h)		< 0,15 %
pH-value		5 – 7,5

As with all natural products slight differences to the above given values may arise.

General references

ARBOCEL® cellulose fibres are environment friendly products, gained from reple
materials.
Among other things, they are used as thickeners, for fibre reinforcement, as an al
diluents or as a carrier and filler in most manifold application fields.

CAS-Nr.: 9004-34-6

JRS

J. RETTENMAIER & SÖHNE GMBH + CO   Telefon: 0 79 67/1 52-39
Fasern aus der Natur   Telefax: 0 79 67/1 52 50
Holzmühle 1
D-73494 Rosenberg

Figure A.1.3 – Specification sheet for JRS's UFC-100

ARBOCEL®

Nano Disperse Cellulose Paste

Characteristics

ARBOCEL NANO MF 40-10 is a nano disperse cellulose , insoluble but dissolvable in water.

Standardanalysis

composition
Nano Disperse Cellulose	9 % - 11 %
water	89 % - 91 %

pH-value (10% suspension)   5 - 7.5

Average particle size of the nano disperse cellulose
(Laser reading with Beckman Coulter LS 230)	approx.	4.5 µm
CIE L* (6% watery dispersion)	approx.	92
Brightness (refexion at 460 nm, dry)	approx.	85 %
Viscosity (6 %, Brookfield, Spindle 3, 20 rpm)	approx.	200 mPas

Delivery form: watery paste; approx. 10 % solid content
Packing: Big Bags
Stability: max. 2 month

Figure A.1.4 – Specification sheet for JRS's MF 40-10

Antioxidant Plaox-1098

**Chemical name:** *N, N'-hexane-1, 6-diylbis [3-(3, 5-di-tert-butyl-4-hydroxyphenyl) propionamide]*
Equivalent: *Irganox 1098 (Ciba SC)/ Lowinox HD98 (Chemtura)*
Molecular formula: $C_{40}H_{64}N_2O_4$
Molecular weight: *636.96*
CAS No.: *23128-74-7*
Structural formula:
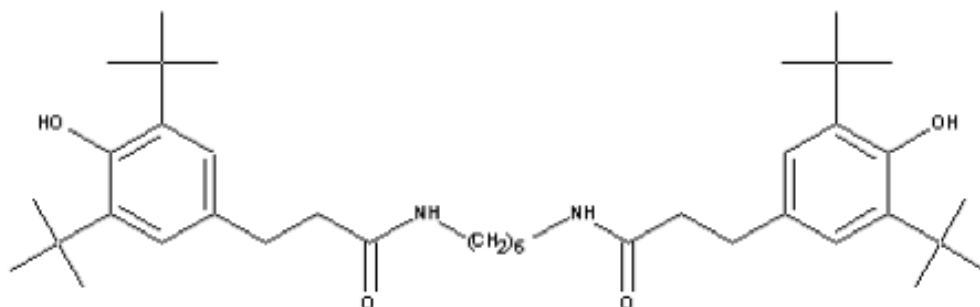
Physical properties

Appearance: White crystal powder
Melting range: 156 ~ 161.5 °C

Flash point: 540 °C
Bulk density: (g/cm3), @20 °C: 1.04

Solubility (g/ 100g solvent), @20 °C

Water: 0.01
Benzene: 0.01
Acetone: 2.8

Methanol: 6.0
N-hexane: 0.01

Specifications

Appearance: White powder
Melting point: 156 ~ 161 °C
Volatile: 0.5% max
Ash: 0.1% max

Transmittance (425nm): 97.0% min
Transmittance (500nm): 98.0% min
Clarity of solution: Clear
Assay: 98% min

Applications

Plaox-1098 is widely used in nylon 6, nylon 66, PE, PP, PA, rubber, etc. It is of low volatility and good extraction-resistance in hot water. The dosage is recommended to be 0.1~0.5 phr.

Figure A.1.5 – Specification sheet for Irganox 1098

Appendix 2 – Particle Size Analysis via DLS

Brookhaven Instruments Corp.
Default Particle Sizing Software Ver. 5.22

Date: Jul 27, 2010
Time: 14:31:59
Batch: 0

Sample ID   **NCC_AL_AFinkle (Combined)**
Operator ID **Ben**
Notes

Measurement Parameters:			
Temperature	= 25.0 deg. C	Runs Completed	= 2
Liquid	= Water	Run Duration	= 00:05:00
Viscosity	= 0.890 cP	Total Elapsed Time	= 00:10:00
Ref.Index Fluid	= 1.330	Average Count Rate	= 406.7 kcps
Angle	= 90.00	Ref.Index Real	= 1.590
Wavelength	= 659.0 nm	Ref.Index Imag	= 0.000
Baseline	= Auto (Slope Analysis)	Dust Filter Setting	= 30.00

NCC_AL_AFinkle (Combined)

Effective Diameter: 103.4 nm
Polydispersity: 0.348
Baseline Index: 6.8/ 98.11%
Elapsed Time: 00:10:00

Multimodal Size Distribution
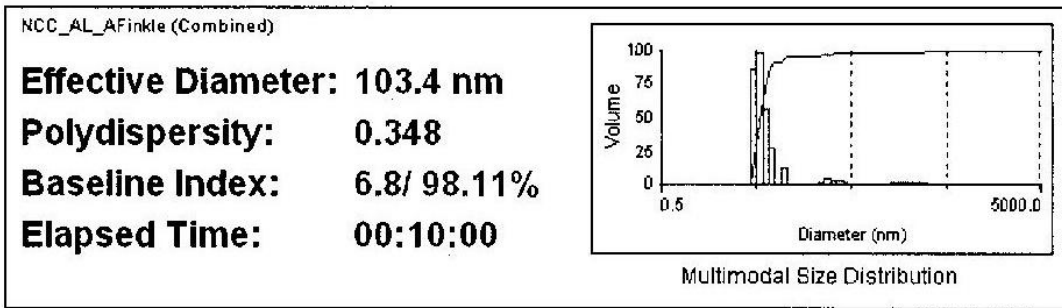
Run	Eff. Diam. (nm)	Half Width (nm)	Polydispersity	Baseline Index	
1	103.1	60.4	0.344	6.4/	96.94%
2	104.3	61.6	0.349	7.9/	99.28%
Mean	103.7	61.0	0.346	7.1/	98.11%
Std. Error	0.6	0.6	0.002	0.8/	1.17
Combined	103.4	61.0	0.348	6.8/	98.11%

Figure A.2.1 – DLS analysis and particle size for NCC-Alb in water

BIC | Brookhaven Instruments Corp.
Default Particle Sizing Software Ver. 5.22

Date: Jul 27, 2010
Time: 14:17:43
Batch: 0

Sample ID   **NCC_FP_AFinkle (Combined)**
Operator ID   **Ben**
Notes

Measurement Parameters:

Temperature	= 25.0 deg. C	Runs Completed	= 2
Liquid	= Water	Run Duration	= 00:05:00
Viscosity	= 0.890 cP	Total Elapsed Time	= 00:10:00
Ref.Index Fluid	= 1.330	Average Count Rate	= 401.6 kcps
Angle	= 90.00	Ref.Index Real	= 1.590
Wavelength	= 659.0 nm	Ref.Index Imag	= 0.000
Baseline	= Auto (Slope Analysis)	Dust Filter Setting	= 30.00

NCC_FP_AFinkle (Combined)

Effective Diameter: 222.9 nm
Polydispersity: 0.368
Baseline Index: 0.0/ 96.48%
Elapsed Time: 00:10:00

Multimodal Size Distribution

Run	Eff. Diam. (nm)	Half Width (nm)	Polydispersity	Baseline Index
1	223.0	133.7	0.359	0.0 / 96.48%
2	222.6	136.6	0.376	0.0 / 96.49%
Mean	222.8	135.2	0.368	0.0 / 96.48%
Std. Error	0.2	1.5	0.009	0.0 / 0.00
Combined	222.9	135.1	0.368	0.0 / 96.48%

Figure A.2.2 – DLS analysis and particle size for NCC-FP in water

# Appendix 3 – Cellulose FTIR Plots
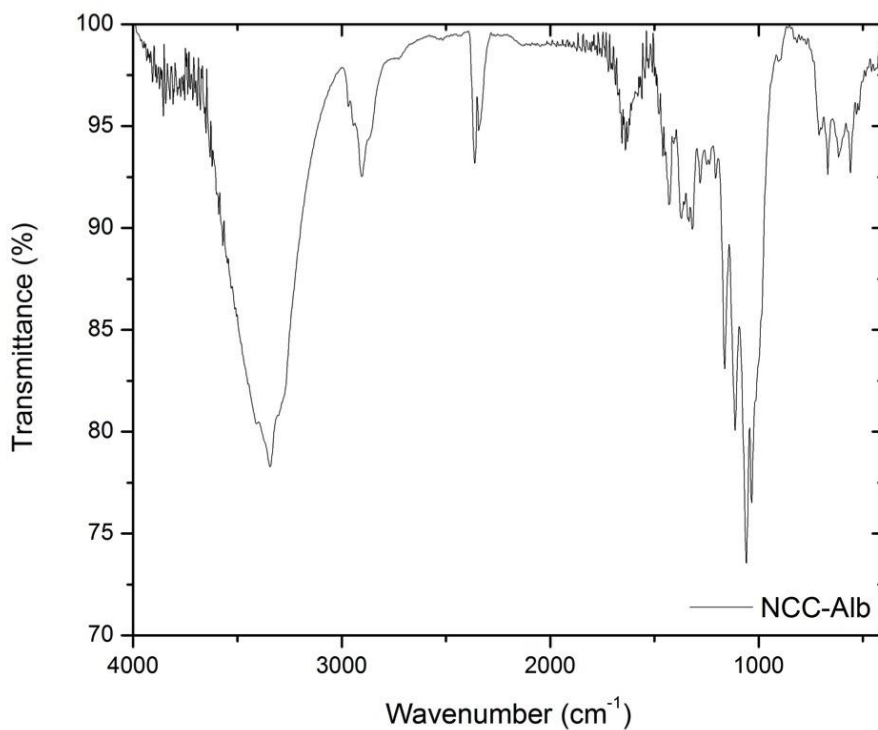
*Figure A.3.1 – FTIR spectrum for NCC-Alb prepared by KBr pellet*
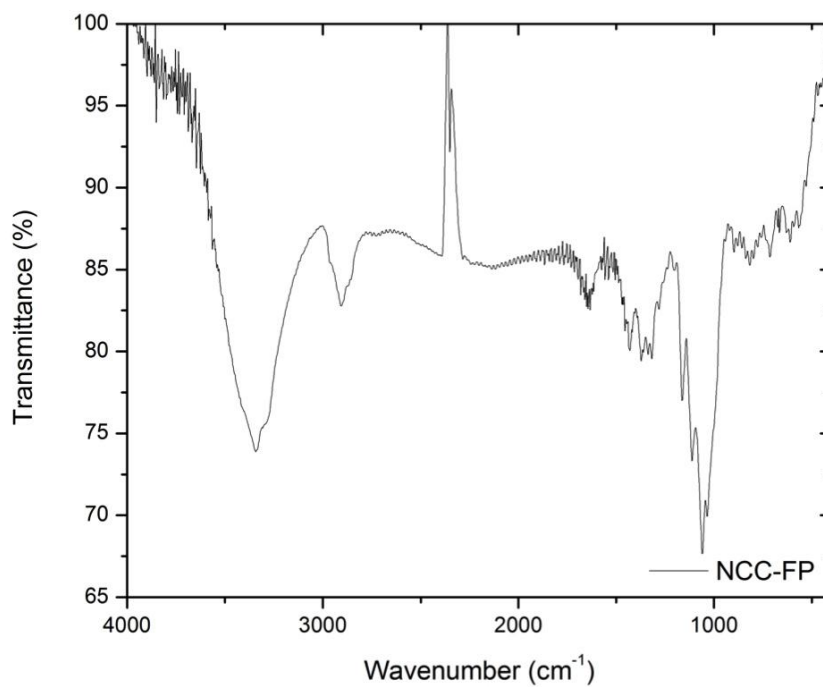
*Figure A.3.2 – FTIR spectrum for NCC-FP prepared by KBr pellet*
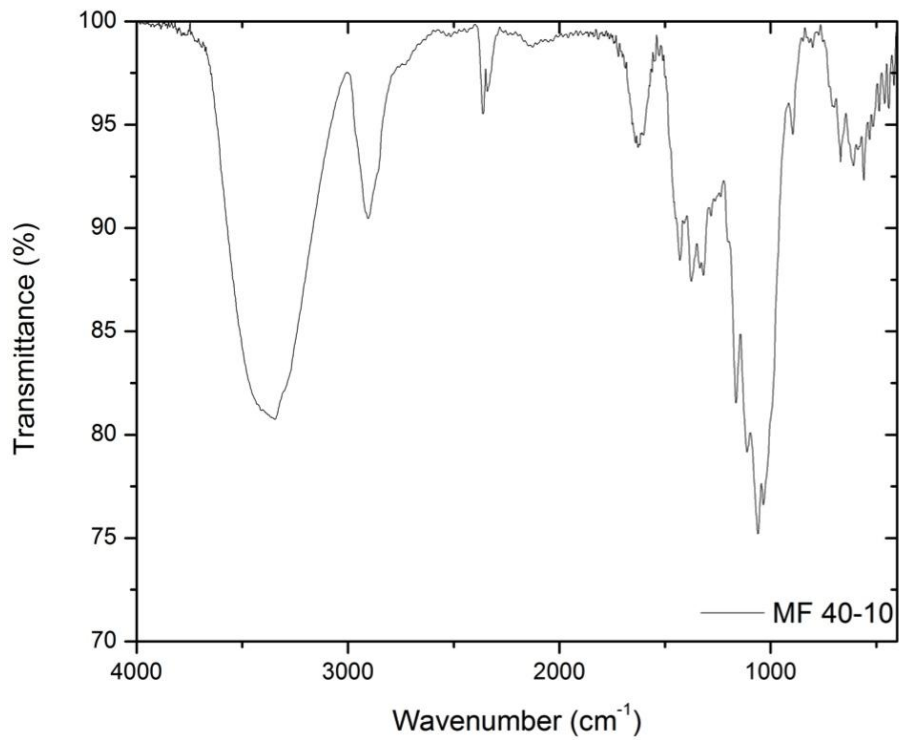
*Figure A.3.3 – FTIR spectrum for MF 40-10 prepared by KBr pellet*
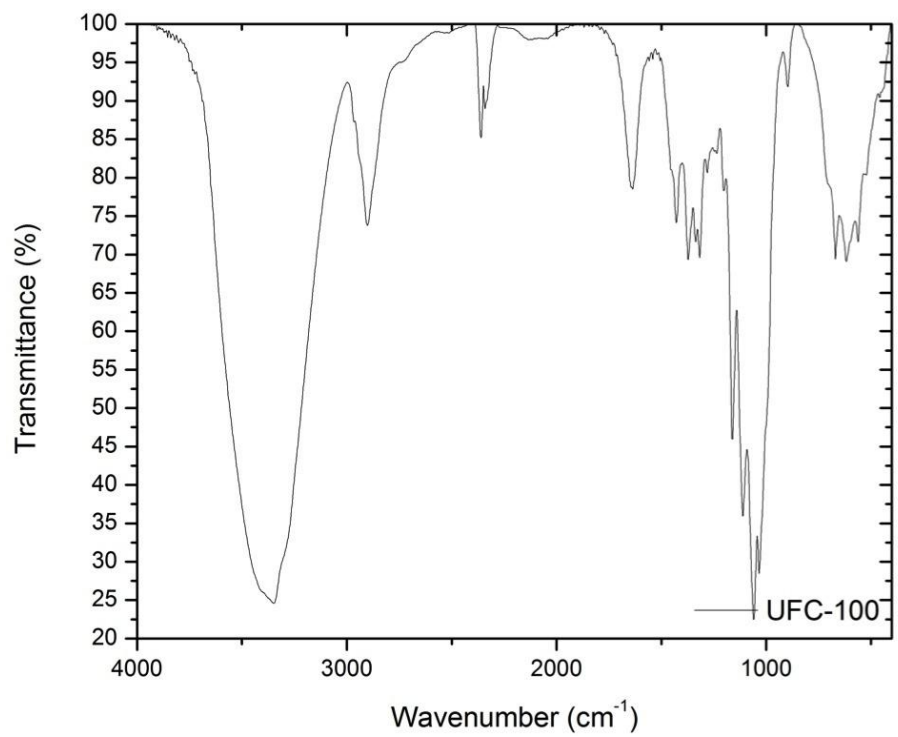
Figure A.3.4 – FTIR spectrum for UFC-100 prepared by KBr pellet

Appendix 4 – Cellulose XRD

a)

b)

c)
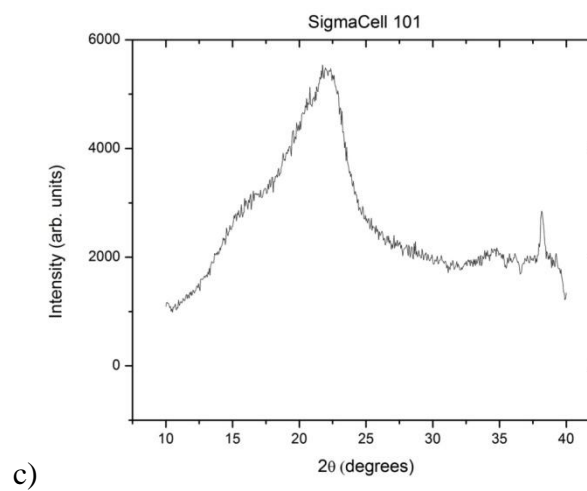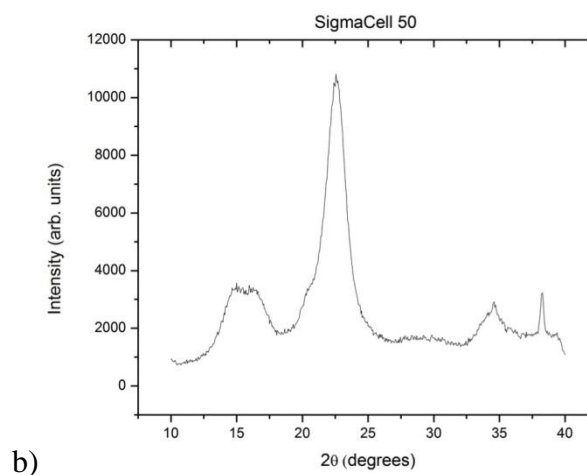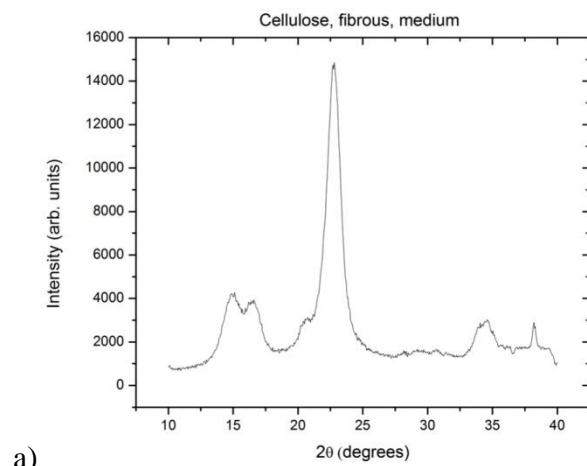
*Figure A.4.1 – XRD pattern for a) Cellulose, fib. Med, b) SigmaCell50 and c) SigmaCell 101*
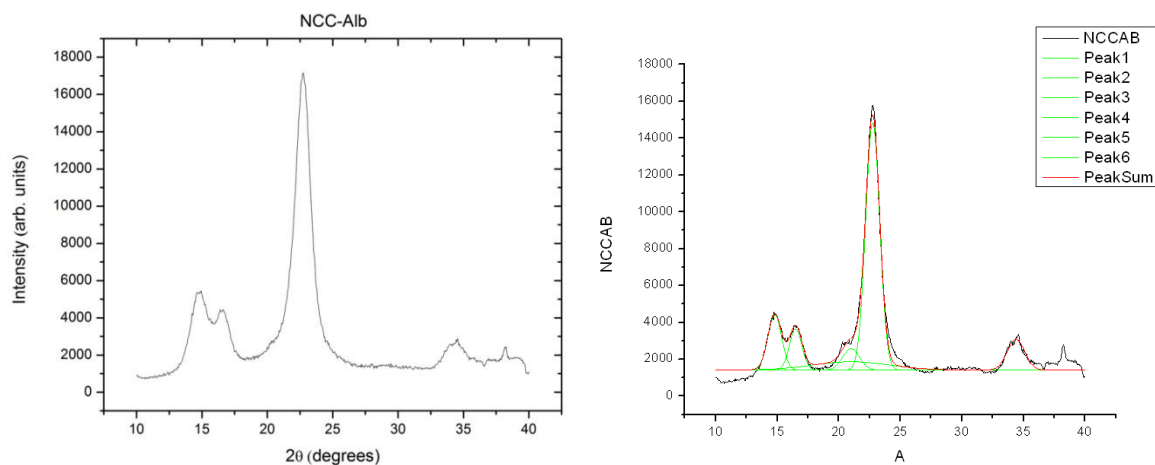
Figure A.4.2 – XRD pattern for NCC-Alb
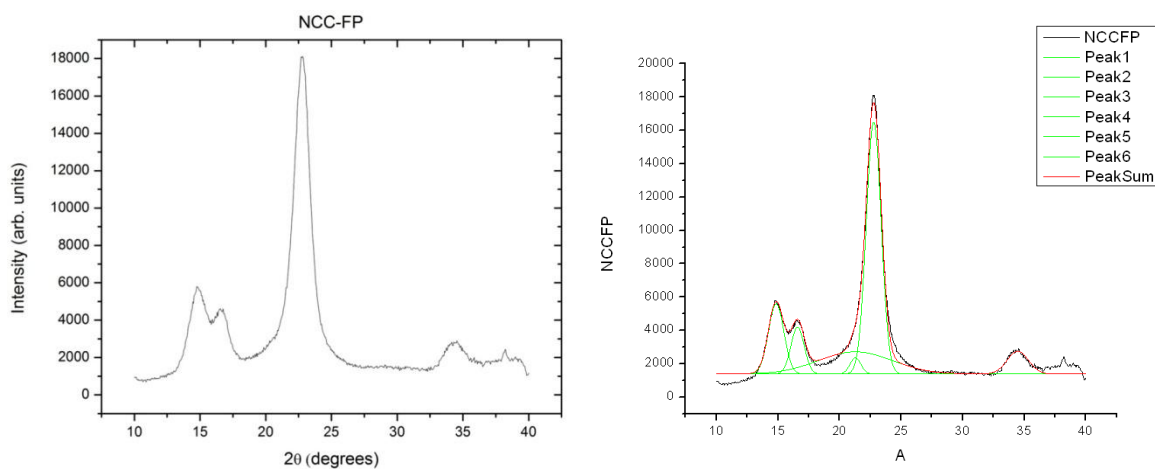

Figure A.4.3 – XRD pattern for NCC-FP
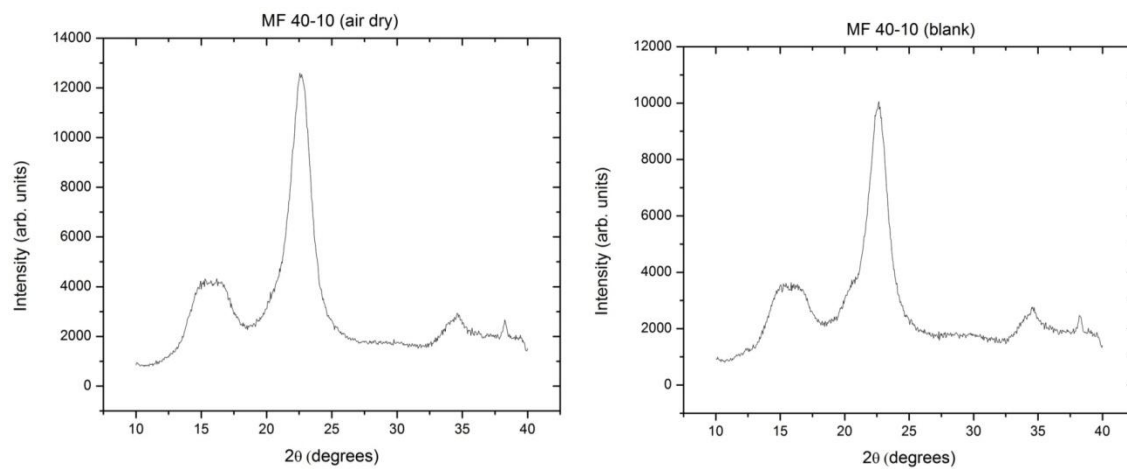
*Figure A.4.4 – XRD pattern for MF 40-10 (air dried) and MF 40-10 (solution mixed)*

148
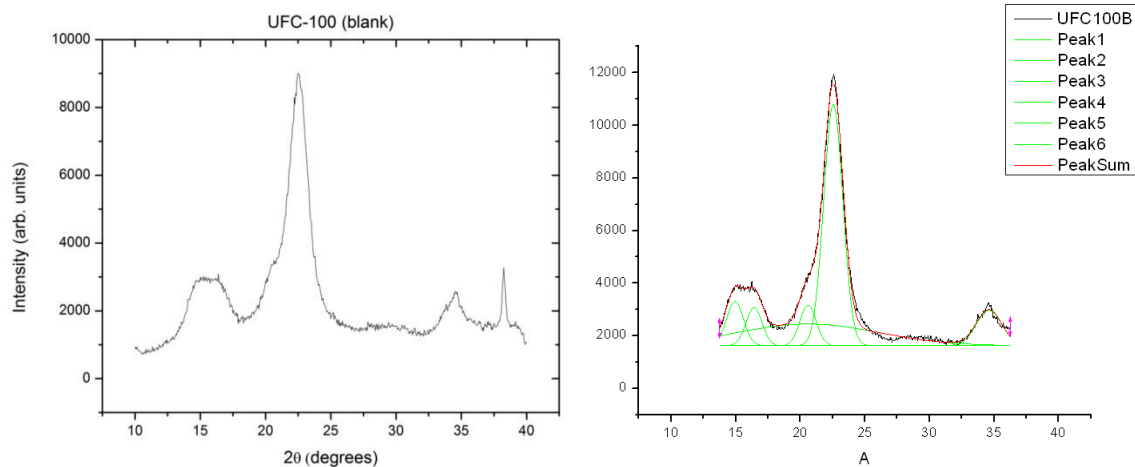
Figure A.4.5 – XRD pattern for UFC-100 (blank)

Reflection	101		10-1		021		002		040	
Sample	2Theta	Beta	2Theta	Beta	2Theta	Beta	2Theta	Beta	2Theta	Beta
UFC-100	14.94645	1.54832	16.42157	1.46469	20.60156	1.48958	22.55437	1.74434	34.60728	2.32638
NCC-FP	14.85241	1.46933	16.5906	1.26605	21.29414	1.03777	22.77672	1.42049	34.46964	2.03533
NCC-Alb	14.8071	1.45407	16.54403	1.24223	21.40915	1.27996	22.75219	1.3826	34.4565	1.99034
NCC-Alb (Blank)	14.80391	1.30528	16.49863	1.17891	20.9985	1.5807	22.75435	1.34216	34.39637	1.66496
Average	14.85247		16.51371		21.07584		22.7094075		34.48245	

Reflection	101	10-1	021	002
Sample	d (nm)	d (nm)	d (nm)	d (nm)
UFC-100	5.75	6.09	6.02	5.16
NCC-FP	6.06	7.05	8.65	6.34
NCC-Alb	6.12	7.18	7.02	6.51
NCC-Alb (Blank)	6.82	7.57	5.68	6.71

Figure A.4.6 – Scherrer equation data for calculating grain / crystallite Size

149

	Value	Error
y0	1621.0693	98.51256
xc1	14.94645	0.07737
w1	1.31502	0.11807
A1	2762.23029	395.74108
sigma1	0.65751	
FWHM1	**1.54832**	**2.70E-02**
Height1	1675.97571	
xc2	16.42157	0.08408
w2	1.24399	0.10946
A2	2265.9045	342.80412
sigma2	0.62199	
FWHM2	**1.46469**	**2.56E-02**
Height2	1453.33278	
xc3	20.60146	0.48464
w3	10.98251	2.08474
A3	11353.75919	3002.37332
sigma3	5.49125	
FWHM3	**12.93092**	**2.26E-01**
Height3	824.85607	
xc4	20.60156	0.0331
w4	1.26513	0.06348
A4	2446.52876	156.67488
sigma4	0.63256	
FWHM4	**1.48958**	**2.60E-02**
Height4	1542.96241	
xc5	22.55437	0.00604
w5	1.4815	0.01309
A5	17029.40869	195.90173
sigma5	0.74075	
FWHM5	**1.74434**	**3.04E-02**
Height5	9171.42308	
xc6	34.60728	0.02983
w6	1.97585	0.10316
A6	3316.60246	296.85447
sigma6	0.98792	
FWHM6	**2.32638**	**4.06E-02**
Height6	1339.30818	

	Area	Center	Width	Height
1	2762.23029	14.94645	1.31502	1675.97571
2	2265.9045	16.42157	1.24399	1453.33278
3	11353.75919	20.60146	10.9825	824.85607
4	2446.52876	20.60156	1.26513	1542.96241
5	17029.40869	22.55437	1.4815	9171.42308
6	3316.60246	34.60728	1.97585	1339.30818

Total Crystalline	27820.6747
Total	39174.43389
%CI	**71.02%**

DF	432
COD (R^2)	0.99597
ReducedChiSq	19991.59207

Figure A.4.7 – Peak Deconvolution data used to calculate %CI for UFC-100

	Value	Error
y0	1381.09771	23.23442
xc1	14.85241	0.02171
w1	1.24793	0.04343
A1	6586.49458	227.89883
sigma1	0.62397	
FWHM1	**1.46933**	**2.56E-02**
Height1	4211.17651	
xc2	16.5906	0.0301
w2	1.07528	0.06363
A2	3788.3309	277.33953
sigma2	0.53764	
FWHM2	**1.26605**	**2.21E-02**
Height2	2811.0263	
xc3	21.29385	0.19695
w3	6.00732	0.51167
A3	10010.75227	527.0419
sigma3	3.00366	
FWHM3	**7.07308**	**1.23E-01**
Height3	1329.61451	
xc4	22.77672	0.00655
w4	1.20645	0.01437
A4	22848.3929	341.6844
sigma4	0.60323	
FWHM4	**1.42049**	**2.48E-02**
Height4	15110.72106	
xc5	34.46964	0.04845
w5	1.72865	0.10525
A5	2952.14454	178.21788
sigma5	0.86433	
FWHM5	**2.03533**	**3.55E-02**
Height5	1362.60406	
xc6	21.29414	0.08625
w6	0.8814	0.16284
A6	1070.29082	268.48429
sigma6	0.4407	
FWHM6	**1.03777**	**1.81E-02**
Height6	968.87991	

	Area	Center	Width	Height
1	6586.49458	14.85241	1.24793	4211.17651
2	3788.3309	16.5906	1.07528	2811.0263
3	10010.75227	21.29385	6.00732	1329.61451
4	22848.3929	22.77672	1.20645	15110.72106
5	2952.14454	34.46964	1.72865	1362.60406
6	1070.29082	21.29414	0.8814	968.87991

Total Crystalline	37245.65374
Total	47256.40601
%CI	**78.82%**

DF	582
COD (R^2)	0.99077
ReducedChiSq	89365.25477

Figure A.4.8 – Peak Deconvolution data used to calculate %CI for NCC-FP

	Value	Error
y0	1327.31046	22.2982
xc1	14.8071	0.02091
w1	1.23497	0.04255
A1	6167.74358	206.60894
sigma1	0.61749	
FWHM1	**1.45407**	**2.54E-02**
Height1	3984.82387	
xc2	16.54403	0.02847
w2	1.05505	0.06044
A2	3580.17406	247.22684
sigma2	0.52752	
FWHM2	**1.24223**	**2.17E-02**
Height2	2707.51909	
xc3	21.40915	0.20087
w3	6.04151	0.57889
A3	8624.05289	497.88817
sigma3	3.02076	
FWHM3	**7.11334**	**1.24E-01**
Height3	1138.9533	
xc4	22.75219	0.01405
w4	1.17428	0.02037
A4	21013.50853	534.83101
sigma4	0.58714	
FWHM4	**1.3826**	**2.41E-02**
Height4	14278.03351	
xc5	34.4565	0.04775
w5	1.69044	0.10359
A5	2766.22957	167.82203
sigma5	0.84522	
FWHM5	**1.99034**	**3.47E-02**
Height5	1305.65854	
xc6	21.40915	0.17216
w6	1.0871	0.24164
A6	1464.3941	526.78143
sigma6	0.54355	
FWHM6	**1.27996**	**2.23E-02**
Height6	1074.80041	

	Area	Center	Width	Height
1	6167.74358	14.8071	1.23497	3984.82387
2	3580.17406	16.54403	1.05505	2707.51909
3	8624.05289	21.40915	6.04151	1138.9533
4	21013.50853	22.75219	1.17428	14278.03351
5	2766.22957	34.4565	1.69044	1305.65854
6	1464.3941	21.40915	1.0871	1074.80041

Total Crystalline	34992.04984
Total	43616.10273
%CI	80.23%

DF	582
COD (R^2)	0.99035
ReducedChiSq	81487.55101

Figure A.4.9 – Peak Deconvolution data used to calculate %CI for NCC-Alb (as received)

	Value	Error
y0	1411.35308	25.63034
xc1	14.80391	0.02607
w1	1.1086	0.05677
A1	4156.40991	233.53915
sigma1	0.5543	
FWHM1	**1.30528**	**2.28E-02**
Height1	2991.46468	
xc2	16.49863	0.03356
w2	1.00127	0.07571
A2	2809.7559	261.65264
sigma2	0.50064	
FWHM2	**1.17891**	**2.06E-02**
Height2	2239.01094	
xc3	20.9985	0.72011
w3	6.26038	2.03653
A3	3532.10821	623.71959
sigma3	3.13019	
FWHM3	**7.37103**	**1.29E-01**
Height3	450.16703	
xc4	22.75435	0.00837
w4	1.13992	0.01595
A4	19180.69373	378.65108
sigma4	0.56996	
FWHM4	**1.34216**	**2.34E-02**
Height4	13425.44172	
xc5	34.39637	0.0387
w5	1.41409	0.08312
A5	2949.72232	169.23908
sigma5	0.70704	
FWHM5	**1.66496**	**2.91E-02**
Height5	1664.35201	
xc6	20.9985	0.10378
w6	1.34252	0.23124
A6	1966.02123	491.1691
sigma6	0.67126	
FWHM6	**1.5807**	**2.76E-02**
Height6	1168.43949	

	Area	Center	Width	Height
1	4156.40991	14.80391	1.1086	2991.46468
2	2809.7559	16.49863	1.00127	2239.01094
3	3532.10821	20.9985	6.26038	450.16703
4	19180.69373	22.75435	1.13992	13425.44172
5	2949.72232	34.39637	1.41409	1664.35201
6	1966.02123	20.9985	1.34252	1168.43949

Total Crystalline	31062.60309
Total	34594.7113
%CI	89.79%

DF	582
COD (R^2)	0.98394
ReducedChiSq	104004.3761

Figure A.4.10 – Peak Deconvolution data used to calculate %CI for NCC-Alb (blank)

Appendix 5 – Moisture Content Plots
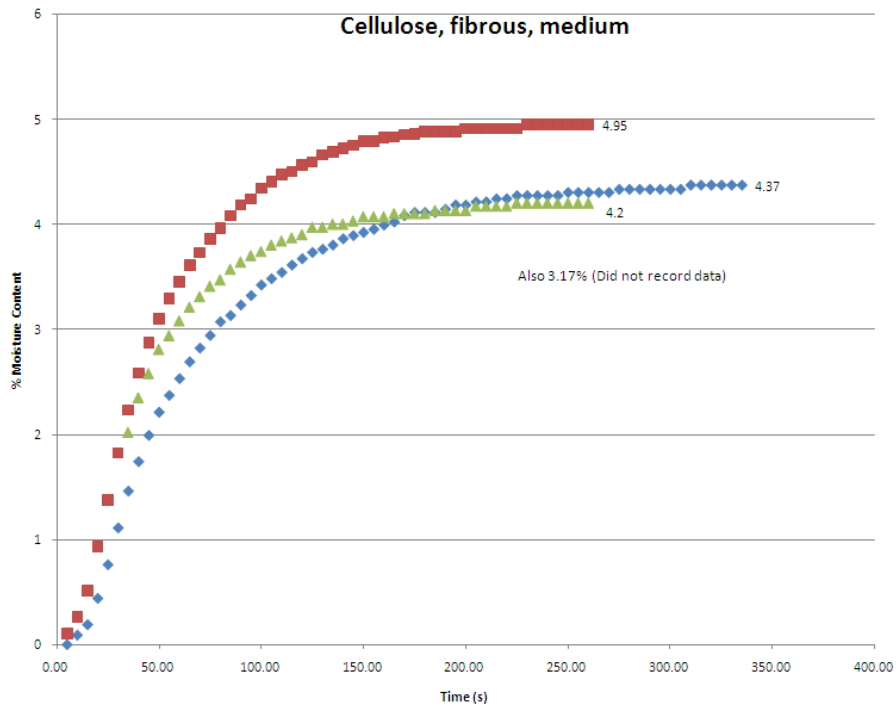
Figure A.5.1 – Moisture content analysis curves for Cellulose, fib, med.
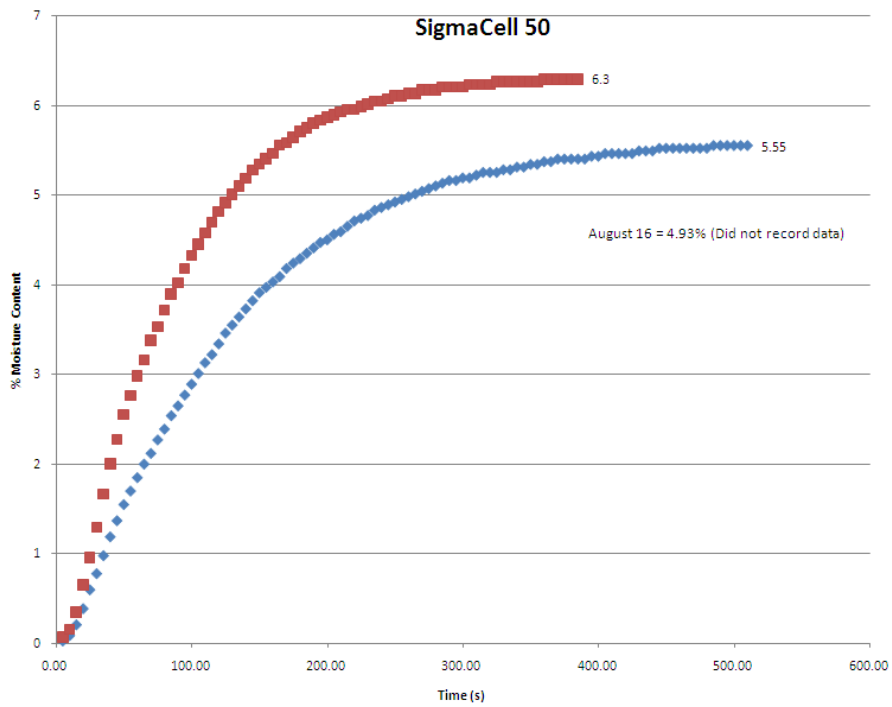

*Figure A.5.2 – Moisture content analysis curves for SigmaCell 50*
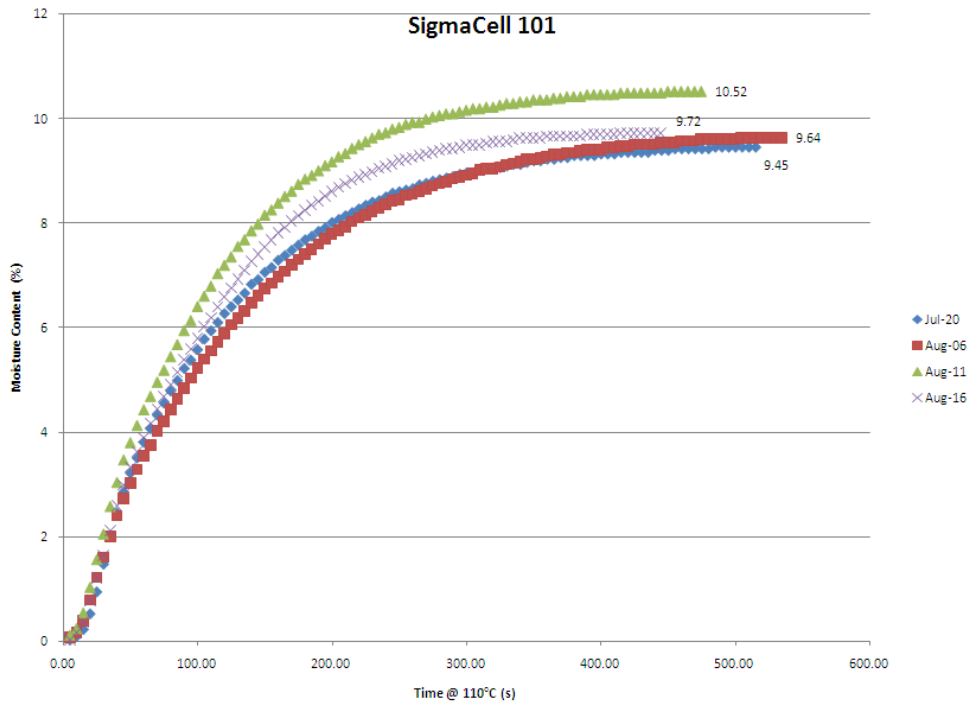
*Figure A.5.3 – Moisture content analysis curves for SigmaCell 101*
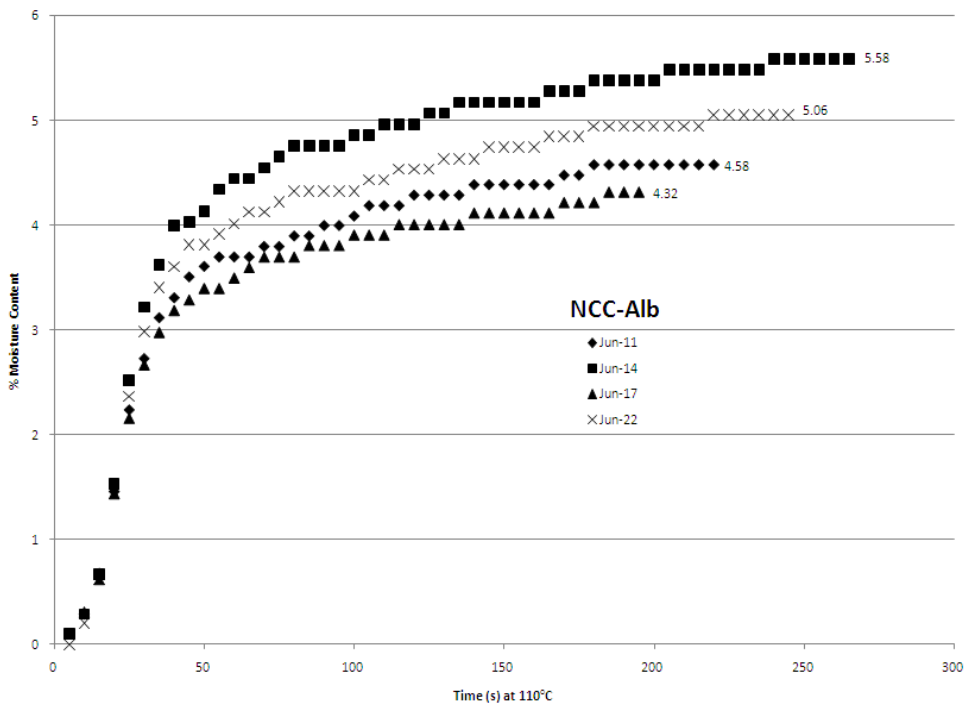
*Figure A.5.4 – Moisture content analysis curves for NCC-Alb*

153
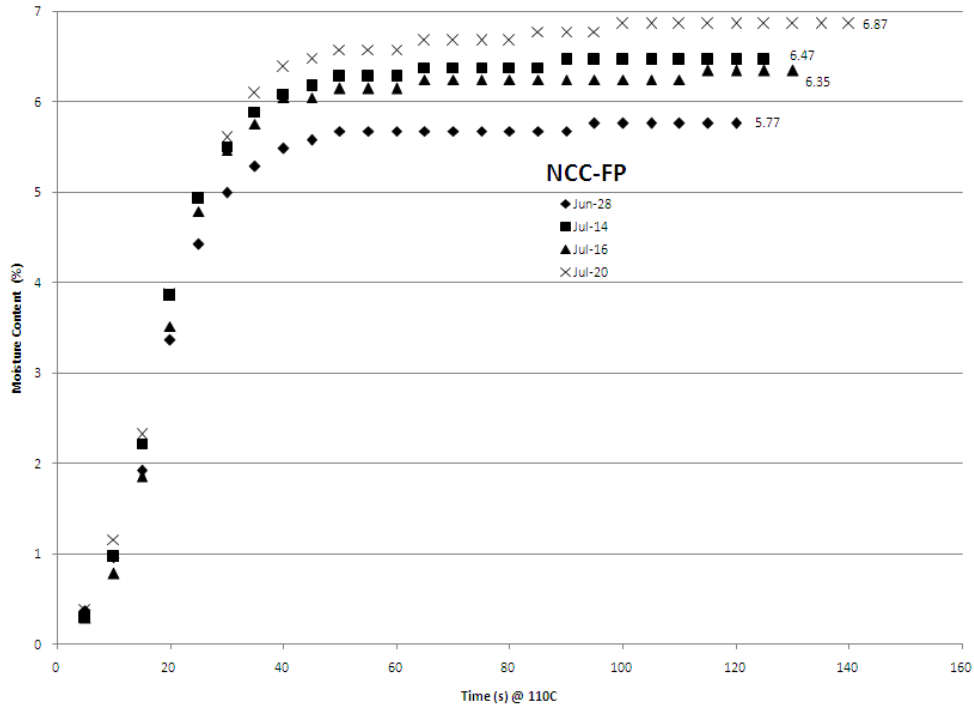
*Figure A.5.5 – Moisture content analysis curves for NCC-FP*
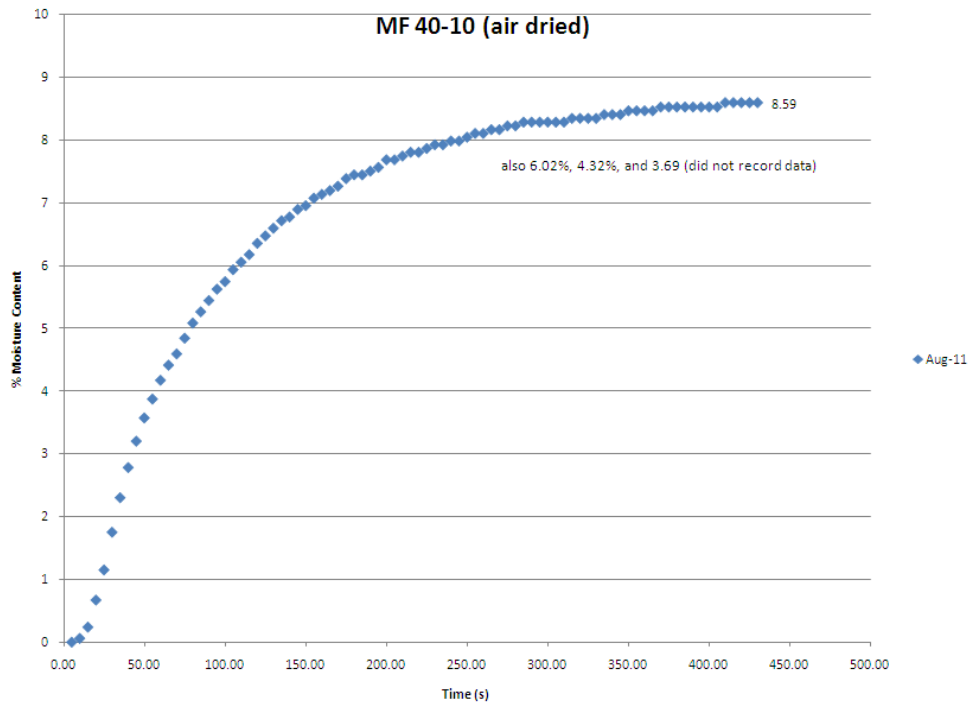
*Figure A.5.6 – Moisture content analysis curves for MF 40-10 (after drying)*

154
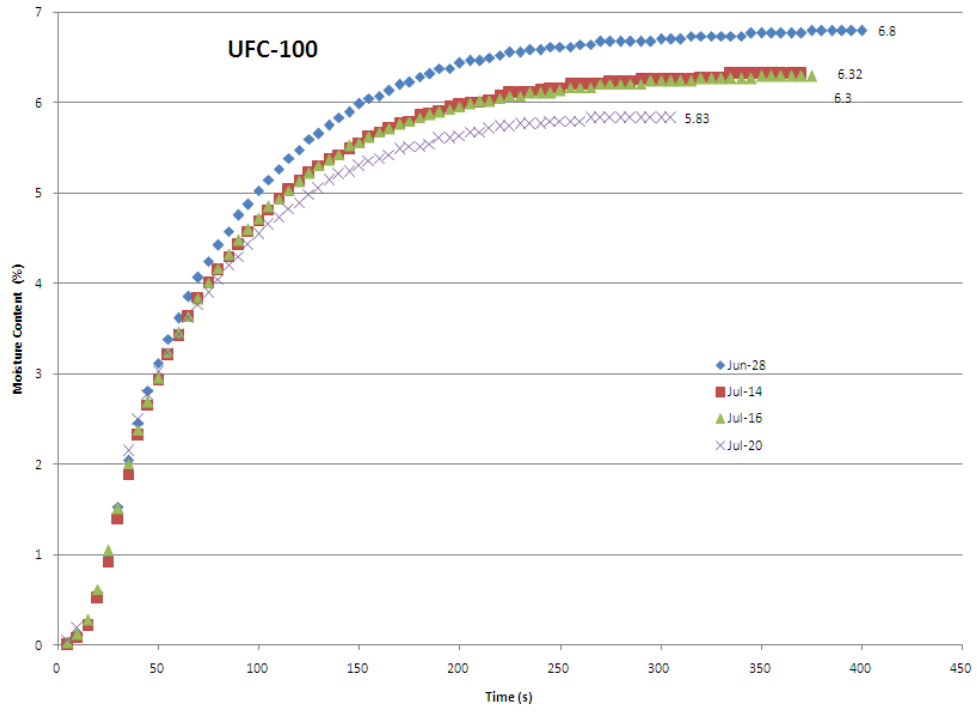
Figure A.5.7 – Moisture content analysis curves for UFC-100

Appendix 6 – OFW Activation Energy Plots
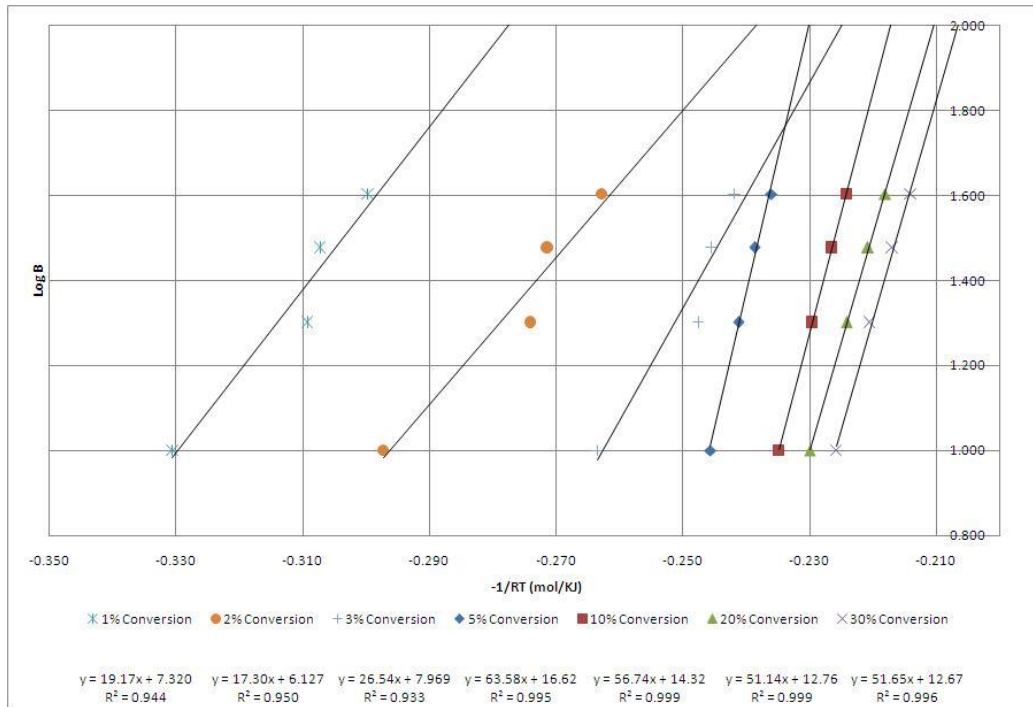
Figure A.6.1 – OFW calculations for activation energy of NCC-Alb (in air)
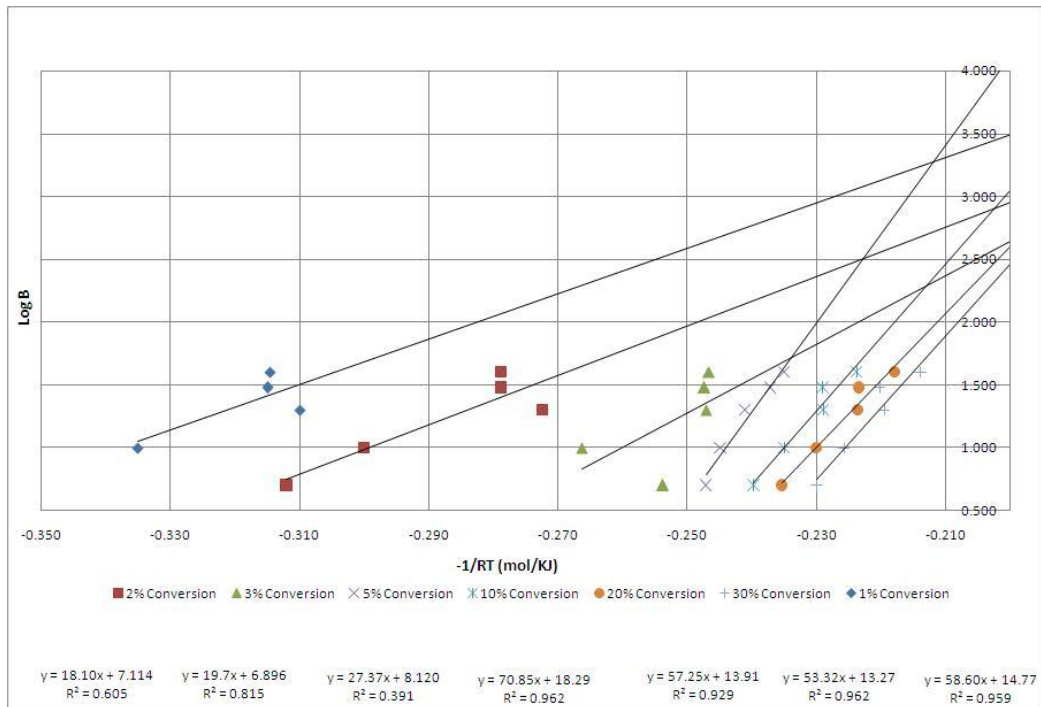
Figure A.6.2 – OFW calculations for activation energy of NCC-Alb (in nitrogen)
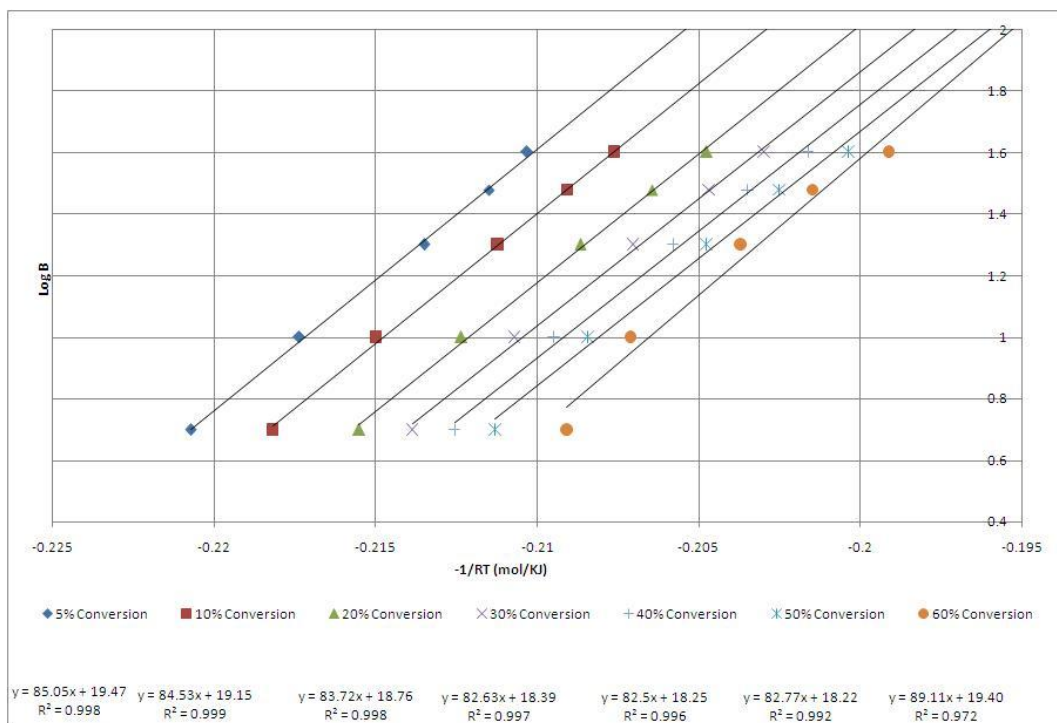
Figure A.6.3 – OFW calculations for activation energy of NCC-FP (in air)
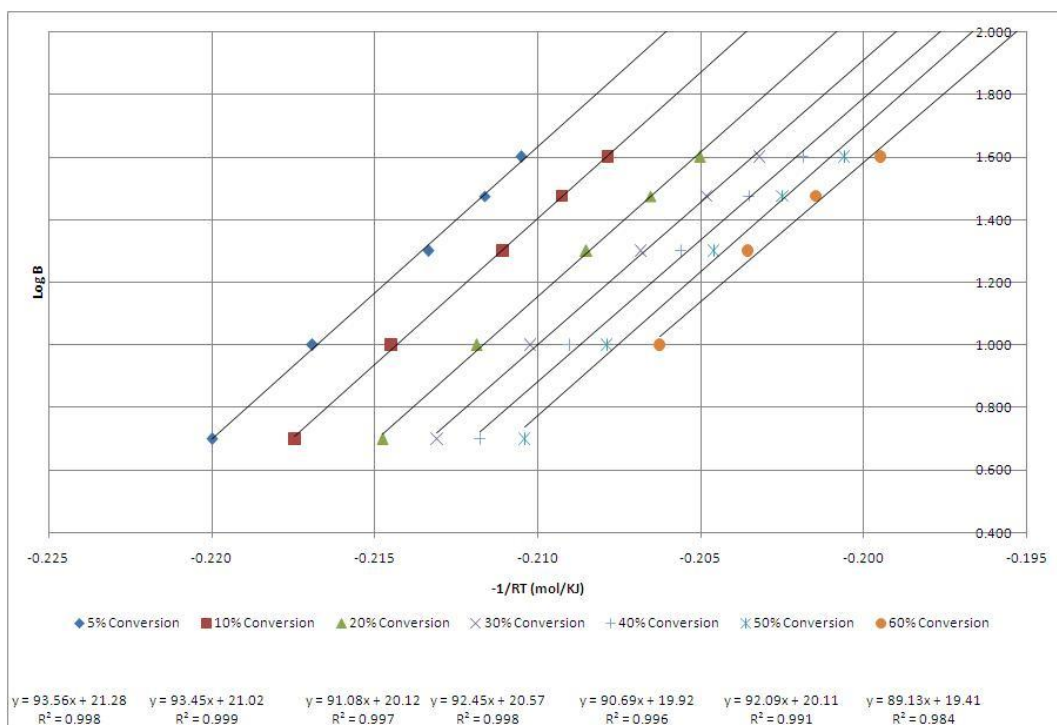
Figure A.6.4– OFW calculations for activation energy of NCC-FP (in nitrogen)

157
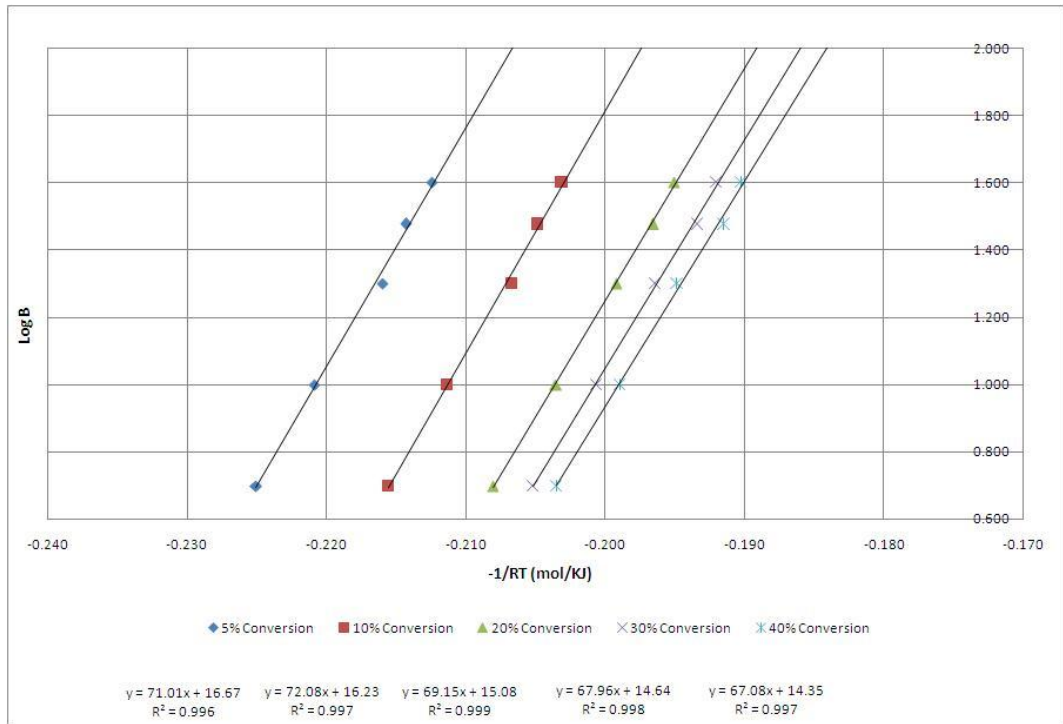
Figure A.6.5 – OFW calculations for activation energy of MF 40-10 (in air)
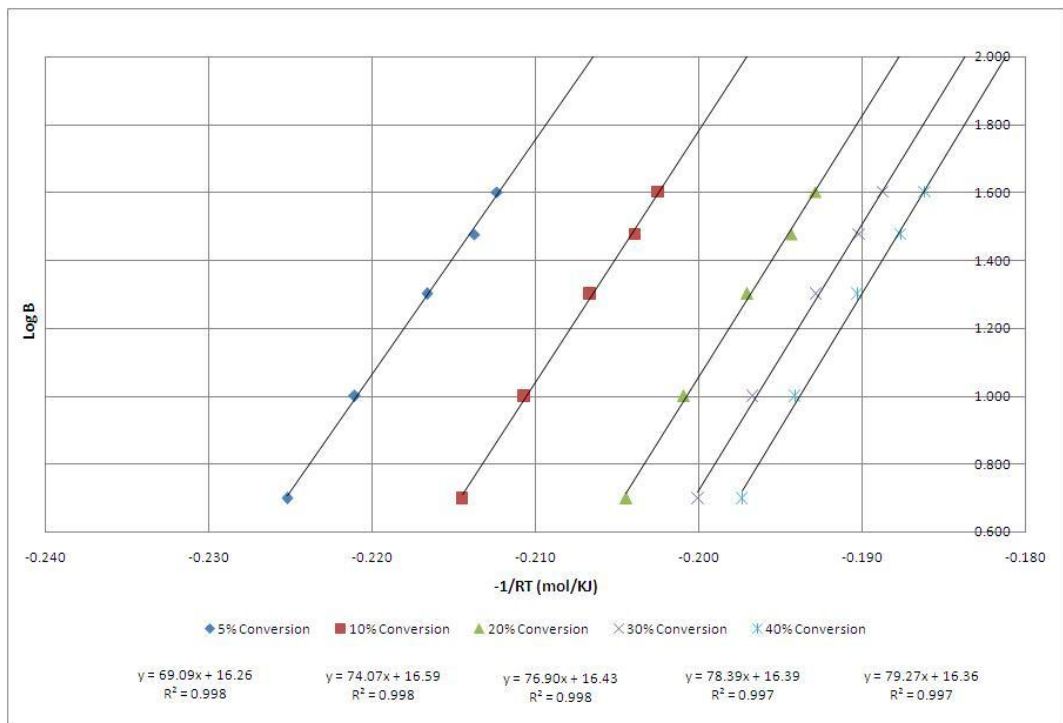
Figure A.6.6– OFW calculations for activation energy of MF 40-10 (in nitrogen)

158
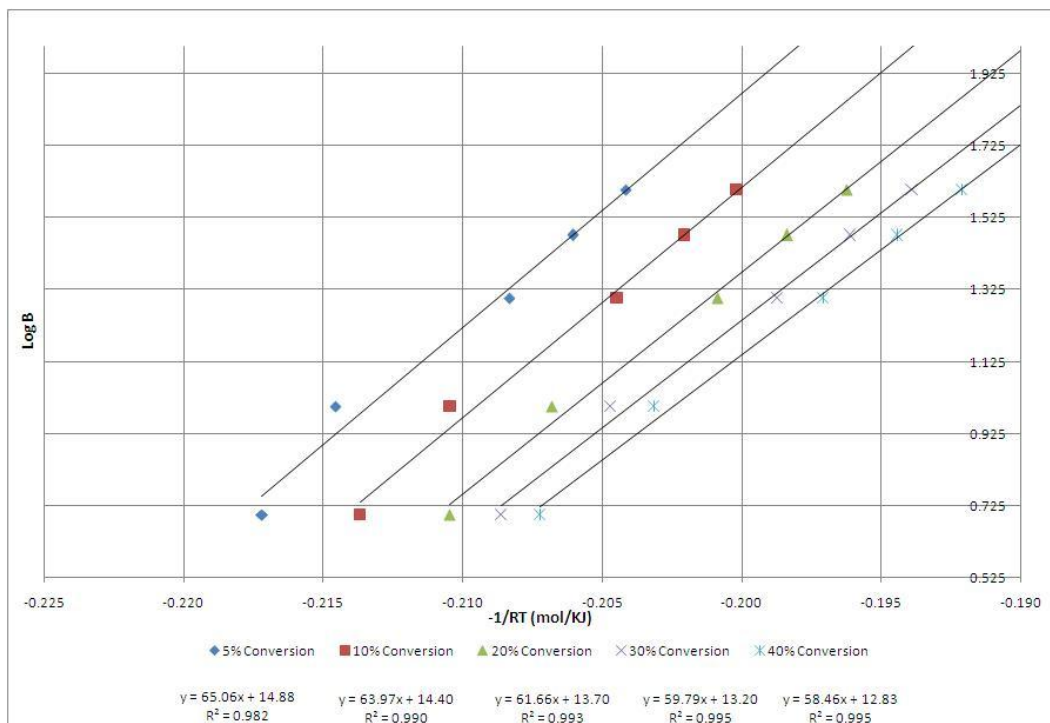
Figure A.6.7 – OFW calculations for activation energy of UFC-100 (in air)
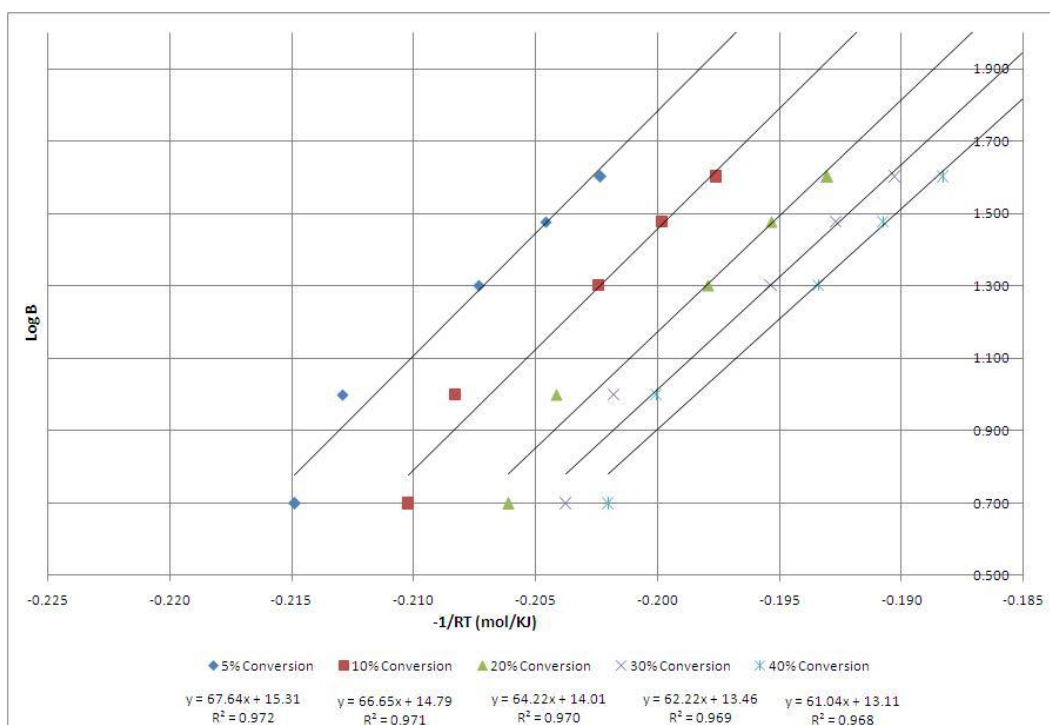
Figure A.6.8 – OFW calculations for activation energy of UFC-100 (in nitrogen)

159

Appendix 7 – Composite FTIR Plots
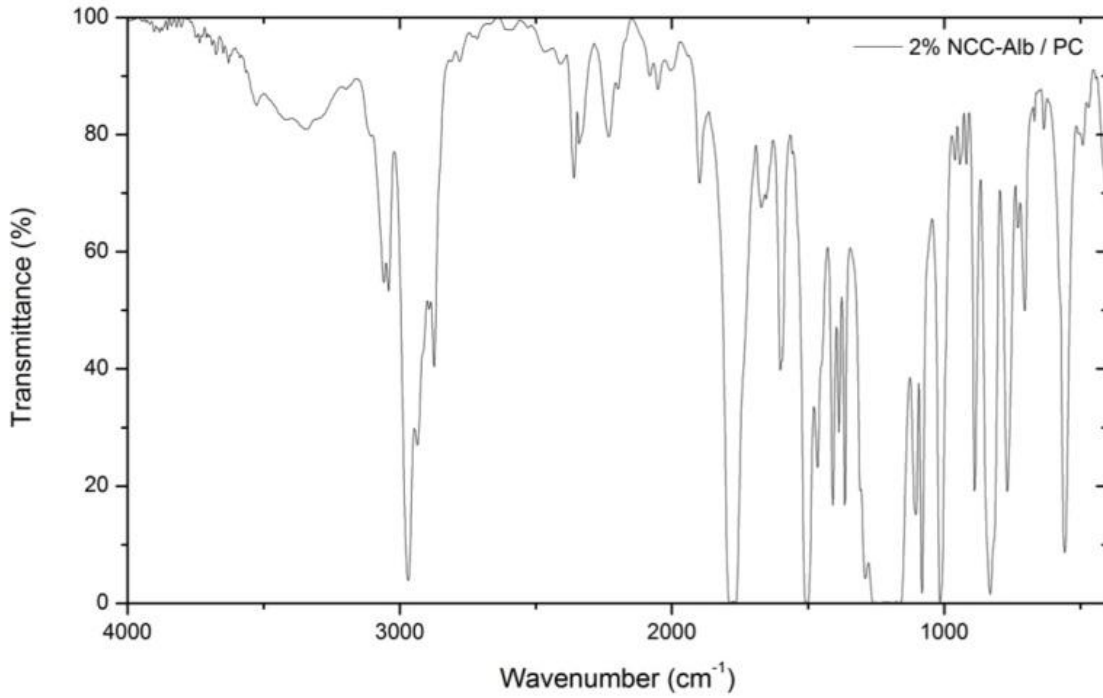
Figure A.7.1 – FTIR spectrum for 2% NCC-Alb / PC prepared by thin film
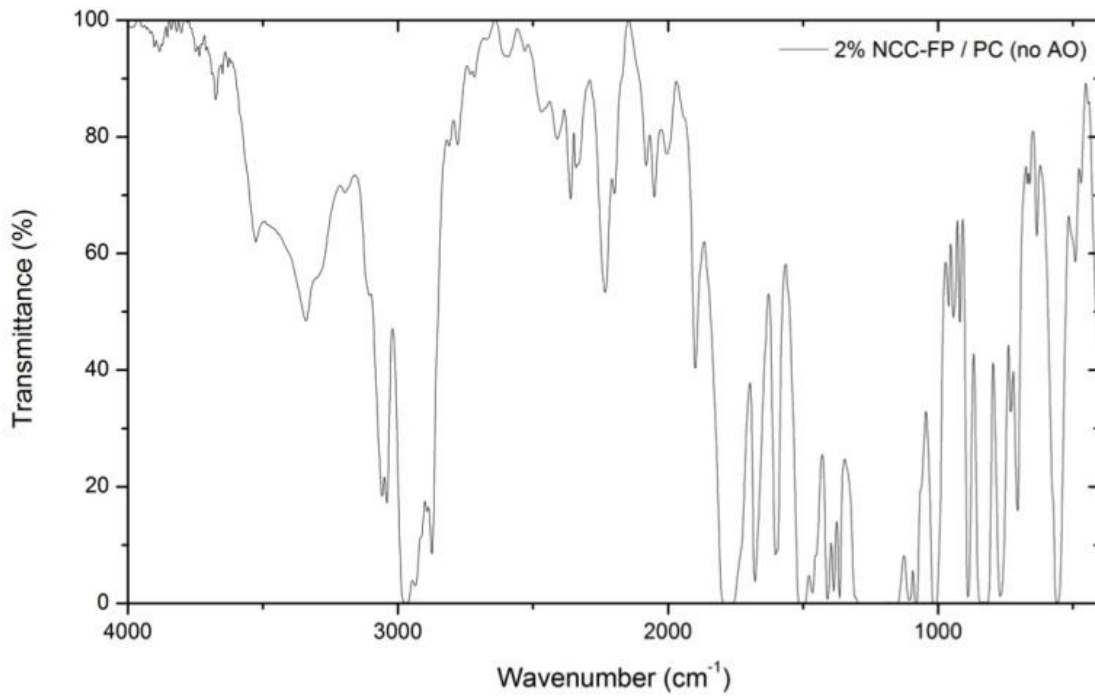
Figure A.7.2 – FTIR spectrum for 2% NCC-FP / PC (no AO) prepared by thin film
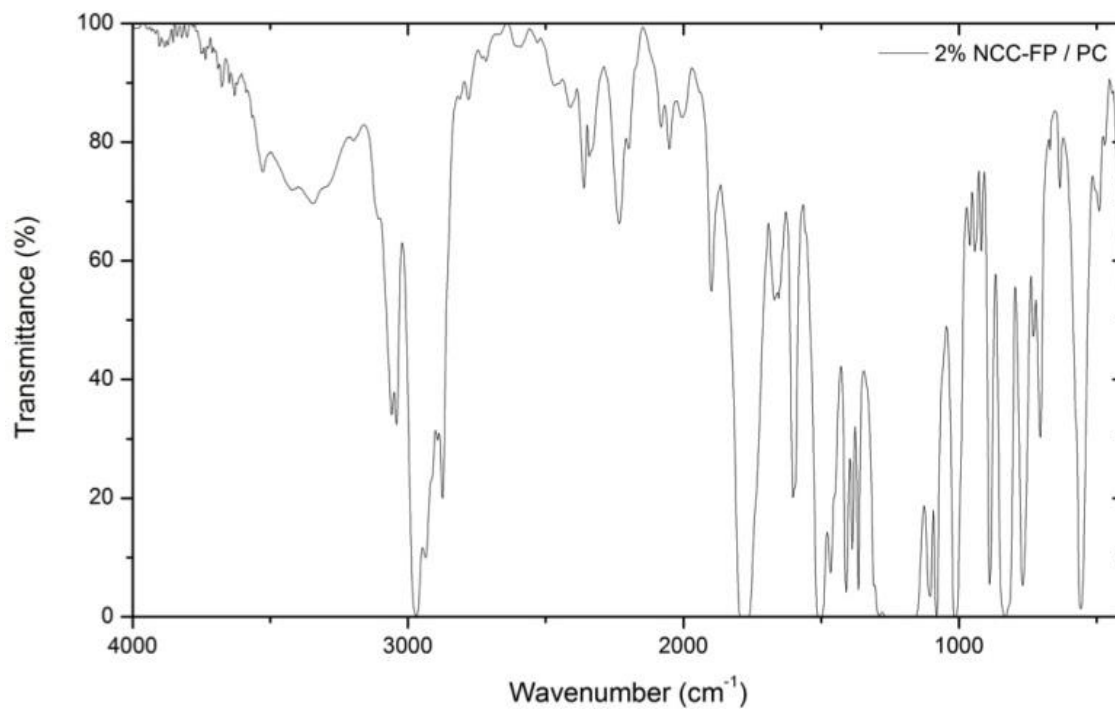
*Figure A.7.3 – FTIR spectrum for 2% NCC-FP / PC prepared by thin film*
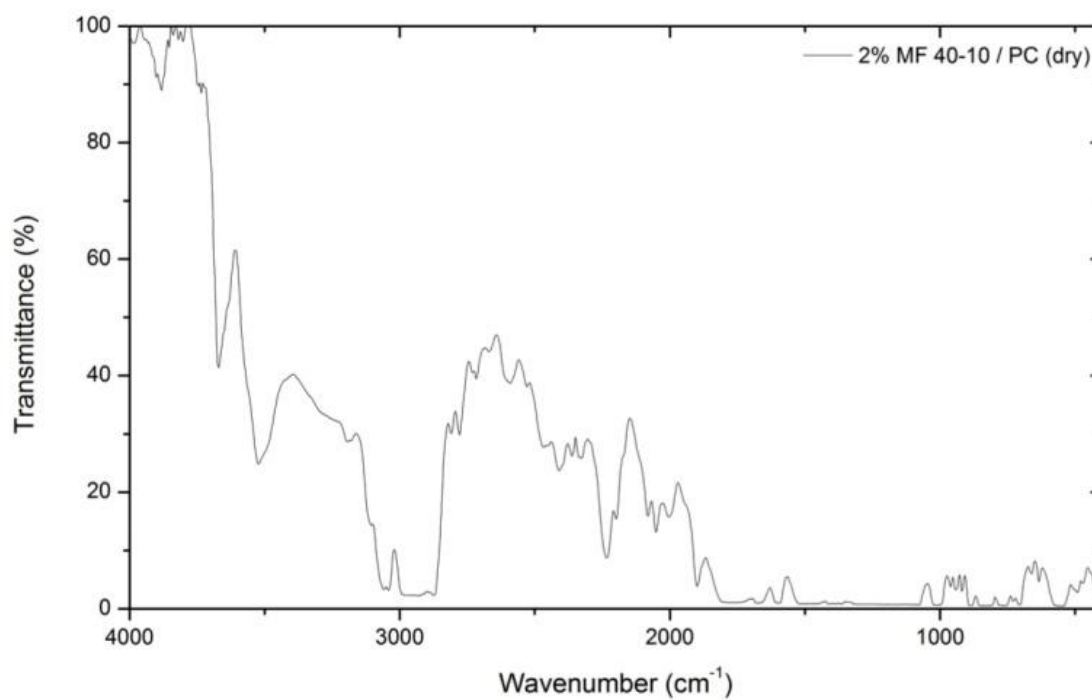
Figure A.7.4 – FTIR spectrum for 2% MF 40-10 / PC (dried) prepared by thin film
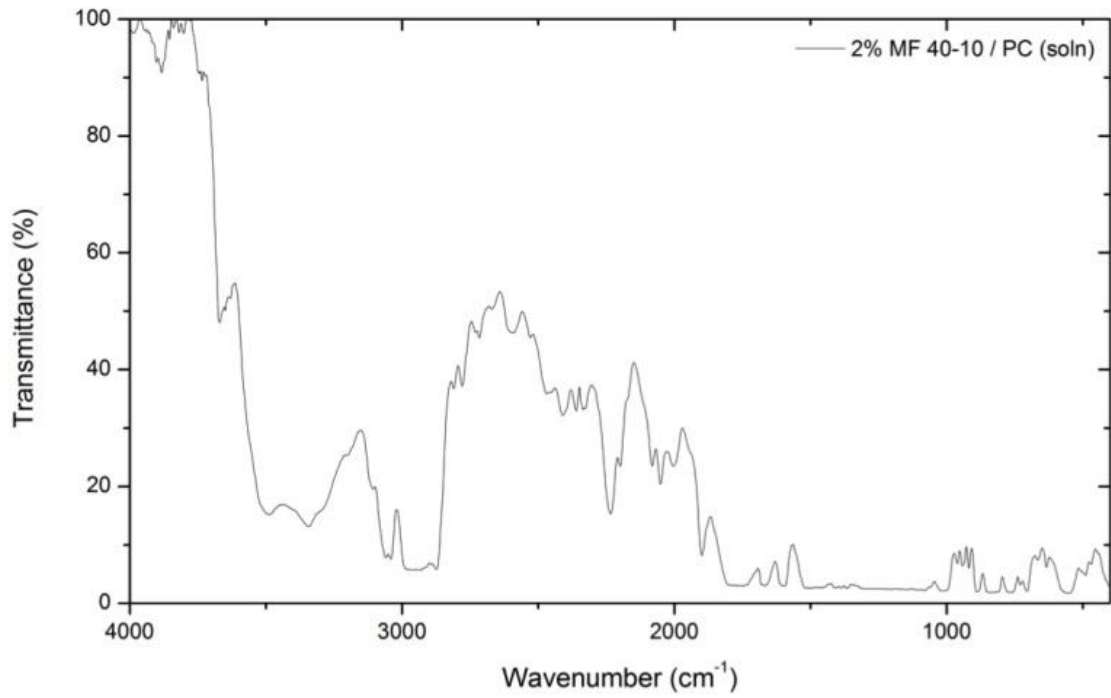
Figure A.7.5 – FTIR spectrum for 2% MF 40-10 / PC (soln) prepared by thin film
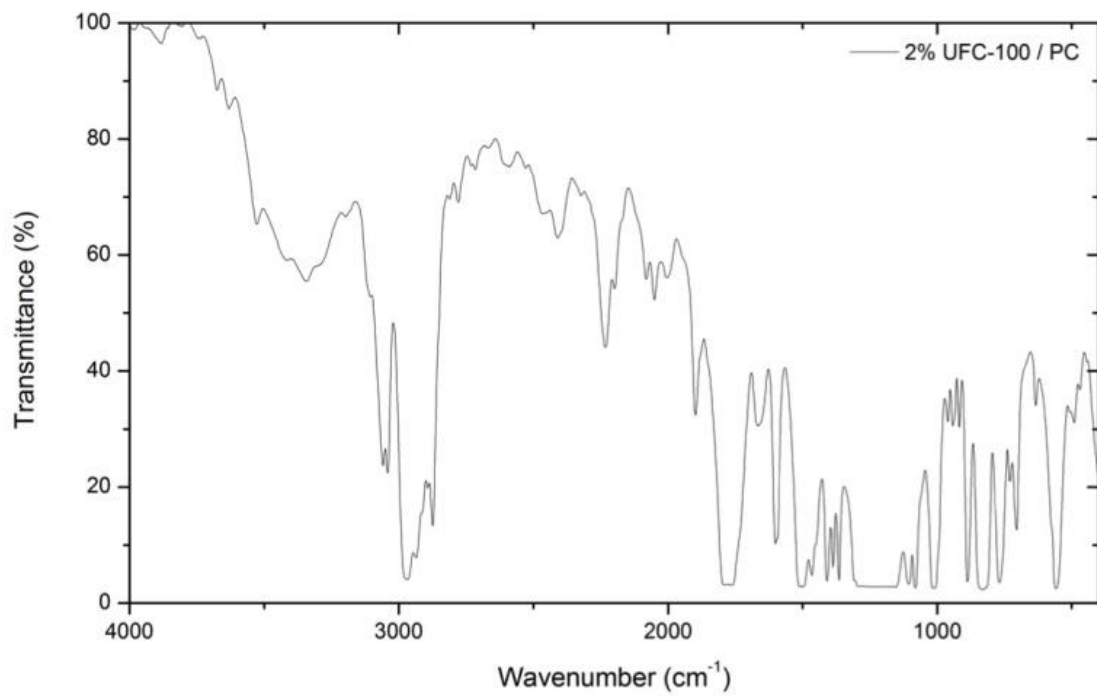

Figure A.7.6 – FTIR spectrum for 2% UFC-100 / PC prepared by thin film

162